



**INSTITUTO POTOSINO DE INVESTIGACIÓN  
CIENTÍFICA Y TECNOLÓGICA, A.C.**

**POSGRADO EN CIENCIAS APLICADAS**

**On repetitive control for harmonic compensation in power electronic systems**

Tesis que presenta:

**M.I. Pánfilo Raymundo Martínez Rodríguez**

Para obtener el grado de:

**Doctor en Ciencias Aplicadas**

En la opción de:

**Control y Sistemas Dinámicos**

**Directores de Tesis:**

Dr. Gerardo Escobar Valderrama

Dr. Jesús Leyva Ramos

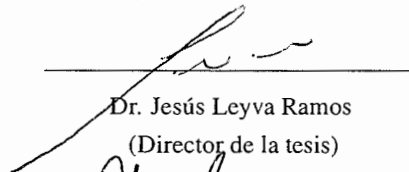
San Luis Potosí, S.L.P., agosto de 2007

## Constancia de aprobación de la tesis

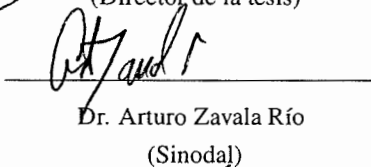
La tesis (**On repetitive control for harmonic compensation in power electronic systems**) presentada para obtener el Grado de Doctor en Ciencias Aplicadas en la opción de Control y Sistemas Dinámicos fue elaborada por el M.I. Pánfilo Raymundo Martínez Rodríguez y aprobada el **7 de agosto de 2007** por los suscritos, designados por el Colegio de Profesores de la División de Matemáticas Aplicadas y Sistemas Computacionales del Instituto Potosino de Investigación Científica y Tecnológica, A.C.



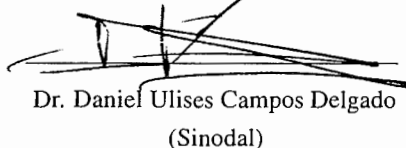
Dr. Gerardo Escobar Valderrama  
(Director de la tesis)



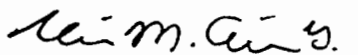
Dr. Jesús Leyva Ramos  
(Director de la tesis)



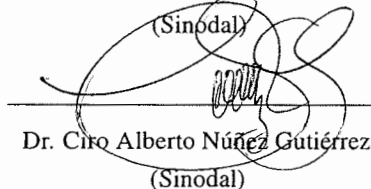
Dr. Arturo Zavala Río  
(Sinodal)



Dr. Daniel Ulises Campos Delgado  
(Sinodal)



Dr. Víctor Manuel Cárdenas Galindo  
(Sinodal)



Dr. Ciro Alberto Núñez Gutiérrez  
(Sinodal)



## **Créditos Institucionales**

Esta tesis fue elaborada en la División de Matemáticas Aplicadas y Sistemas Computacionales del Instituto Potosino de Investigación Científica y Tecnológica, A.C., bajo la dirección de los Doctores: Dr. Gerardo Escobar Valderrama y Dr. Jesús Leyva Ramos.

Durante la realización del trabajo el autor recibió una beca académica del Consejo Nacional de Ciencia y Tecnología (No. de registro 166569) y del Instituto Potosino de Investigación Científica y Tecnológica, A. C.

Parte de esta tesis fue elaborada en el Departamento de Ingeniería Electrónica de la Escuela Superior de Ingenieros en la Universidad de Sevilla.



**IPICYT**

# Instituto Potosino de Investigación Científica y Tecnológica, A.C.

## Acta de Examen de Grado

El Secretario Académico del Instituto Potosino de Investigación Científica y Tecnológica, A.C., certifica que en el Acta 003 del Libro Primero de Actas de Exámenes de Grado del Programa de Doctorado en Ciencias Aplicadas en la opción de Control y Sistemas Dinámicos está asentado lo siguiente:

En la ciudad de San Luis Potosí a los 7 días del mes de agosto del año 2007, se reunió a las 17:00 horas en las instalaciones del Instituto Potosino de Investigación Científica y Tecnológica, A.C., el Jurado integrado por:

<b>Dr. Daniel Ulises Campos Delgado</b>	<b>Presidente</b>	<b>UASLP</b>
<b>Dr. Gerardo Escobar Valderrama</b>	<b>Secretario</b>	<b>IPICYT</b>
<b>Dr. Arturo Zavala Río</b>	<b>Sinodal</b>	<b>IPICYT</b>
<b>Dr. Ciro Alberto Núñez Gutiérrez</b>	<b>Sinodal externo</b>	<b>UASLP</b>
<b>Dr. Jesús Leyva Ramos</b>	<b>Sinodal</b>	<b>IPICYT</b>
<b>Dr. Víctor Manuel Cárdenas Galindo</b>	<b>Sinodal externo</b>	<b>UASLP</b>

a fin de efectuar el examen, que para obtener el Grado de:

**DOCTOR EN CIENCIAS APLICADAS  
EN LA OPCIÓN DE CONTROL Y SISTEMAS DINÁMICOS**

sustentó el C.

**Pánfilo Raymundo Martínez Rodríguez**

sobre la Tesis intitulada:

*On repetitive control for harmonic compensation in power electronics systems*

que se desarrolló bajo la dirección de

**Dr. Gerardo Escobar Valderrama**  
**Dr. Jesús Leyva Ramos**

El Jurado, después de deliberar, determinó

**APROBARLO**

Dándose por terminado el acto a las 19:00 horas, procediendo a la firma del Acta los integrantes del Jurado. Dando fé el Secretario Académico del Instituto.

A petición del interesado y para los fines que al mismo convengan, se extiende el presente documento en la ciudad de San Luis Potosí, S.L.P., México, a los 7 días del mes agosto de 2007.

**L.C.C. Ivonne Lizette Cuevas Velez**  
Jefa del Departamento de Asuntos Escolares

**Dr. Marcial Bortolotto**  
Secretario Académico



# Agradecimientos

Agradezco a todas las personas que de alguna u otra manera estuvieron involucradas con el desarrollo del presente trabajo, por su apoyo y motivación brindados. En especial agradezco a mi esposa Judith por su gran apoyo, amor, comprensión y paciencia a través de este largo proceso de formación, así como a mis pequeños hijos, Raymundo y Mariana por su amor incondicional, quienes junto con Judith han sido el motor que me impulsa a seguir mejorando siempre. De igual manera Agradezco a mis padres Pánfilo Raymundo y María Guadalupe por guiarme en el buen camino a lo largo de mi vida, por sus valiosos consejos y el apoyo incondicional que siempre me han brindado, además de ser unos padres maravillosos. Agradezco también a mis hermanos Alejandra y Carlos por el apoyo y amistad que siempre he recibido de ellos.

En forma muy especial agradezco al Dr. Gerardo Escobar Valderrama quien más que un director de tesis ha sido un gran amigo, gracias por la amistad, la confianza, los consejos brindados a lo largo de mi formación, y por todo el conocimiento que he adquirido a lo largo de estos años. Además de agradecer con toda humildad y respeto a la familia del Dr. Gerardo quienes siempre abrieron las puertas de su hogar brindándome su amistad.

De igual manera agradezco al Dr. Juan Pablo Loyola Rodríguez y su esposa Dra. Patricia Leyva de Loyola por su amistad, consejos y apoyo incondicional brindados a lo largo de mi vida. Agradezco también a mis suegros Sr. Eduardo Martínez y Sra. María Dolores López, quienes me han acogido como un hijo, por su apoyo y cariño incondicional. En general agradezco a mi familia por todo su apoyo, a mis abuelos, tíos, primos, sobrinos.

De igual manera agradezco a mis profesores por sus consejos y lecciones brindadas. A mis sinodales por que gracias a sus observaciones y consejos he podido completar esta etapa.

También manera agradezco a Michael, Raymundo, Héctor, Andrés, Juan Luís, Perla, Demetrio, Misael, Vrani, Luís Adolfo, Hugo Oscar, Octavio, Eugenia, Pablo, Blanca y Pilar, por su amistad y apoyo.

A mis compañeros y amigos del ITESI , Sacramento, Alfonso, Marcos, Homero, Gabriel y Sergio, por su amistad y apoyo para poder concluir con esta etapa.

Pánfilo Raymundo Martínez Rodríguez, San Luis Potosí, México, agosto del 2007.

*A mi amada y bella esposa Judith, a mis amados hijos Raymundo y Mariana,  
y a mis padres y hermanos con agradecimiento y cariño.*

# Resumen

PARA atacar el problema de distorsión armónica distintas técnicas de control han sido utilizadas, entre las que destacan: el control por modos deslizantes, los controladores basados en pasividad, el control adaptable, los controladores basados en modelo interno, etc. Como resultado de estas técnicas diversos esquemas de control han sido generados, pudiendo clasificar a estos en directos o indirectos, de naturaleza selectiva o no. Quizá los más comúnmente utilizados, son los de control indirecto o también conocidos como controladores en modo corriente, esto debido a las características de desempeño que ofrecen. Normalmente estos esquemas contienen algunos términos adicionales o de refinamiento para garantizar la compensación de la distorsión armónica. Estos términos de refinamiento actúan sobre un conjunto determinado de componentes armónicos, los cuales, corresponden con los componentes armónicos que se desea compensar. Debido a esta característica este tipo de controladores son denominados como selectivos. Un ejemplo de estos esquemas lo constituye el control basado en un banco filtros resonantes, siendo precisamente el banco de filtros resonantes el término de refinamiento para garantizar la compensación armónica, donde cada filtro resonante debe estar sintonizado a la frecuencia armónica que se desea compensar.

Entre las principales contribuciones del presente trabajo en el área de control aplicado a electrónica de potencia se mencionan, el desarrollo de un par de nuevos esquemas de control repetitivo, así como la observación de que un banco infinito de filtros resonantes, bajo ciertas condiciones, es equivalente uno a uno a los esquemas de control repetitivo propuestos. Esto último deriva del hecho de que un banco infinito tiene una representación equivalente en términos de una función hiperbólica en el dominio de la frecuencia, que a su vez puede ser expresada como un cociente de funciones de términos exponenciales, esto es, retardos puros.

En particular el arreglo de control repetitivo propuesto en este trabajo consiste de un retardo en retroalimentación, más una trayectoria de prealimentación "feedforward". Esta retroalimentación puede ser positiva o negativa, asociándole a la prealimentación el mismo signo. Además se muestra que el esquema con retroalimentación y prealimentación positiva es equivalente a una suma infinita de filtros resonantes centrados en todos los múltiplos enteros de la fundamental (incluyendo al cero), mientras que el esquema con retroalimentación y prealimentación negativa es equivalente a una suma infinita de filtros resonantes centrados en múltiplos impares enteros de la fundamental. Es importante mencionar que la implementación de dichos esquemas repetitivos resulta relativa-

mente sencilla requiriendo solamente recrear un retardo puro, y realizar las operaciones de retroalimentación y prealimentación. Por lo que la implementación de estos esquemas se puede hacer de manera analógica o digital.

En la presente tesis se aplican técnicas de control basadas en los esquemas repetitivos mencionados anteriormente para la reducción de distorsión armónica en diversos sistemas de electrónica de potencia, a saber, convertidores DC-DC, PFC, filtro activo monofásico en dos topologías, de puente completo y de medio puente.

En el convertidor DC-DC, el esquema de control presentado se enfoca a compensar el rizo de voltaje a la salida del convertidor, debido a las perturbaciones en el voltaje de entrada. La estructura de este controlador se conserva muy parecida a la del controlador convencional, que incluye un lazo interno y un lazo externo. El esquema de control repetitivo, es utilizado para cancelar casi cualquier remanente de contaminación armónica en el voltaje de salida mientras se mantiene regulado a escalones de carga. En el PFC se tiene un objetivo diferente. En este sistema se busca mantener un voltaje regulado a la salida del convertidor, manteniendo las características ideales de corriente en la red eléctrica, esto es, una corriente proporcional al voltaje y en fase con éste. En el filtro activo, el objetivo es compensar la distorsión lineal distorsionante para mantener el factor de potencia cercano a la unidad. La topología seleccionada para este sistema es un VSI de medio puente, el cual consiste en una rama de interruptores más una rama de dos capacitores. Dos problemas adicionales surgen en este tipo de dispositivos: balance en los capacitores y regulación de la suma de los voltajes en los capacitores a un valor de referencia deseado. Por último se presenta un esquema de control repetitivo para la compensación de distorsión armónica y potencia reactiva usando un filtro activo paralelo basado en un VSI monofásico de puente completo. El controlador propuesto logra que el sistema compuesto por el filtro activo y carga se comporten como un elemento resistivo ante la red eléctrica manteniendo un factor de potencia cercano a la unidad.

Los prototipos de cada uno de los sistemas electrónicos de potencia anteriormente mencionados, fueron desarrollados en el Laboratorio de Procesamiento y Calidad de la Energía del IPICYT, de los cuales fue posible extraer resultados experimentales, que se presentan para validar el comportamiento práctico de los controladores propuestos.



# Contents

<b>Resumen</b>	<b>xi</b>
<b>Notation</b>	<b>vii</b>
<b>List of figures</b>	<b>ix</b>
<b>List of tables</b>	<b>xv</b>
<b>1 Introduction</b>	<b>1</b>
1.1 Overview of the harmonic phenomena in power systems . . . . .	1
1.2 Existing solutions for harmonic compensation . . . . .	2
1.3 Repetitive control as a practical solution for the harmonic compensation issue . . .	3
1.4 Repetitive control without feedforward path . . . . .	4
1.4.1 Numerical simulations of the repetitive schemes . . . . .	7
1.5 Outline of the dissertation . . . . .	12
<b>2 Repetitive schemes with feedforward modification</b>	<b>15</b>
2.1 Introduction . . . . .	15
2.2 Repetitive schemes plus feedforward path . . . . .	17
2.3 Practical modifications to the proposed compensator . . . . .	19
2.4 Analog implementation of the repetitive schemes . . . . .	23

2.5	Stability analysis of the closed-loop system . . . . .	29
<b>3</b>	<b>Harmonic compensation in a DC-DC boost converter</b>	<b>35</b>
3.1	Introduction . . . . .	35
3.2	Problem formulation . . . . .	36
3.3	Repetitive-based controller . . . . .	39
3.3.1	Stability analysis . . . . .	42
3.4	Experimental results . . . . .	45
<b>4</b>	<b>Boost-based PFC with harmonic compensation</b>	<b>51</b>
4.1	Introduction . . . . .	51
4.2	Switch-regulated boost converter as a PFP . . . . .	53
4.2.1	Inner control loop . . . . .	54
4.2.2	Outer control loop . . . . .	57
4.3	Stability analysis . . . . .	59
4.4	Experimental results . . . . .	61
<b>5</b>	<b>A repetitive controller for a half bridge active filter</b>	<b>67</b>
5.1	Introduction . . . . .	67
5.2	System Description . . . . .	68
5.3	Controller design . . . . .	70
5.3.1	Inner control loop . . . . .	70
5.3.2	Voltage control loops . . . . .	72
5.4	Experimental results . . . . .	75
<b>6</b>	<b>A repetitive controller for a single phase active filter</b>	<b>79</b>
6.1	Introduction . . . . .	79

<i>Contents</i>	<b>xv</b>
6.2 Problem formulation . . . . .	80
6.2.1 Inner control loop . . . . .	82
6.2.2 Outer control loop . . . . .	84
6.3 Experimental results . . . . .	86
<b>7 Concluding remarks and future work</b>	<b>91</b>
7.1 Concluding remarks . . . . .	91
7.2 Future Work . . . . .	93
<b>Bibliography</b>	<b>94</b>



# Notation and Acronyms

## Frequent Acronyms

AC	Alternating current.
BIBO	bounded input bounded output.
BBD	bucket brigade delay.
DC	direct current.
DC-DC	direct current to direct current.
EMI	electro magnetic interference.
DSP	digital signal processor.
ESR	equivalent series resistances.
FFT	fast Fourier transform.
HPF	High Pass Filter
HR	harmonic Reducer.
IC	integrated circuit.
IGBT	isolated gate bipolar transistor.
LPF	low Pass Filter.
LTI	linear time invariant.
MOSFET	metal-oxide-semiconductor field-effect transistor.
PCC	point of common connection.
PF	power factor.
PFC	power factor correctors or unit power factor converter.
PI	proportional integral.
PIS	synchronous Proportional integral.
PWM	pulse width modulation.
SPWM	sinusoidal pulse width modulation.
RHS	right hand side.
RMS	root mean square.
THD	total harmonic distortion.
VSI	Voltage source inverter.

**Most common mathematical symbols**

$\mathbb{R}$	field of real numbers.
$\mathbb{C}$	field of complex numbers.
$\mathbb{R}^n$	linear space of ordered $n$ -tuples in $\mathbb{R}$ .
$\in$	belong to.
$\triangleq$	“defined as”.
$(\cdot)^\top$	transpose operator.
$(\cdot)^{-1}$	inverse operator.
$\bar{\sigma}(\cdot)$	denotes the largest singular value of the matrix.
$Re(\alpha)$	The real part of $\alpha \in \mathbb{C}$ .
$\mathcal{L}^{-1}$	The inverse Laplace transform.
$\ A\ _\infty$	Induced $\infty$ -norm of a transfer matrix $A$ .
$\mathcal{L}_2$	Space of square integral functions.
$\mathcal{L}_\infty$	Space of bounded functions.
$\mathcal{H}_\infty$	The set of $\mathcal{L}_\infty$ analytic in $Re(s) > 0$ .
prefix $\mathcal{R}$	real rational, e.g., $\mathcal{RH}_\infty$ , $\mathcal{RH}_2$ .
$t$	time, $t \in \mathbb{R}_{\geq 0}$ .
$\frac{d}{dt}(\cdot)$ , $(\dot{\cdot})$	differentiation operator.
$(\cdot)_k^p$ ,	$k$ -th harmonic coefficients for the positive sequence representation.
$(\cdot)_k^n$	$k$ -th harmonic coefficients for the negative sequence representation.
$I_n$	The identity matrix of dimension $n$ .
$\mathcal{J}$	the skew symmetric matrix $\begin{bmatrix} 0 & -1 \\ 1 & 0 \end{bmatrix}$
$e^{(\cdot)}$	exponential function
$\mathcal{H}$	The set of indexes of the considered harmonic components
$\rho(\cdot)$	The rotation vector defined as $\begin{bmatrix} \cos(\cdot) \\ \sin(\cdot) \end{bmatrix}$ .
$\hat{(\cdot)}$	estimate of $(\cdot)$ .
$\tilde{(\cdot)}$	error between a quantity and its reference.
	$(\cdot) - (\cdot)^*$ , $\hat{(\cdot)} - (\cdot)$ .
$(\cdot)^*$	desired external references.

# List of Figures

1.1	Repetitive control system proposed in [18]. . . . .	4
1.2	Block diagram and poles location of: <b>(a)</b> positive feedback (all harmonics) compensator, and <b>(b)</b> negative feedback (odd harmonics) compensator. . . . .	6
1.3	Block diagram of: <b>(a)</b> positive feedback (all harmonics) compensator, and <b>(b)</b> negative feedback (odd harmonics) compensator whit K and LPF. . . . .	7
1.4	Theoretical Bode plots of traditionally repetitive scheme for different values of $K$ (x-axis Hz, y-axis dB): <b>(dotted line)</b> $K = 0.95$ , <b>(dashed line)</b> $K = 0.75$ , and <b>(solid line)</b> $K = 0.5$ . . . . .	8
1.5	Theoretical Bode plots of $R_p(s; d_1, K)$ different values of $K$ (x-axis Hz, y-axis dB): <b>(dotted line)</b> $K = 0.95$ , <b>(dashed line)</b> $K = 0.75$ , and <b>(solid line)</b> $K = 0.5$ . . . . .	9
1.6	Theoretical Bode plots of $R_n(s; d_2, K)$ different values of $K$ (x-axis Hz, y-axis dB): <b>(dotted line)</b> $K = 0.95$ , <b>(dashed line)</b> $K = 0.75$ , and <b>(solid line)</b> $K = 0.5$ . . . . .	9
1.7	Theoretical Bode plot of $R_p(s; d_1, K)$ for different values of $\tau$ and $K = 0.95$ (x-axis Hz, y-axis dB): <b>(dotted line)</b> without LPF, <b>(solid line)</b> $\tau = 1.3263 \times 10^{-5}$ s (12 kHz) , and <b>(dashed line)</b> $\tau = 1.3263 \times 10^{-4}$ s ( 1.2 kHz). . . . .	10
1.8	Theoretical Bode Bode plot of $R_n(s; d_2, K)$ for different values of $\tau$ and $K = 0.95$ (x-axis Hz, y-axis dB): <b>(dotted line)</b> without LPF , <b>(solid line)</b> $\tau = 1.3263 \times 10^{-5}$ s (12 kHz), and <b>(dashed line)</b> $\tau = 1.3263 \times 10^{-4}$ s ( 1.2 kHz). . . . .	10
1.9	Amplitude of $\mathcal{S}_K^{R_n} _{s=j\omega}$ for different values of $\tau$ and $K = 0.95$ (x-axis Hz, y-axis dB): <b>(dotted line)</b> without LPF and with LPF for different values of $\tau$ : <b>(solid line)</b> $\tau = 1.3263 \times 10^{-5}$ s (12 kHz), and <b>(dashed line)</b> $\tau = 1.3263 \times 10^{-4}$ s ( 1.2 kHz). . . . .	11

1.10	Amplitude of $\mathcal{S}_d^{R_n} _{s=j\omega}$ for different values of $\tau$ and $K = 0.95$ (x-axis Hz, y-axis dB): <b>(dotted line)</b> without LPF and with LPF for different values of $\tau$ : <b>(From top to bottom in solid line)</b> $\tau = 1.3263 \times 10^{-5}$ s (12 kHz), and $\tau = 1.3263 \times 10^{-4}$ s (1.2 kHz). . . . .	11
2.1	Continuous-time model and zero-pole locations of: <b>(a)</b> positive feedback (all harmonics) compensator with feedforward, and <b>(b)</b> negative feedback (odd harmonics) compensator with feedforward. . . . .	17
2.2	Pole-zero locations of the repetitive compensators: <b>(a)</b> positive feedback (all harmonics) compensator with feedforward, and <b>(b)</b> negative feedback (odd harmonics) compensator with feedforward. . . . .	20
2.3	Block diagram representation of the repetitive compensators with feedforward and practical modifications: <b>(a)</b> $R_{pf}(s; d_1, K)$ , and <b>(b)</b> $R_{nf}(s; d_2, K)$ . . . . .	20
2.4	Theoretical Bode plots of $R_{pf}(s; d_1, K)$ for different values of $K$ (x-axis Hz, y-axis dB): <b>(dotted line)</b> $K = 0.95$ , <b>(dashed line)</b> $K = 0.75$ , and <b>(solid line)</b> $K = 0.5$ . . . . .	21
2.5	Theoretical Bode plots of $R_{nf}(s; d_2, K)$ for different values of $K$ (x-axis Hz, y-axis dB): <b>(dotted line)</b> $K = 0.95$ , <b>(dashed line)</b> $K = 0.75$ , and <b>(solid line)</b> $K = 0.5$ . . . . .	22
2.6	Theoretical Bode plots of $R_{pf}(s; d_1, K)$ for different values of $\tau$ and $K=0.95$ (x-axis Hz, y-axis dB): <b>(dotted line)</b> without LPF, <b>(solid line)</b> $\tau = 1.3263 \times 10^{-5}$ s (12 kHz), and <b>(dashed line)</b> $\tau = 1.3263 \times 10^{-4}$ s (1.2 kHz). . . . .	22
2.7	Theoretical Bode plots of $R_{nf}(s; d_2, K)$ for different values of $\tau$ and $K=0.95$ (x-axis Hz, y-axis dB): <b>(dotted line)</b> without LPF, <b>(solid line)</b> $\tau = 1.3263 \times 10^{-5}$ s (12 kHz), and <b>(dashed line)</b> $\tau = 1.3263 \times 10^{-4}$ s (1.2 kHz). . . . .	23
2.8	Implemented positive feedback feedforward (all harmonics) compensator. . . . .	24
2.9	Implemented negative feedback feedforward (odd harmonics) compensator. . . . .	25
2.10	Time responses of <b>(Top)</b> output signal and <b>(Bottom)</b> input signal of the MN3004 circuit. . . . .	26
2.11	Experimental frequency response for the positive feedback compensator with feedforward (x-axis 125 Hz/div and y-axis 10 dB/div): <b>(top)</b> $K = 0.824$ , and <b>(bottom)</b> $K = 0.955$ . . . . .	27
2.12	Experimental frequency response for the negative feedback compensator with feedforward (x-axis 62.5 Hz/div and y-axis 10 dB/div): <b>(top)</b> $K = 0.824$ , and <b>(bottom)</b> $K = 0.955$ . . . . .	27



2.13	Experimental time response for the negative feedback compensator with $K = 0.955$ to a sinusoidal signal of frequency 120 Hz and amplitude 50 mV (x-axis 4 ms/div). <b>(from top to bottom)</b> : output $y(t)$ with feedforward (y-axis 2 V/div), output $y(t)$ without feedforward (y-axis 2 V/div), and input $e(t)$ (y-axis 100 mV/div). . . . .	28
2.14	Experimental time response for the negative feedback compensator with $K = 0.955$ to a sinusoidal signal of frequency 240 Hz and amplitude 1 V (x-axis 4 ms/div), (y-axis 1 V/div). <b>(from top to bottom)</b> : output $y(t)$ with feedforward, output $y(t)$ without feedforward, and input $e(t)$ . $K = 0.955$ . . . . .	28
2.15	Experimental time response for the negative feedback compensator with $K = 0.955$ to a sinusoidal signal of frequency 600 Hz and amplitude 50 mV (x-axis 4 ms/div). <b>(from top to bottom)</b> : output $y(t)$ with feedforward (y-axis 2 V/div), output $y(t)$ without feedforward (y-axis 2 V/div), and input $e(t)$ (y-axis 100 mV/div). . . . .	29
2.16	General control system with a positive feedback plus feedforward repetitive compensator. . . . .	30
2.17	An equivalent system for the overall closed-loop system. . . . .	32
3.1	Boost converter circuit. . . . .	37
3.2	Block diagram of the adaptive controller using a bank of resonant filters for the compensation of the output voltage harmonic distortion. . . . .	39
3.3	Frequency response of the positive feedback feedforward repetitive scheme, with low pass filter with cutoff frequency $f = 12$ kHz and, different values of cutoff frequency of derivative term of limited bandwidth . . . . .	41
3.4	Block diagram of the proposed repetitive-based controller. . . . .	42
3.5	Block diagram of the output voltage error dynamics in closed loop with the repetitive scheme. . . . .	43
3.6	Block diagram of the proposed repetitive-based controller. . . . .	44
3.7	Bode plot of the BIBO Stability condition (3.16) for repetitive controller for a DC-DC converter . . . . .	45
3.8	Transient responses after enabling the harmonic compensation, with $R = 12.5\Omega$ . <b>(From top to bottom)</b> Capacitor voltage $x_2$ , inductor current $x_1$ and the inductor reference current $I_d$ . . . . .	47

3.9	Transient responses after disabling the harmonic compensation, with $R = 25\Omega$ . <b>(from top to bottom)</b> Capacitor voltage $x_2$ , inductor current $x_1$ and the inductor reference current $I_d$ . . . . .	47
3.10	Frequency spectrum of capacitor voltage $x_2$ , with $R = 12.5\Omega$ . <b>(top)</b> Without har- monic compensation, and <b>(bottom)</b> under harmonic compensation. . . . .	48
3.11	Frequency spectrum of capacitor voltage $x_2$ , with $R = 25\Omega$ . <b>(top)</b> Without har- monic compensation, and <b>(bottom)</b> under harmonic compensation. . . . .	48
3.12	Frequency spectrum of inductor current $x_1$ , with $R = 12.5\Omega$ . <b>(top)</b> Without har- monic compensation, and <b>bottom</b> under harmonic compensation. . . . .	49
3.13	Transient response for a load step change from $R = 25\Omega$ to $R = 12.5\Omega$ . <b>(from</b> <b>top to bottom)</b> Capacitor voltage $x_2$ , inductor current $x_1$ and DC component of the inductor reference current $I_d$ . . . . .	49
3.14	Transient response for a load step change from $R = 12.5\Omega$ to $R = 25\Omega$ . <b>(from</b> <b>top to bottom)</b> capacitor voltage $x_2$ , inductor current $x_1$ and DC component of the inductor reference current $I_d$ . . . . .	50
4.1	Switch-regulated boost-based PFC circuit. . . . .	52
4.2	Block diagram of the proposed repetitive-based controller for the PFC. . . . .	59
4.3	Block diagram of the input current error dynamics in closed-loop with the repetitive scheme. . . . .	59
4.4	Equivalent system of the block diagram shown in Fig. 4.3 for analysis purposes. . .	61
4.5	Bode plot of $(s + 1/\tau_a)/(s + 1/\tau_b)$ for different values of $kr$ to show that their norm is always less than or equal to 1. The Bode plot of $1/(\tau_1 s + 1)$ is also included where the cutoff frequency of the LPF is fixed to 12 KHz, $K_1 = 8$ and $K_r$ is varied from 2 to 8. . . . .	62
4.6	Bode plot of $(s + 1/\tau_a)/(s + 1/\tau_b)$ for different values of $kr$ to show that their norm is always less than or equal to 1. The Bode plot of $1/(\tau_1 s + 1)$ is also included where the cutoff frequency of the LPF is fixed to 12 KHz, $K_1 = 8$ and $K_r$ is varied from 10 to 20. . . . .	62
4.7	Time responses of <b>(top)</b> voltage $v_C$ (y-axis 100 V/div, x-axis 2 s/div), and <b>(bottom)</b> $G$ for a load step change from $R = 850\Omega$ to $R = 500\Omega$ and back (y-axis approx. 250 W/div, x-axis 2 s/div). . . . .	64

4.8	<b>(top)</b> Source voltage $v_S$ (y-axis 100 V/div, x-axis 4 ms/div) and <b>(bottom)</b> harmonic content of $v_S$ (y-axis 20 dB/div, x-axis 125 Hz/div). . . . .	64
4.9	<b>(from top to bottom)</b> Source voltage $v_S(t)$ (y-axis 100 V/div, x-axis 4 ms/div), input current $i_i(t)$ (y-axis 2 A/div, x-axis 4 ms/div), and input current error $\tilde{i}_i(t)$ (y-axis 2 A/div, x-axis 4 ms/div), for a load resistance $R = 500 \Omega$ . . . . .	65
4.10	Harmonic content of <b>(top)</b> the source voltage $v_S(t)$ (y-axis 20 dB/div, x-axis 125 Hz/div) and <b>(bottom)</b> the input current $i_i(t)$ (y-axis 20 dB/div, x-axis 125 Hz/div) under the proposed compensator at a load resistance $R = 500 \Omega$ . . . . .	65
4.11	Time responses of <b>(from top to bottom)</b> input current reference $i_i^*(t)$ (y-axis 4 A/div, x-axis 4 ms/div), input current $i_i(t)$ with harmonic compensation (y-axis 4 A/div, x-axis 4 ms/div), and input current $i_i(t)$ without harmonic compensation (y-axis 5 A/div, x-axis 4 ms/div), all of them at a load resistance $R = 500 \Omega$ . . . . .	66
5.1	Single phase half bridge shunt active filter. . . . .	69
5.2	Block diagram of the proposed controller. . . . .	74
5.3	The analog implementation of the proposed controller for a half bridge active filter	75
5.4	Power leg of the half bridge active filter. . . . .	76
5.5	Time waveforms of <b>(from top to bottom)</b> line voltage $v_S$ (real scale 20 V/div), compensated line current $x_1 = i_S$ (real scale 2.5 A/div), and current error $\tilde{x}_1$ (real scale 0.5 A/div). . . . .	77
5.6	<b>(top)</b> Frequency spectrum of $v_S$ (20 dB/div), and <b>(bottom)</b> frequency spectrum of $x_1 = i_S$ (20 dB/div). . . . .	77
5.7	Time waveforms of <b>(from top to bottom)</b> compensated line current $i_S$ (real scale 2.5 A/div), distorted load current $i_0$ (real scale 2.5 A/div), and injected current $i$ (real scale 2.5 A/div). . . . .	78
5.8	Transient responses of <b>(from top to bottom)</b> capacitor voltages $v_{C1}$ and $v_{C2}$ (5 V/div), voltages difference $x_3 = (v_{C1} - v_{C2})$ (1 V/div) and scaled equivalent conductance $G$ (10 W/div) during load step changes. . . . .	78
6.1	Single phase full-bridge shunt active filter. . . . .	81
6.2	Block diagram of the inner control loop. . . . .	85
6.3	Block diagram of the proposed repetitive-based controller. . . . .	86

6.4	Prototype of single Phase active filter . . . . .	87
6.5	Time responses with the proposed controller of: <b>(from top to bottom)</b> line voltage $v_S(t)$ (250 V/div), compensated current $i_S(t)$ (10 A/div), current load $i_0(t)$ (10 A/div), and injected current $i(t)$ (10 A/div). . . . .	88
6.6	<b>(from top to bottom)</b> Source voltage $v_S(t)$ (250 V/div), source current $i_S(t)$ with harmonic compensation (10 A/div), and source current $i_S(t)$ without harmonic compensation (10 A/div). . . . .	89
6.7	Transient responses during a load step change of <b>(top)</b> capacitor voltage $v_C(t)$ (100 V/div), and <b>(bottom)</b> scaled apparent conductance $\delta(t) = v_{S,RMS}^2 \eta(t)$ observed by the source (500 W/div). . . . .	89
6.8	Spectra of <b>(top)</b> the line voltage $v_S$ (20 dB/div), and <b>(bottom)</b> the compensated current $i_S$ (20 dB/div). . . . .	90

# List of Tables

3.1	Parameters of the boost converter. . . . .	45
3.2	Elements used to implement the delay line. . . . .	46
4.1	Elements used to implement the boost-based PFC converter. . . . .	63



# Chapter 1

## Introduction

### 1.1 Overview of the harmonic phenomena in power systems

THE last few years have witnessed a tremendous growing in the connection of distorting nonlinear loads to the electrical grid. As a result, several negative effects have been produced, which have been in detriment of the quality of the supplied energy. For instance, it is well known that the connection of nonlinear loads to the grid injects distorted currents into the mains, which indirectly produces a harmonic distortion in the voltage at the point of common connection (PCC). Typical examples of nonlinear loads are energy conversion equipments such as switched-mode power supplies, dc arc furnaces, flexible ac transmission components, adjustable speed drives and electronic fluorescent lamp ballast, among others. The non controlled rectifier with smoothing capacitor is perhaps the device most commonly found in industrial, domestic and office electronic equipments, which causes a considerable current distortion.

The introduction of new applications and advances in power electronics equipments have permitted to provide clever solutions to alleviate most electrical conversion, transmission, distribution and generation issues [1]. Active harmonic filters, dynamic voltage restorers, power factor compensators, static and adaptive var compensators and uninterruptable power supplies are examples of power electronic equipment aimed to improve the power quality. In most of these examples, the common issue is the compensation of the harmonic pollution caused by nonlinear loads. Recall that the harmonic description of signals is a tool that facilitates the treatment of distorted though periodic signals, based on the fact that a harmonic component is defined as a sinusoidal signal whose frequency is a multiple of the fundamental frequency. Harmonic distortion is thus defined as a signal composed of the sum of harmonic components at multiples of the fundamental frequency at which the supply system is designed to operate [2].

It is well known that the presence of harmonic distortion in the line current produces losses in the conductors and diminishes the power factor, which somehow limits the capacity to connect

more loads, and makes an inefficient use of the energy. Moreover, it is important to remember that any ac current, flowing through a circuit, produced by a non linear load could generate harmonic voltage drops in the PCC, and thus, the voltage signal at this point may exhibit, at least, a similar harmonic contents depending on the short circuit impedance. It is, however, not surprising that even under the presence of harmonics, a lot of electronics equipments will exhibit a good performance as far as the harmonics voltages do not exceed 5% [1]. Nevertheless, most delicate equipment may suffer premature aging or damage caused by such distortion. Motivated by these issues, this work represents an effort to provide control solutions based in repetitive schemes, for power electronics systems to compensate harmonic distortion produced by nonlinear loads.

## 1.2 Existing solutions for harmonic compensation

This work gathers the study of several power electronics systems where the control solutions for the harmonic distortion issue have been proposed. A first approach, that is revisited, consists on the application of adaptive techniques aimed to reconstruct the harmonic disturbances allowing their cancellation. The controllers obtained following this approach are of selective nature, that is, they reduce specific harmonics, while maintaining an acceptable dynamical performance, and without inclusion of additional hardware. It is important to remark that the harmonic compensation problem can be recast as a tracking reference problem with disturbance rejection, where the reference signal and the disturbances are both periodic signals. The derivation of these adaptive controllers uses the Lyapunov approach to build the estimates for the harmonic components of the disturbances. This process yields a series of adaptive laws which are quite difficult to implement due to presence of rotations in the regressors. Fortunately, the adaptive expressions can be reduced considerably, by means of rotations, into a bank of resonant filters tuned at the frequencies of the harmonics to be compensated (see [3] and [4]).

To better understand these ideas, let us consider the very well known technique used in active filters to compensate the  $\ell$ -th harmonic of the fundamental  $\omega_0$ . This technique consists of the following three steps. First, the system variables are transformed to rotating frame quantities at a rotating frequency  $\ell\omega_0$  ( $\ell$  an integer). Second, once in this synchronous frame, the variables are sent to a compensator, usually a PI. Third, the compensator outputs are converted back to the stationary reference frame [5], [6]. A PI is usually considered as the compensator since it guarantees zero steady state error of dc disturbances. Notice that, in the synchronous frame, rotating at  $\ell\omega_0$ , the  $\ell$ -th harmonic of a disturbance becomes a dc quantity, therefore, the PI in such a rotating frame guarantees zero steady state of such an  $\ell$ -th harmonic. This type of scheme is referred in the literature as synchronous PI associated to a given rotating frame [7], [8], multiple rotating integrator [9], synchronous-frame harmonic controller [6], multiple reference frame controller [5], and multi-synchronous PI controllers [10]. The main drawback of this scheme is the cumbersome implementation. Notice that two frame transformations (two rotations) are involved for each harmonic component to be compensated.



It has been shown, however, that this complexity, linked to the frame transformations, can be considerably reduced by appealing to the modulation properties of the Laplace transform [11], [12], [13], [14]. Application of such ideas to the above synchronous PI, yields the very well known resonant plus proportional compensator referred in the literature as resonant regulator [13], [14], PIS compensator [15], [16], stationary-frame generalized integrator [17], multi-resonant controller [10]. As it will be shown later, all of the proposed controllers maintain a similar structure as the conventional one, that is, they are composed by two control loops. This type of schemes is referred as current control or indirect control in power electronics systems. In these schemes, the bank of resonant filters appears as a refinement term to the final control signal. The resonant filters can be implemented in analog or digital form. The inconvenience here appears whenever the number of harmonics that is necessary to compensate increases. Basically, a resonant filter is required for each harmonic under compensation, that is, a huge bank of resonant filters is required for the compensation of several harmonics.

### **1.3 Repetitive control as a practical solution for the harmonic compensation issue**

The idea behind the bank of resonant filters is the generation of resonant peaks with extremely high gains tuned at the harmonics under compensation, in addition and automatically, notches are created between two consecutive resonant peaks. However, as pointed out before, this type of implementation becomes cumbersome as the harmonics under consideration increase, which evidently represents a bigger computational effort. To overcome this issue, it is proposed in this work to use controllers based on repetitive schemes whose frequency response mimics the bank of resonant filters, and with a much simpler implementation. The repetitive control is aimed to generate an infinite number of resonant peaks tuned at certain multiples of the fundamental frequency. In particular, the type of repetitive schemes used here are conformed by a feedback array of a single delay line in either, positive or negative feedback, and incorporates a feedforward path to create the notches in between every two consecutive resonant peaks to improve the selective nature, which contrast with respect the traditional structures.

The development of repetitive control was originally motivated by the design of a magnet power supply for a proton synchrotron [18]. Actually, the first works aimed to repetitive controllers theory were presented in [19] and [20], those papers were formally gathered in the seminal paper [21]. The stability study of the servo scheme proposed in [18] (see Fig 1.1) was complemented later by [22]. Other interesting theoretical developments of repetitive control were also presented in [23], [24] and the numerous references therein. It is important to remark that repetitive control has found more applicability in the discrete time formulation (see for instance [25],[26] and [27]).

First applications of repetitive control were based on the positive feedback scheme. It is important to notice that a positive feedback structure may have the disadvantage of compensating for

every single harmonic, odd, even and the dc component [3]. The use of repetitive schemes is not new in the power electronics field, for instance, some interesting applications of conventional positive feedback repetitive schemes can be found in [28], [29], [30] and [31] where the advantages of the feedback-feedforward structures respect to traditional structures will be described in the next chapters. The positive repetitive schemes without feedforward path based on a negative feedback approach were introduced in [3] [32], [33] and [34]. The negative based repetitive scheme, in contrast to the positive feedback approach, is aimed to compensate odd harmonics only, and thereby reduces the possibility of reinjecting unnecessary distortion into the system, a feature very well appreciated in the harmonic compensation in power electronics systems.

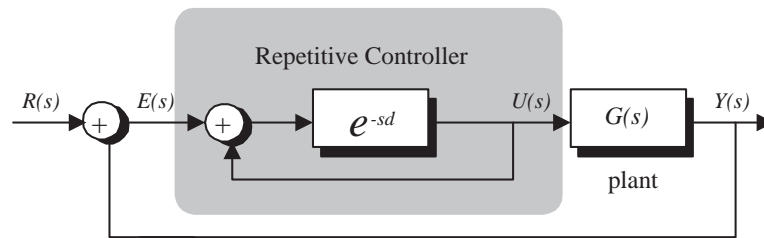


Figure 1.1: Repetitive control system proposed in [18].

It is important to remark that both controllers, using a bank of resonant filters or using repetitive schemes, are based on the well known *internal model principle* [35]. This principle states that a controlled output can track or reject a class of reference signals without steady error if the model (or generator) of the reference is included in the stable closed loop system.

Recall that the idea is to compensate periodic signals, which are the most commonly found in electrical power systems which arise as harmonic perturbations. To facilitate the study of this type of signals the infinite Fourier series representation is used. It is well known that a harmonic component, i.e., a sinusoidal signal, can be generated by means of a harmonic oscillator, i.e., a resonant filter. Therefore, as each harmonic component should be compensated, then it is necessary a bank of resonant filters to compensate them. However, as pointed out before, as the harmonics to compensate increase, this solution is not longer practical. Fortunately, in repetitive control approach, a simple delay line in a feedback array can be used to produce an infinite number of harmonic oscillators. Thereby, with an appropriate repetitive controller, it is possible to emulate a bank of a large number of harmonic oscillators tuned at the harmonics of interest.

## 1.4 Repetitive control without feedforward path

This section describe two repetitive controllers which are referred as the positive and the negative feedback schemes. The main interest of this section is to establish the bases for the develop of repetitive compensators aimed to harmonic compensation in power electronics systems, as well as

to establish the main difference between the traditional approach proposed by Hara, et. al. in [19] and [20] and the approach proposed in this work. It has been observed that in the traditionally schemes the delay line are located more frequently in the direct path, while, in this work it is proposed to locate the delay line in the feedback path. It can be shown that by placing the delay in the feedback path, the dynamic response of the phase is improved. therefore ,this work focuses in this type of schemes only. It is important to remark that the positive scheme of the repetitive controller is aimed to compensate all harmonics of the fundamental (like in traditional approach), while the negative scheme of repetitive controller consists of a negative feedback loop of the delay line aimed to compensate odd harmonics of the fundamental only.

Consider the single-input single-output (SISO) continuous-time systems described by

$$\begin{aligned} y(t) &= e(t) + y(t - d_1) \\ y(t) &= e(t) - y(t - d_2) \end{aligned} \quad (1.1)$$

where  $d_1$  and  $d_2$  are two positive real numbers representing the period of the reference signal (or perturbation) to be compensated. Notice that, the real numbers 1 and 2 have been used to differentiate between the repetitive schemes (1 for positive scheme and 2 for negative scheme)

The corresponding transfer functions of the above systems, after application of the Laplace transform, are given by the next expressions:

$$R_p(s; d_1) = \frac{1}{1 - e^{-sd_1}} \quad (1.2)$$

$$R_n(s; d_2) = \frac{1}{1 + e^{-sd_2}} \quad (1.3)$$

and the corresponding block diagrams are shown in Fig.1.2, where  $E(s)$  and  $Y(s)$  are Laplace transform of the input and the output signals.

For  $R_p(s; d_1)$  the poles can be found from  $e^{-sd_1} = 1$ , while for  $R_n(s; d_2)$  the poles of the system can be calculated from  $e^{-sd_2} = -1$ . Notice that, the complex functions  $e^{-sd_1}|_{s=j\omega} = 1$ , for  $\omega d_1 = 2\pi k$  ( $\forall k \in \{0, \pm 1, \pm 2, \dots, \pm\infty\}$ ). Therefore, if  $d_1 = 2\pi/\omega_0 = 1/f_0$  (one period) is proposed, then the transfer function of the positive feedback scheme has infinite many imaginary poles located at every single multiple of the fundamental frequency  $\omega_0$  ( $f_0 = \omega_0/2\pi$ ). On the other hand, the complex function  $e^{-sd_2}|_{s=j\omega} = -1$  for  $\omega d_2 = \pi(2k + 1)$  ( $\forall k \in \{0, \pm 1, \pm 2, \dots, \pm\infty\}$ ). Therefore, if  $d_2 = \pi/\omega_0 = 1/(2f_0)$  (half a period) then the transfer function of the negative feedback scheme has infinite many poles located at the odd multiples of  $\omega_0$ .

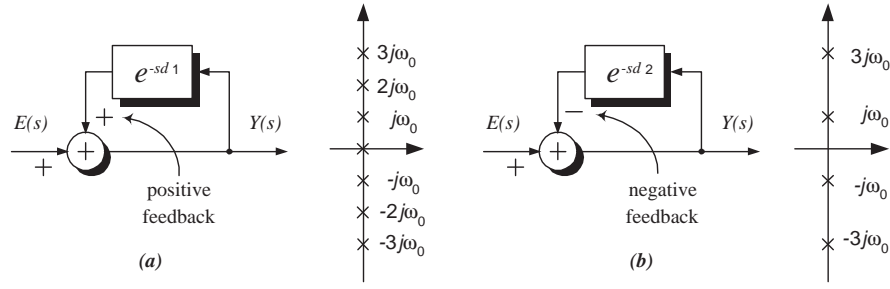


Figure 1.2: Block diagram and poles location of: **(a)** positive feedback (all harmonics) compensator, and **(b)** negative feedback (odd harmonics) compensator.

The corresponding transfers functions can also be written as

$$\begin{aligned}
 R_p(s; d_1) &= \frac{1}{1 - e^{-\frac{2s\pi}{\omega_0}}} = \frac{e^{\frac{s\pi}{\omega_0}}}{e^{\frac{s\pi}{\omega_0}} - e^{-\frac{s\pi}{\omega_0}}} \\
 &= \frac{e^{\frac{s\pi}{\omega_0}}}{2 \sinh(\frac{s\pi}{\omega_0})} = \frac{e^{\frac{s\pi}{\omega_0}}}{\frac{2s\pi}{\omega_0} \prod_{k=1}^{\infty} (\frac{s^2}{k^2\omega_0^2} + 1)} \quad (1.4)
 \end{aligned}$$

$$\begin{aligned}
 R_n(s; d_2) &= \frac{1}{1 + e^{-\frac{s\pi}{\omega_0}}} = \frac{e^{\frac{s\pi}{2\omega_0}}}{e^{\frac{s\pi}{2\omega_0}} + e^{-\frac{s\pi}{2\omega_0}}} \\
 &= \frac{e^{\frac{s\pi}{2\omega_0}}}{2 \cosh(\frac{s\pi}{2\omega_0})} = \frac{e^{\frac{s\pi}{2\omega_0}}}{2 \prod_{k=1}^{\infty} (\frac{s^2}{(2k-1)^2\omega_0^2} + 1)} \quad (1.5)
 \end{aligned}$$

where it is more evident that, for  $R_p(s; d_1)$ , the first pole lies at the origin and the rest of the poles lie at every single multiple of  $\omega_0$ , while the poles for  $R_n(s; d_2)$  lie at odd multiples of  $\omega_0$ , and there is not a pole at the origin (see Fig. 1.2).

The Bode plots of the repetitive above repetitive compensators consist of a set of peaks centered at the harmonic frequencies. The gain at these resonant frequencies is, in theory, infinite and thus, it may lead to asymptotic stability problems. To overcome this issue, it is proposed to add damping to all the poles by slightly shifting them to the left of the imaginary axis. It has been observed that, with the pole shifting process, the amplitude becomes limited. The shifting process can be realized as follow  $R_p(s + a; d_1) = R_p(s; d_1, K)$  for the positive feedback scheme, and  $R_n(s + a; d_2) = R_n(s; d_2, K)$  for the negative feedback scheme. In exponential terms the shifting process is expressed as  $e^{-(s+a)d} = e^{-ad}e^{-sd}$ . Notice that, a gain factor of the form  $K = e^{-ad}$  is applied to the exponential function as shown in Fig.1.3. Conversely, if we propose a gain  $K > 1$  the poles move to the right, but if  $0 < K < 1$  then they move to the left. Moreover, it is easy to show that, after this modification, the peaks reach a maximum magnitude of  $1/(1 - K)$  and the valleys a minimum magnitude of  $1/(1 + K)$  for both schemes.

In what follows the sensitivity function is used to study the robustness of the proposed schemes with respect to variations in the delay  $d_i$  ( $i \in 1, 2$ ) and the gain  $K$ , which are the main parameters

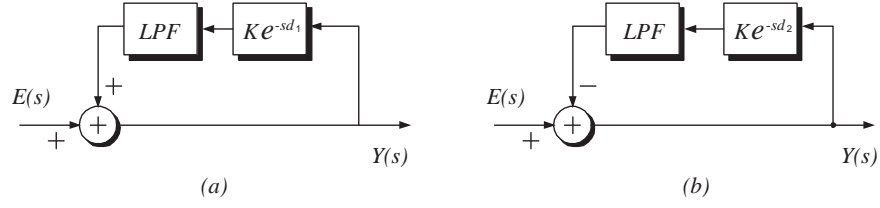


Figure 1.3: Block diagram of: **(a)** positive feedback (all harmonics) compensator, and **(b)** negative feedback (odd harmonics) compensator with  $K$  and LPF.

in these control schemes. For the negative feedback case the sensitivity function  $\mathcal{S}$  with respect to parameters  $d_i$  ( $i \in 1, 2$ ) and  $K$  can be calculated, respectively, according to the following expressions

$$\mathcal{S}_{d_i}^{R_n} = \frac{\partial R_n / R_n}{\partial d_i / d_i} \quad , \quad \mathcal{S}_K^{R_n} = \frac{\partial R_n / R_n}{\partial K / K}$$

For the negative feedback repetitive scheme the following expressions are obtained

$$\mathcal{S}_{d_2}^{R_n} = \frac{sd_2 K e^{-sd_2}}{1 + K e^{-sd_2}} \quad , \quad \mathcal{S}_K^{R_n} = -\frac{-K e^{-sd_2}}{1 + K e^{-sd_2}}$$

Notice that, the sensitivity function  $\mathcal{S}_K^{R_n}$  is bounded by  $\|\mathcal{S}_K^{R_n}\| < \frac{K}{1-K}$ , with  $0 < K < 1$ . However, the sensitivity function  $\mathcal{S}_{d_2}^{R_n}$  is unbounded, that is,  $\mathcal{S}_{d_2}^{R_n}|_{j\omega} \rightarrow \infty$  as  $\omega \rightarrow \infty$ . This means that, for higher frequencies a slight error in the tuning of parameter  $d_2$  will cause a very poor compensation. To alleviate this issue a low pass filter (LPF) can be introduced as shown in Fig. 1.3. In fact in the physical implementation this filter is introduced necessarily to eliminate the noise due to the sampling process involved. This would in principle restrict the bandwidth of the controller. The proposed LPF is of the form  $1/(\tau s + 1)$ , i.e., a first order filter with pole located at  $s = -1/\tau$ . It is important to remark that the pole of the LPF should be located at frequencies well above the fundamental frequency. After introduction of the LPF, the sensitivity function for the negative repetitive scheme yields

$$\mathcal{S}_{d_2}^{R_n} = \frac{sd_2 K e^{-sd_2}}{\tau s + 1 + K e^{-sd_2}} \quad , \quad \mathcal{S}_K^{R_n} = -\frac{-K e^{-sd_2}}{\tau s + 1 + K e^{-sd_2}}$$

Notice that, after this practical modification, the sensitivity function is now bounded by  $\|\mathcal{S}_d^{R_n}\| < \frac{d_2 K}{\tau(1-K)}$ . Similar procedure to study the sensitivity of  $R_p(s; d_1, K)$  can be performed, which yields in principle similar results.

### 1.4.1 Numerical simulations of the repetitive schemes

Numerical simulations have been carried out to better visualize the response of the above controllers. First the bode plots of the negative feedback scheme with the delay line in the direct path, as in most traditional schemes, is shown in Fig 1.4 for different values of the gain  $K$ .

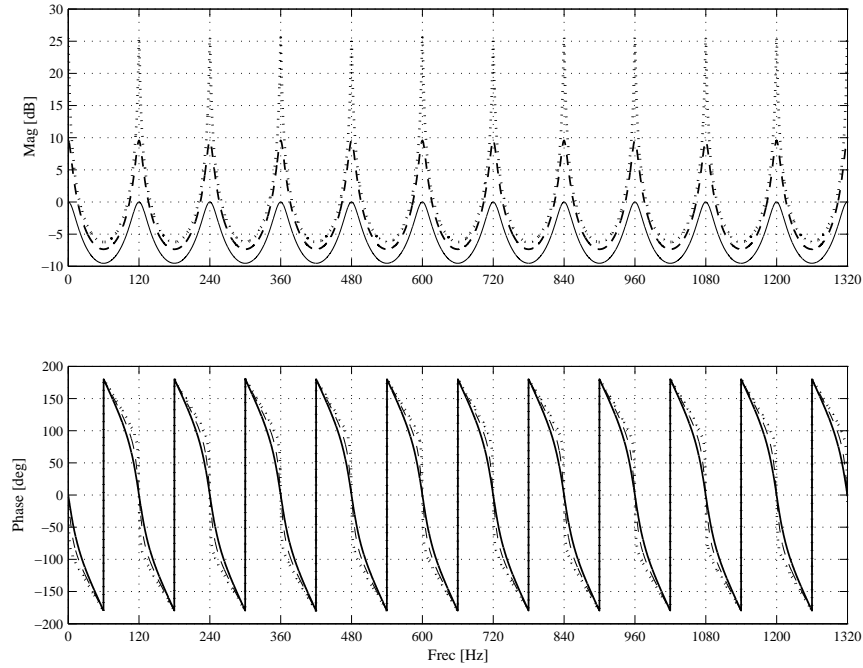


Figure 1.4: Theoretical Bode plots of traditionally repetitive scheme for different values of  $K$  (x-axis Hz, y-axis dB): (**dotted line**)  $K = 0.95$ , (**dashed line**)  $K = 0.75$ , and (**solid line**)  $K = 0.5$ .

Figures 1.5 and 1.6 show the theoretical Bode plots of  $R_p(s; d_1, K)$  and  $R_n(s; d_2, K)$  respectively. For these simulations the compensation of harmonics of 120 Hz has been considered, that is,  $f_0 = 120$  Hz ( $\omega_0 = 754$  rad/s). The corresponding delays are  $d_1 = 8.3333$  ms for the positive feedback compensator and  $d_2 = 4.1666$  ms for the negative feedback compensator. Several plots are presented for different values of  $K$  without the introduction of a LPF. It is observed that, for  $K = 0.95$  the resonant peaks reach a gain of 26.02 dB, while the valleys reach a minimum magnitude of  $-5.8$  dB. However, if the gain is reduced to  $K = 0.75$  the corresponding maximum and minimum magnitudes are 12.04 dB and  $-4.86$  dB, respectively. A further reduction to  $K = 0.5$  results in a maximum and minimum magnitudes of 6.02 dB and  $-3.52$  dB, respectively. All these values apply to both compensators. These plots show clearly that as gain  $K$  decreases, the peak amplitude is reduced while the bandwidth of each peak increases, thus increasing its robustness with respect to frequency variations.

The bode plot for both repetitive schemes  $R_n(s; d_2, K)$  and  $R_p(s; d_1, K)$  considering a LPF are shown in Figs. 1.7 and 1.8 where the corresponding delays are  $d_1 = 8.3333$  ms for the positive feedback compensator and  $d_2 = 4.1666$  ms for the negative feedback compensator, and considering in both cases a gain  $K = 0.95$ . These plots include the response without a LPF, and the responses considering a LPF with two different cutoff frequencies: 1.2 KHz and 12 kHz. Notice that, the LPF has a vanishing effect over the resonant peaks amplitude and phase shift. Moreover, the resonant peaks are not kept at the expected resonant frequencies. That is, a considerable phase shift arise, due to the introduction of the LPF.

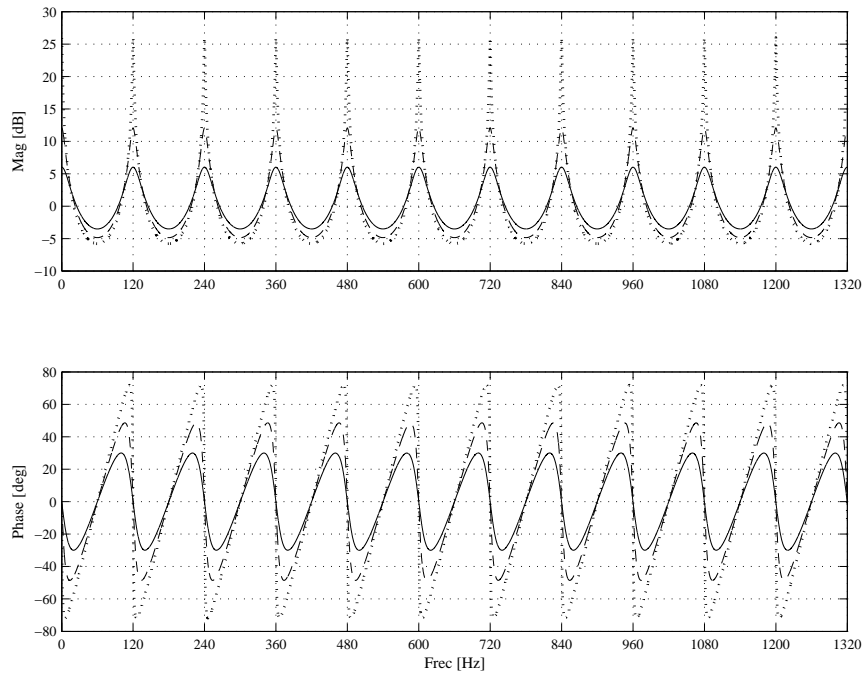


Figure 1.5: Theoretical Bode plots of  $R_p(s; d_1, K)$  different values of  $K$  (x-axis Hz, y-axis dB): (dotted line)  $K = 0.95$ , (dashed line)  $K = 0.75$ , and (solid line)  $K = 0.5$ .

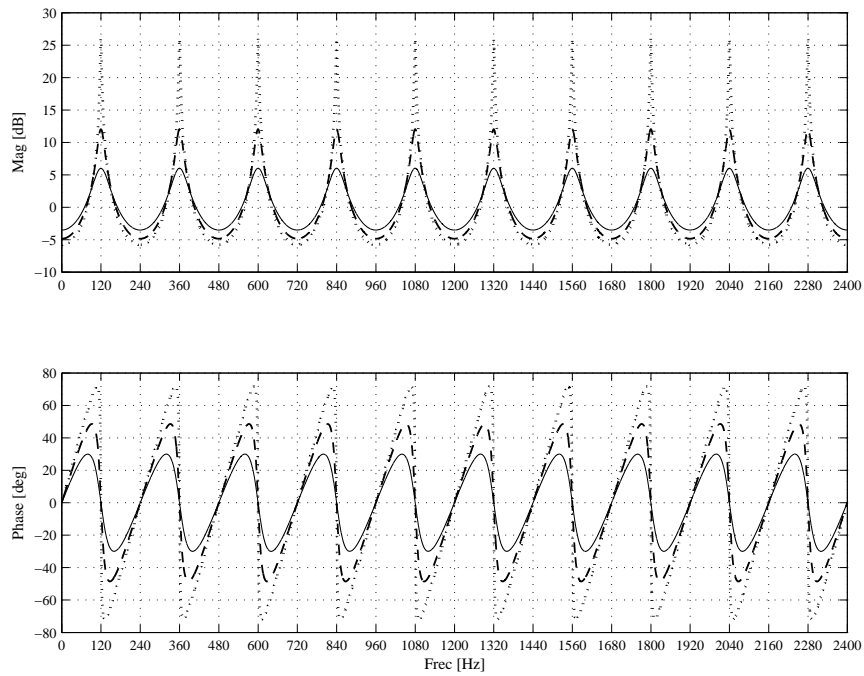


Figure 1.6: Theoretical Bode plots of  $R_n(s; d_2, K)$  different values of  $K$  (x-axis Hz, y-axis dB): (dotted line)  $K = 0.95$ , (dashed line)  $K = 0.75$ , and (solid line)  $K = 0.5$ .

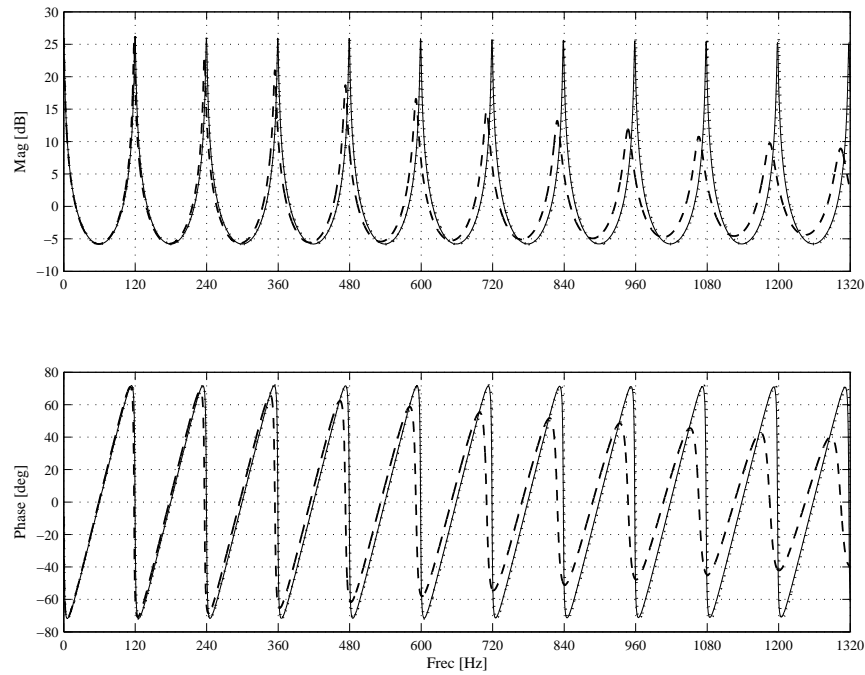


Figure 1.7: Theoretical Bode plot of  $R_p(s; d_1, K)$  for different values of  $\tau$  and  $K = 0.95$  (x-axis Hz, y-axis dB): (**dotted line**) without LPF, (**solid line**)  $\tau = 1.3263 \times 10^{-5}$  s (12 kHz), and (**dashed line**)  $\tau = 1.3263 \times 10^{-4}$  s (1.2 kHz).

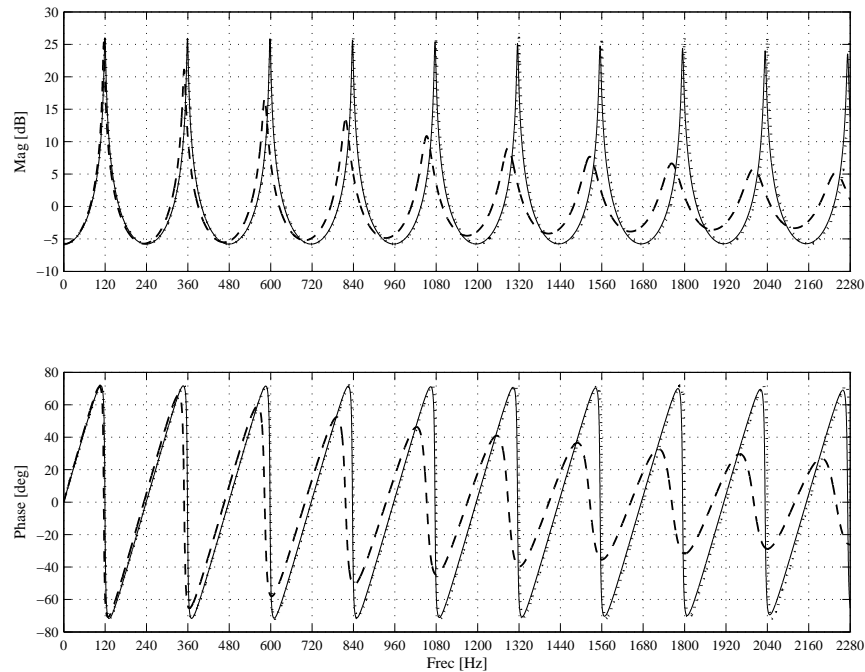


Figure 1.8: Theoretical Bode plot of  $R_n(s; d_2, K)$  for different values of  $\tau$  and  $K = 0.95$  (x-axis Hz, y-axis dB): (**dotted line**) without LPF, (**solid line**)  $\tau = 1.3263 \times 10^{-5}$  s (12 kHz), and (**dashed line**)  $\tau = 1.3263 \times 10^{-4}$  s (1.2 kHz).



Figures 1.9 and 1.10 show the amplitude response of the sensitivity function with respect to  $K$  and  $d_2$  for the negative feedback scheme, respectively. They have been evaluated at  $K = 0.95$  and  $d_2 = 4.1666$  ms, i.e., considering the compensation of harmonics of 120 Hz. The two solid lines on each plot represent the responses considering a LPF at two different cutoff frequencies, that is, at 1.2 kHz and 12 kHz. In these plots The dotted line represents the response without introduction of the LPF.

Figure 1.9 shows that  $\mathcal{S}_K^{R_n}$  in all three curves is bounded and that the maximum sensitivity peaks are presented around the resonant frequencies. Notice that, the LPF has a vanishing effect over the amplitude of  $\mathcal{S}_K^{R_n}$ .

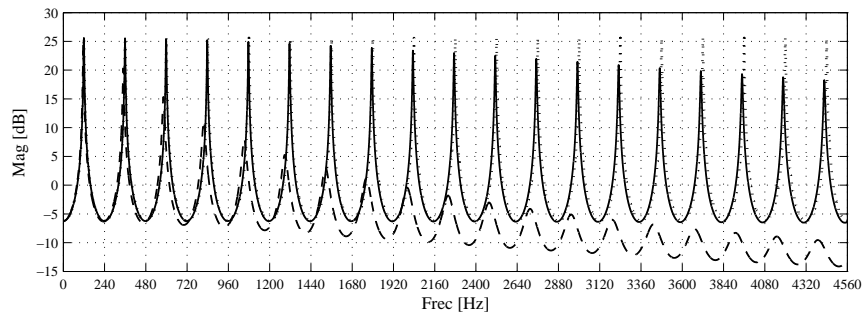


Figure 1.9: Amplitude of  $\mathcal{S}_K^{R_n}|_{s=j\omega}$  for different values of  $\tau$  and  $K = 0.95$  (x-axis Hz, y-axis dB): **(dotted line)** without LPF and with LPF for different values of  $\tau$ : **(solid line)**  $\tau = 1.3263 \times 10^{-5}$  s (12 kHz), and **(dashed line)**  $\tau = 1.3263 \times 10^{-4}$  s (1.2 kHz).

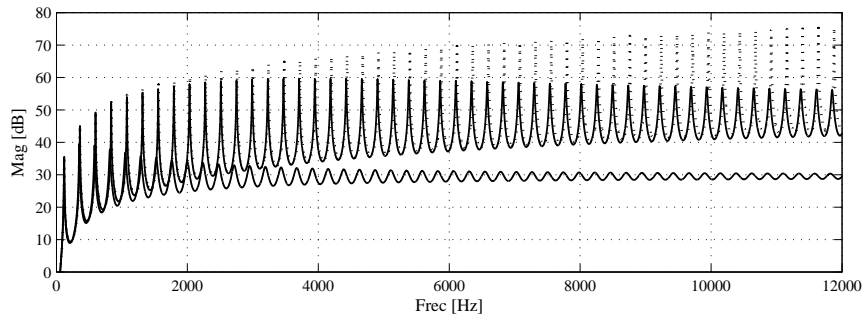


Figure 1.10: Amplitude of  $\mathcal{S}_d^{R_n}|_{s=j\omega}$  for different values of  $\tau$  and  $K = 0.95$  (x-axis Hz, y-axis dB): **(dotted line)** without LPF and with LPF for different values of  $\tau$ : **(From top to bottom in solid line)**  $\tau = 1.3263 \times 10^{-5}$  s (12 kHz), and  $\tau = 1.3263 \times 10^{-4}$  s (1.2 kHz).

Figure 1.10 shows that the effect of the LPF keeps the amplitude of  $\mathcal{S}_d^{R_n}$  bounded. However, if LPF is introduced, then the sensitivity grows indefinitely as  $\omega \rightarrow \infty$ , as shown by the dotted line plot. Notice that, for  $\tau = 1.3263 \times 10^{-4}$  s/rad (equivalent to 1.2 kHz cut off frequency ) the maximum value of the function is  $\|\mathcal{S}_d^{R_n}\| = 39.54$  dB, while for  $\tau = 1.3263 \times 10^{-5}$  s/rad

(equivalent to 12 kHz cut off frequency ) the maximum value of the function is  $\|\mathcal{S}_d^{R_n}\| = 59.61$  dB

## 1.5 Outline of the dissertation

The contents of the present dissertation has been divided into six chapters. It is important to mention that the work related to the resonant filters scheme has not been capture in the chapters as an independent study. Instead, the resonant filter controllers are presented as a previous step to the proposal of repetitive schemes. Roughly speaking, controllers design is based on a frequency domain description of the periodic disturbances. Adaptation is then introduced to cope with uncertainties in the disturbance signals and system parameters. As explained before, the adaptations are reduced to a bank of resonant filters by means of suitable rotations. These filters are tuned at the frequencies of the harmonics under compensation, hence, providing precise selective harmonic compensation despite the low control bandwidth. Finally, the repetitive schemes can replace the bank of resonant filters under certain conditions.

- ▷ In chapter 2 two repetitive compensators are developed based on the feedback-feedforward structure. The proposed repetitive feedback feedforward schemes are, in fact, modifications to the schemes presented earlier in [18], [19], [20], [34] and [36]. Those schemes were conformed by a single feedback array of a delay line in either positive, or negative feedback. The modification consist in the introduction of a feedforward path which is aimed to introduce notches in between every two consecutive resonant peaks, thus enhancing the selectivity of this type of controllers. The contribution of this chapter consists in the developed of the repetitive feedback feedforward schemes and in the observation that, after the feedforward modification, it is possible to establish an exact equivalence between the proposed repetitive schemes and a bank of resonant filters. Moreover, sufficient conditions for BIBO stability of the modified repetitive control system are derived. Finally, simple analog circuitry is presented to implement both positive and negative feedback repetitive schemes. the Main results of this chapters were presented in [3] [34] and [36]. It is important to mention that a similar structure for a discrete time passive systems was presented in [32].
- ▷ In Chapter 3, an application of the positive feedback feedforward repetitive scheme for the compensation of harmonic distortion in a dc-to-dc boost converter is presented. The introduction of the repetitive scheme is aimed to compensate the harmonic distortion in the output voltage due to the harmonic pollution present in the input voltage. An analog implementation of the repetitive based controller is proposed, which simplifies enormously the implementation. The repetitive strategy is able to cancel almost every remaining harmonic distortion component while maintaining an acceptable dynamical performance. Some of the results obtained in this chapter were presented in [37] and [38].
- ▷ A repetitive based control for a PFC is presented in Chapter 4. The control is aimed to

cope with the harmonic distortion produced by the cascade connection of a non controlled rectifier feeding a dc-dc converter, guaranteeing voltage regulation on the dc side. It is shown that the expression of the system model is represented in terms of the input current instead of the inductor current as usually done is instrumental for the developments. The controller presented here, is composed by the cascade interconnection of two loops referred as inner and outer loops. This structure is very similar to the conventional one, with the difference that a bank of resonant filters is included in the inner loop to fulfill the tracking objective. This bank of oscillators is aimed to compensate odd harmonics of the fundamental, and thus it is proposed to replace it by the negative feedback feedforward compensator. The BIBO stability analysis of the system in closed loop with such an infinite dimensional system is presented. Experimental results in a 400W prototype are shown. The main results of this chapter were appeared in [39].

- ▷ In Chapter 5, a repetitive scheme is proposed for a harmonic reducer. The latter consists of a non controlled rectifier to which an active filter is connected in parallel to compensate harmonic distortion in the line current. The active filter is built using a half-bridge topology consisting of a single branch of two switches plus a branch of two capacitors on the dc side (split dc-capacitor), thus reducing the number of switching devices. The repetitive-based controller proposed is aimed to compensate reactive power and current harmonic distortion guaranteeing a power factor close to unity. Additionally, the controller guarantees the regulation and balance of the two capacitor voltages. The contents of this chapter is based on [40]
- ▷ Chapter 6 presents a repetitive-based controller for an active filter to compensate for reactive power and current harmonic distortion in a single phase system, i.e., to guarantee a power factor close to unity. The topology selected for the active filter consists of a single phase full-bridge VSI. Adaptive controller is then proposed which can be reduced to a bank of resonant filter tuned at odd harmonics. As mentioned before, an equivalence between this control scheme and the negative feedback plus feedforward scheme is established. The bank of resonant filters is thus replaced by the repetitive scheme, which reduces considerably the implementation of the proposed controller. The proposed control scheme has been implemented in a 1.5 kVA prototype and the experimental results are presented here contents of this chapter is based on in [41].



## Chapter 2

# Repetitive schemes with feedforward modification

---

### *Summary*

In this chapter are proposed two repetitive schemes that include either positive or negative feedback plus a feedforward path, where, the delay line is placed in a common path. In these schemes, is showed that the introduction of a feedforward path to a conventional repetitive scheme, either in positive or negative feedback, considerably improves the frequency response and performance, thus providing higher gains with enhanced selectivity. In this chapter, is observed that such repetitive schemes with the feedforward modification are equivalent, under certain conditions, to a bank of resonant filters. Moreover, sufficient conditions are derived for the BIBO stability of an LTI system in closed loop with a repetitive based controller. The latter is composed of an LTI block plus a repetitive scheme, as a refinement term to guarantee harmonic distortion compensation. Finally, simple analog circuitry is presented to implement both positive and negative feedback plus feedforward repetitive schemes.

---

## 2.1 Introduction

Based on the need of compensating higher harmonics of the fundamental frequency, repetitive strategies have emerged in different engineering domains. In particular, there has been a good acceptance of such schemes in power electronics applications [28], [29], [30] and [31]. Indeed, as shown in these papers, the repetitive techniques offer some advantages over conventional solutions, which is demonstrated by the industrial applications in recent equipment.

In most of these works, the authors used a positive feedback scheme to implement the repetitive controller (see Fig. 1.1). Some of them place the delay line in the direct path and others in the feedback path. It is important to notice that a positive feedback structure has the disadvantage of

compensating for every single harmonic either odd or even, including the dc component. Moreover, depending on the position of the delay line in the structure, it may even deteriorate the phase shift.

Although the positive feedback based scheme may apparently solve the harmonics compensation problem, it may lead to more distortion in certain cases. Consider, for instance, a system where even harmonics do not exist originally (like in many power electronic systems) in this case, the positive feedback repetitive controller would try to amplify, and indeed reinject, any small noise which has components on the even frequencies. This behavior evidently has the danger of producing polluted responses with such harmonics which were not present before.

To alleviate this issue, it is proposed in [42], [33] and [34] a negative feedback scheme. It was shown that this type of structure restricts the compensation to only odd harmonics of the fundamental, and it does not have a pole in the origin. This negative feedback repetitive compensator is thus more appropriate for harmonic compensation in the power electronics field.

In this chapter are proposed two repetitive schemes with feedback and feedforward path for positive and negative schemes. With the introduction of feedforward path the selectivity of both negative and positive repetitive schemes are improved. The idea behind this modification is the introduction of zeros lying in between every two consecutive poles, the zeros in their turn will produce notches in between every two consecutive resonant peaks, therefore substituting the original valleys in the conventional repetitive schemes presented in [19], [20], [21], [32], [33] and [34]. This modification clearly improves the selective nature of the whole controller, which will in principle allow higher gains and better performance.

This chapter presents the properties of such modified compensators. The input-output proprieties of each controller are studied. Basically, expressions are obtained for the pole-zero locations, as well as, the Bode plot of the transfer function. As in the previous chapter, some practical modifications are also introduced, namely, a gain  $K$  and a LPF. An analog implementation of the controller is also presented and some experimental results are given. For this implementation, the special purpose IC MN3004 is used. Besides, the repetitive scheme is plugged in to a quite general closed loop control system. And, sufficient conditions are obtained to guarantee stability of the overall closed loop system.

The notation used in this chapter is the following.  $\mathcal{L}^{-1}[\cdot]$  means the inverse Laplace transform. A function  $g(t)$  is called an  $\mathcal{L}_2$  denoted by  $g(t) \in \mathcal{L}_2$ , if  $\int_0^\infty g(t)^2 dt < \infty$ . A rational function is said to be stable if it is analytic in the closed right-half complex plane, proper if it is finite at  $s = \infty$ , and strictly proper if it is zero at  $s = \infty$ . The set of all proper and real rational stable transfer functions are denoted by  $\mathcal{RH}_\infty$ . The infinity norm of  $G(s) \in \mathcal{RH}_\infty$  is defined by  $\|G\|_\infty \triangleq \sup_\omega \bar{\sigma} |G(j\omega)|$ .

## 2.2 Repetitive schemes plus feedforward path

The block diagrams of the repetitive compensators, with either positive and negative feedback, including the feedforward path and the pole-zero location, are shown in Fig. 2.1. In these diagrams  $Y(s)$  represents the output,  $E(s)$  is the input, and  $d_1$  and  $d_2$  are real numbers representing the delay times for the positive and negative feedback schemes, respectively<sup>1</sup>.

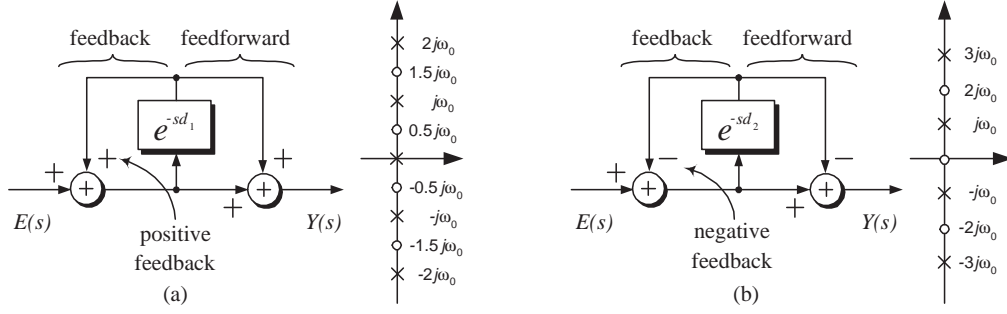


Figure 2.1: Continuous-time model and zero-pole locations of: **(a)** positive feedback (all harmonics) compensator with feedforward, and **(b)** negative feedback (odd harmonics) compensator with feedforward.

The corresponding transfer functions for both positive and negative feedback plus feedforward path repetitive compensators are given by

$$R_{pf}(s; d_1) = \frac{1 + e^{-sd_1}}{1 - e^{-sd_1}} \quad (2.1)$$

$$R_{nf}(s; d_2) = \frac{1 - e^{-sd_2}}{1 + e^{-sd_2}} \quad (2.2)$$

The poles for those representations can be found as follow, for the positive feedback plus feedforward repetitive scheme  $d_1\omega_0 = 2\pi k$  for every  $k = 0, \pm 1, \pm 2, \dots, \pm\infty$ . For the negative feedback plus feedforward repetitive scheme  $d_2\omega_0 = \pi(2k + 1)$  for every  $k = 0, \pm 1, \pm 2, \dots, \pm\infty$ . That is, for  $R_{pf}(s; d_1)$ , the poles can be found from  $e^{-sd_1} = 1$ , while for  $R_{nf}(s; d_2)$  from  $e^{-sd_2} = -1$ . According to this, for  $R_{pf}(s; d_1)$  the first pole lies at the origin and the rest of the poles lie at the integer multiples of  $\omega_0$ . Notice that, the poles for  $R_{nf}(s; d_2)$  are located at odd harmonics of  $\omega_0$  and there is not pole at the origin. Notice also that, each zero of  $R_{pf}(s; d_1)$  lies exactly in the middle point between two consecutive poles. In a similar way, the zeros for  $R_{nf}(s; d_2)$  are located in the middle points between every two consecutive poles, that is, at even harmonics of  $\omega_0$ , including a zero in the origin.

In many power electronics applications, compensation of harmonics of 120 Hz and 60 Hz are

<sup>1</sup>Subindex 1 and 2 have been used to differentiate between the positive and negative feedback feedforward schemes, respectively.

required, therefore, delays ranging from 4.166 ms to 16.666 ms should be implemented. The lower bound corresponds to the compensation of harmonics of 120 Hz using the negative feedback compensator, i.e.,  $d_2 = \pi/\omega_0 = 1/(2f_0) = 1/240 = 4.166$  ms, while the upper bound corresponds to the compensation of 60 Hz using the positive feedback compensator, i.e.,  $d_1 = 2\pi/\omega_0 = 1/f_0 = 1/60 = 16.666$  ms.

**Remark 2.1** As pointed out before, the delay times can be computed as  $d_1 = 2\pi/\omega_0 = 1/f_0$  ( $\omega_0 = 2\pi f_0$ ) for the positive feedback to compensate for every single harmonic of the fundamental frequency  $\omega_0$ , and  $d_2 = \pi/\omega_0 = 1/(2f_0)$  for the negative feedback to compensate odd harmonics of  $\omega_0$ . For instance, if compensation of harmonics of  $f_0 = 120$  Hz is required, then the corresponding delays are  $d_1 = 8.333$  ms for the positive feedback compensator and  $d_2 = 4.166$  ms for the negative feedback compensator respectively.  $\square$

Since the time delays of the block diagrams in Fig. 2.1 are computed as  $d_1 = 2\pi/\omega_0$  and  $d_2 = \pi/\omega_0$ , then the transfer function for each compensator can also be written as follows

$$\begin{aligned} R_{pf}(s; d_1) &= \frac{1 + e^{-\frac{2s\pi}{\omega_0}}}{1 - e^{-\frac{2s\pi}{\omega_0}}} = \frac{e^{\frac{s\pi}{\omega_0}} + e^{-\frac{s\pi}{\omega_0}}}{e^{\frac{s\pi}{\omega_0}} - e^{-\frac{s\pi}{\omega_0}}} \\ &= \frac{\cosh(\frac{s\pi}{\omega_0})}{\sinh(\frac{s\pi}{\omega_0})} = \frac{\prod_{k=1}^{\infty} \left( \frac{s^2}{((\frac{2k-1}{2})^2 \omega_0^2} + 1) \right)}{\frac{s\pi}{\omega_0} \prod_{k=1}^{\infty} \left( \frac{s^2}{k^2 \omega_0^2} + 1 \right)} \end{aligned} \quad (2.3)$$

$$\begin{aligned} R_{nf}(s; d_2) &= \frac{1 - e^{-\frac{s\pi}{\omega_0}}}{1 + e^{-\frac{s\pi}{\omega_0}}} = \frac{e^{\frac{s\pi}{2\omega_0}} - e^{-\frac{s\pi}{2\omega_0}}}{e^{\frac{s\pi}{2\omega_0}} + e^{-\frac{s\pi}{2\omega_0}}} \\ &= \frac{\sinh(\frac{s\pi}{2\omega_0})}{\cosh(\frac{s\pi}{2\omega_0})} = \frac{\frac{s\pi}{2\omega_0} \prod_{k=1}^{\infty} \left( \frac{s^2}{(2k)^2 \omega_0^2} + 1 \right)}{\prod_{k=1}^{\infty} \left( \frac{s^2}{(2k-1)^2 \omega_0^2} + 1 \right)} \end{aligned} \quad (2.4)$$

where it is more evident that the above compensators provide an infinite set of resonant peaks centered at given harmonic frequencies as it is observed in the pole-zero location shown in Fig. 2.1. Notice also that, due to the presence of the zeros, notches appear between every two consecutive poles.

A very interesting observation here is that the above schemes can also be expressed as infinite sums of resonant compensators as follows [43],

$$R_{pf}(s; d_1) = \coth\left(\frac{s\pi}{\omega_0}\right) = \frac{2}{s} + \frac{\omega_0}{\pi} \sum_{\ell=1}^{\infty} \frac{4s}{s^2 + (\ell\omega_0)^2} \quad (2.5)$$

$$R_{nf}(s; d_2) = \tanh\left(\frac{s\pi}{2\omega_0}\right) = \frac{\omega_0}{\pi} \sum_{\ell=1}^{\infty} \frac{4s}{s^2 + (2\ell-1)^2 \omega_0^2} \quad (2.6)$$



**Remark 2.2** The expressions given in (2.5) and (2.6) show that these schemes reproduce exactly the frequency response of an infinite bank of resonant filters tuned at selected harmonic frequencies. The above is clearly in agreement with the internal model principle [35]. Thus, it is expected that the repetitive schemes under study can provide appropriate solutions in power electronics applications for harmonic compensation.  $\square$

Summarizing, the feedforward modification introduces zeros which produce notches located in between two consecutive resonant peaks. The latter has the advantage of making the compensators more selective, in the sense that, the original overlapping (represented by the valleys) or interaction between consecutive resonant peaks is removed by the notches. This would allow, in principle, peaks of higher gains and slightly wider bandwidth, avoiding, at the same time, the excitation of harmonics located in between two consecutive peaks. For instance, the negative feedback compensator with feedforward would compensate the odd harmonics while the even harmonics would be simply ignored.

## 2.3 Practical modifications to the proposed compensator

These repetitive compensators are, however, not ready to be used in a real application yet. Notice from Fig. 2.1 that their expected Bode plots consist in a set of resonant peaks and notches which have, in theory, an infinite magnitude ( $+\infty$  dB at the resonance frequencies and  $-\infty$  dB at the notches). Moreover, notice that the resonant peaks are very narrow, therefore, not only robustness problems but also instabilities may arise. As the resonant peaks may affect unmodeled dynamics at high frequencies, and also they can amplify unavoidable noise. In order to solve these issues it is proposed to add damping to all the poles/zeros by slightly shifting them to the left of the imaginary axis [33], [34]. This shifting process is realized in the same way of the feedback scheme as follows:  $R_{pf}(s + a; d)$  and  $R_{nf}(s + a; d)$  for the positive and the negative repetitive schemes, respectively. Applying the shifting to the exponential term results in  $e^{-d(s+a)} = e^{-ad}e^{-sd}$ . Notice that, this is equivalent to multiply the exponential function by a gain factor  $K = e^{-ad}$  as shown in Fig. 2.3.

Notice that, For a gain  $K > 1$  the poles/zeros move to the right, but if  $0 < K < 1$  then they move to the left. Moreover, it is easy to show that the gain of the resonant peaks at the resonant frequencies, originally of infinite magnitude, reach a maximum magnitude of  $(1 + K)/(1 - K)$ , while the notches reach a minimum magnitude of  $(1 - K)/(1 + K)$ . Then, this pole/zero shifting process, limits the peaks amplitude of the repetitive scheme. After the shifting process, the zeros and poles of the new systems are located at  $s = -a \pm jk\omega_0$  for  $R_{pf}(s; d_1, K)$  and  $s = -a \pm j(2k + 1)\omega_0$  for  $R_{nf}(s; d_2, K)$ , as shown in Fig. 2.2.

It is also recommended in [3] to include a simple LPF in the studied schemes as shown in Fig. 2.3. The idea of this filter is to cope with the noise produced by the sampling process inherent to the physical implementation. The effect of this modification produces some slight inaccuracies as de-

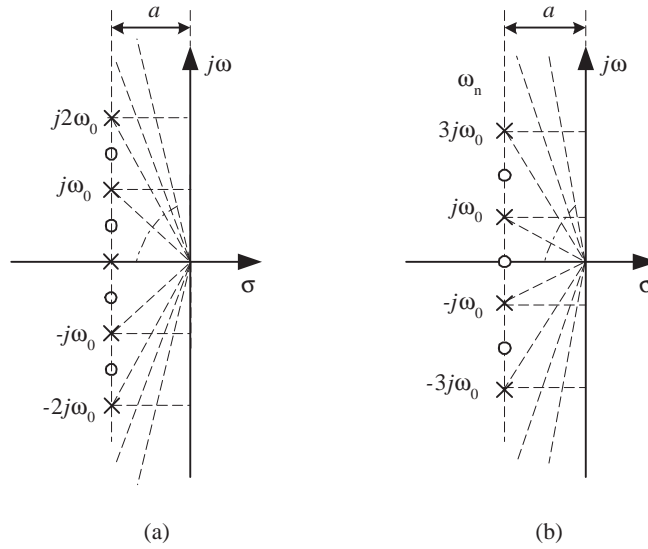


Figure 2.2: Pole-zero locations of the repetitive compensators: **(a)** positive feedback (all harmonics) compensator with feedforward, and **(b)** negative feedback (odd harmonics) compensator with feedforward.

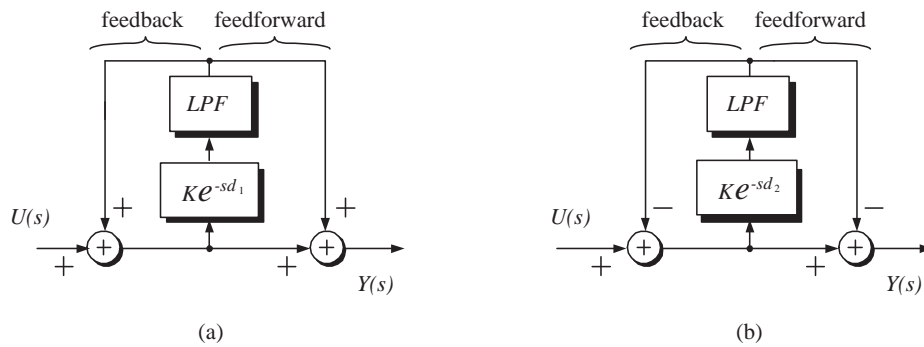


Figure 2.3: Block diagram representation of the repetitive compensators with feedforward and practical modifications: **(a)**  $R_{pf}(s; d_1, K)$ , and **(b)**  $R_{nf}(s; d_2, K)$ .

scribed next. First, resonant peaks and notches are slightly shifted with respect to the corresponding expected harmonic frequency, and second, an almost imperceptible phase shift appears at the tuned harmonic frequencies.

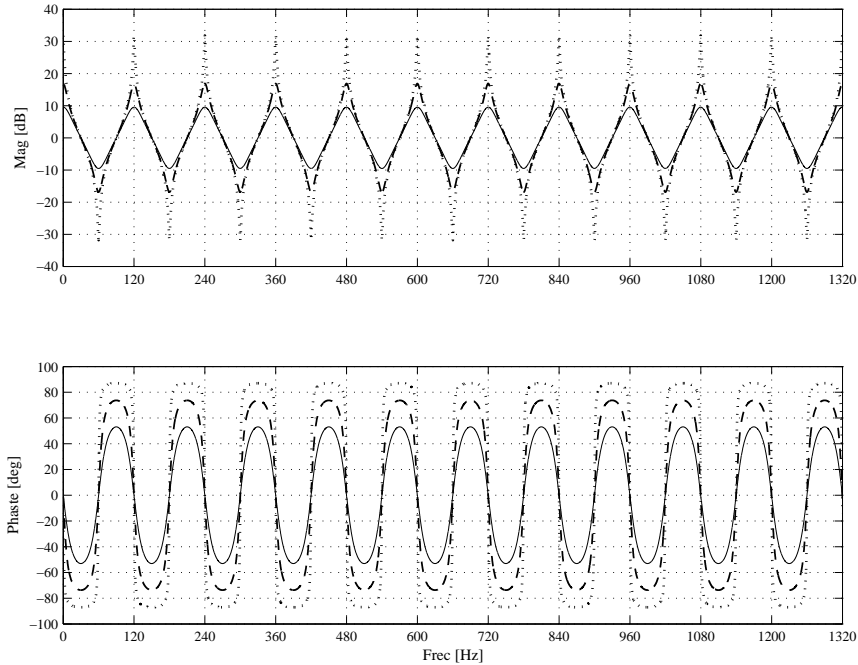


Figure 2.4: Theoretical Bode plots of  $R_{pf}(s; d_1, K)$  for different values of  $K$  (x-axis Hz, y-axis dB): (**dotted line**)  $K = 0.95$ , (**dashed line**)  $K = 0.75$ , and (**solid line**)  $K = 0.5$ .

Figures 2.4 and 2.5 show the theoretical Bode plots of  $R_{pf}(s; d_1, K)$  and  $R_{nf}(s; d_2, K)$  for the compensation of harmonics of 120 Hz and for several values of  $K$ . In this case, the delay times are fixed to  $d_1 = 8.333$  ms and  $d_2 = 4.166$  ms for the positive and negative feedback compensators, respectively. For  $K = 0.95$  the plot goes from 31.82 dB at the resonant frequencies to  $-31.82$  dB at the notches. However, if the gain is reduced to  $K = 0.75$  the corresponding maximum and minimum magnitudes reach 16.90 dB and  $-16.90$  dB, respectively. A further reduction to  $K = 0.5$  results in a maximum and minimum magnitudes of 9.54 dB and  $-9.54$  dB, respectively. All these gains are valid for both compensators. These plots show clearly that as gain  $K$  decreases, the peak amplitude is reduced. In consequence, the selective nature of the filter is decreased when the  $K$  gain decreases. It can also be interpreted as an increment in the bandwidth at resonant peaks which, in its turn, increases its robustness with respect to frequency variations. Notice that, with the introduction of gain  $K$  and without the LPF, the phase plots have the interesting feature that the phase shift is zero exactly at the resonant frequency and are bounded by 90 and -90 degrees.

The Bode plot of the compensator output with LPF for both schemes are shown in Figs. 2.6 and 2.7. The LPF is of the form  $1/(\tau s + 1)$  and the cut off frequency is located in either 1200 Hz or 12000 Hz, for each one of the repetitive schemes. These figures show three bode plots for a fixed  $K = 0.95$ , and for different values of  $\tau$  including a theoretical bode plot without LPF. Notice that,

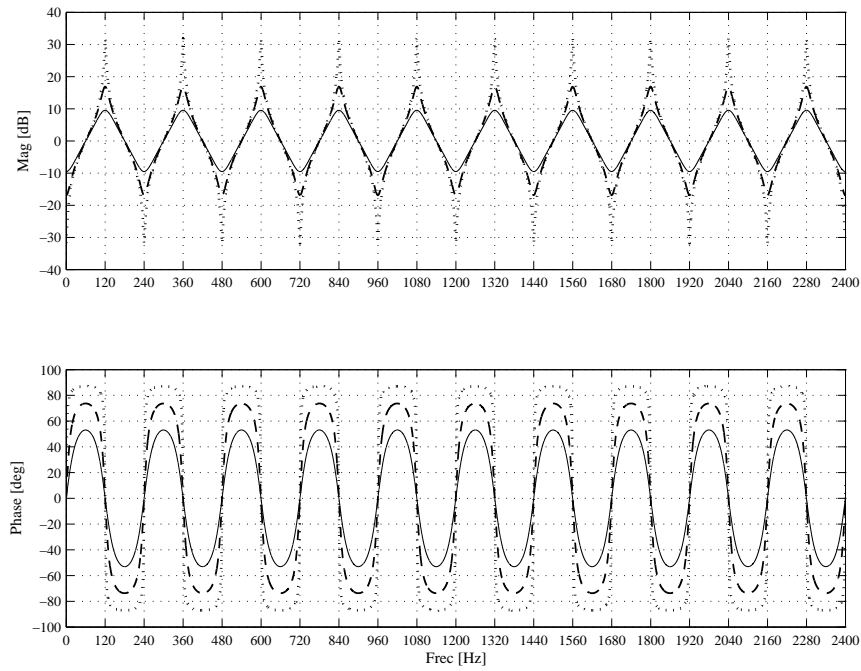


Figure 2.5: Theoretical Bode plots of  $R_{rf}(s; d_2, K)$  for different values of  $K$  (x-axis Hz, y-axis dB): (**dotted line**)  $K = 0.95$ , (**dashed line**)  $K = 0.75$ , and (**solid line**)  $K = 0.5$ .

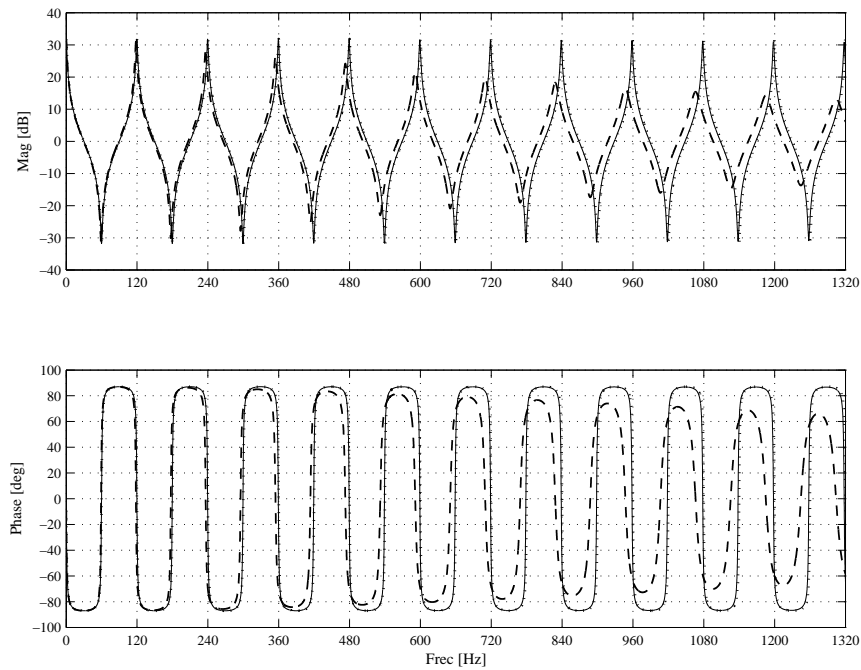


Figure 2.6: Theoretical Bode plots of  $R_{pf}(s; d_1, K)$  for different values of  $\tau$  and  $K=0.95$  (x-axis Hz, y-axis dB): (**dotted line**) without LPF, (**solid line**)  $\tau = 1.3263 \times 10^{-5}$  s (12 kHz), and (**dashed line**)  $\tau = 1.3263 \times 10^{-4}$  s (1.2 kHz).

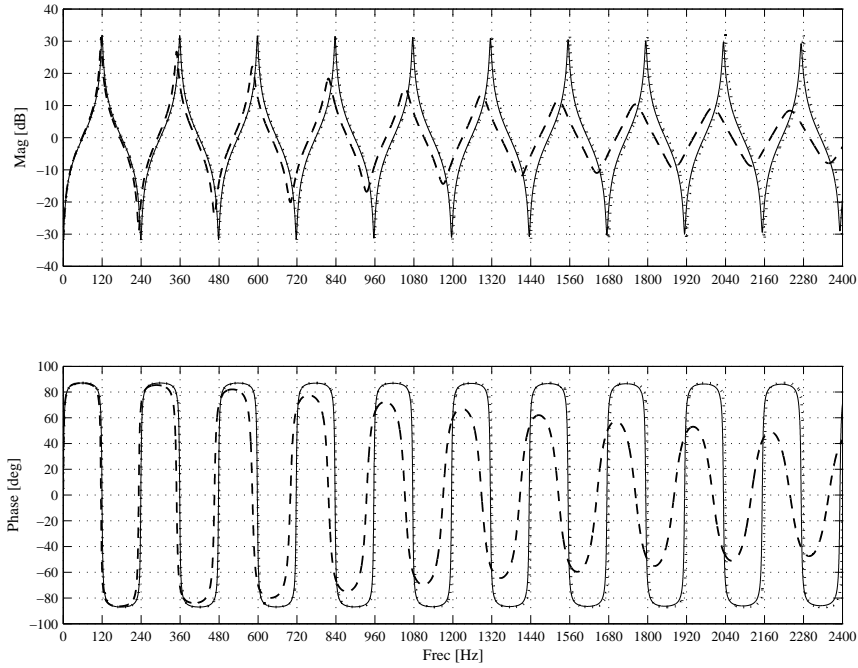


Figure 2.7: Theoretical Bode plots of  $R_{nf}(s; d_2, K)$  for different values of  $\tau$  and  $K=0.95$  (x-axis Hz, y-axis dB): (**dotted line**) without LPF, (**solid line**)  $\tau = 1.3263 \times 10^{-5}$  s (12 kHz), and (**dashed line**)  $\tau = 1.3263 \times 10^{-4}$  s (1.2 kHz).

in both schemes, the LPF affects mainly the resonant gain, and it has an effect on the phase shift at the resonant frequency.

## 2.4 Analog implementation of the repetitive schemes

The two schematics of the implemented circuits for the positive and negative feedback compensators with the feedforward modification are given in Figs. 2.8 and 2.9, respectively. The delay line appearing in both repetitive schemes is implemented using a special purpose IC MN3004. This IC, known in the music industry as a 512-stage *Bucket Brigade Delay* (BBD), allows the implementation of relatively large delays in the range of 2.5 ms to 25 ms.

The basic operation of the BBD MN3004 is described next. The MN3004 uses the auxiliary external clock MN3101, to programme the delay time. In the clock generator MN3101 the oscillation frequency  $f_{cp}$  is fixed by the array of two resistances  $R_1$ ,  $R_2$  and one capacitor  $C_1$ . This frequency is computed approximately by  $f_{cp} = 1/(2R_2C_1)$  for a fixed  $R_1$  slightly larger than  $R_2$ . The MN3101 delivers two complementary pulse signals indicated by CP1 and CP2 both oscillating at  $f_{cp}$ . Thus, since the MN3004 is a 512-stage, the resulting delay is computed as  $d = 512/(2f_{cp})$ . Notice that these analog implementations use a conventional voltage source of 15 V<sub>DC</sub> and non special sources

are required. To exhibit the delay produced by the BBD it is shown in Fig. 2.10 the AC component of the output signal (top plot) of the BBD MN3004 circuit in response to a sinusoidal signal of relatively small frequency, 30 Hz, used as input (bottom plot). Notice that the output signal has approximately a delay of 4.16 ms with respect to the input signal, which corresponds to the delay required for the negative feedback compensator. Notice also that, the output signal is polluted by a higher order harmonic due to the sampling process involved, hence, the use of a LPF is essential.

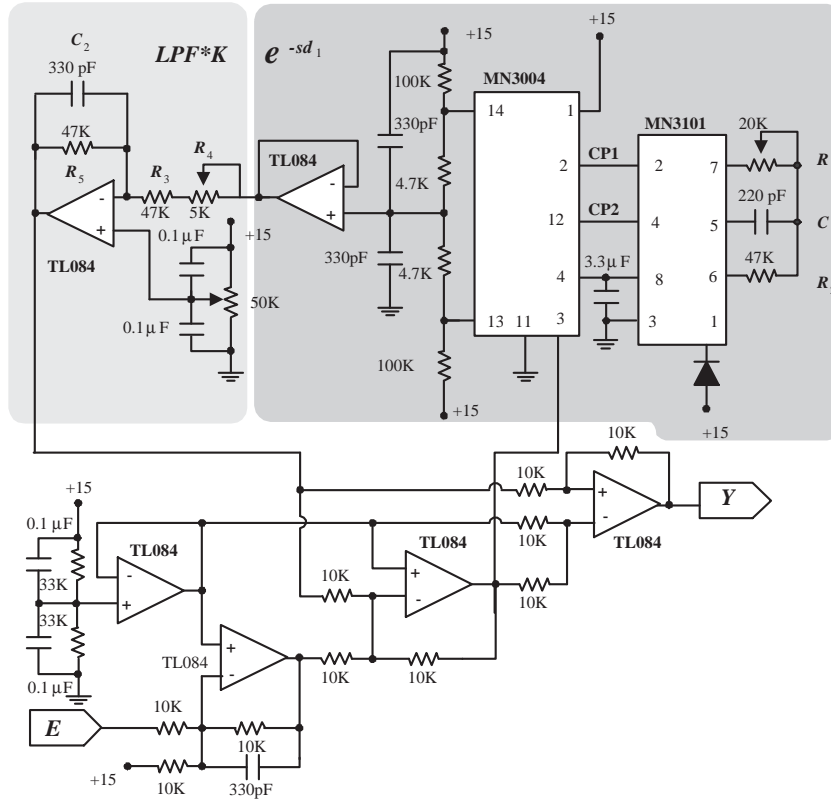


Figure 2.8: Implemented positive feedback feedforward (all harmonics) compensator.

For harmonic compensation of 120 Hz and 60 Hz delays ranging from 4.166 ms to 16.666 ms should be implemented. These delays are included in the delay times range offered by the MN3004. For the experimental tests presented here, the compensation of harmonics of 120 Hz has been chosen. Therefore, delays of  $d_1 = 8.333$  ms and  $d_2 = 4.166$  ms are implemented for the positive and negative feedback compensators, respectively.

In both circuits, the value of gain  $K$  is fixed according to  $K = R_5/(R_3 + R_4)$ . Two values for  $K$  have been tested, namely,  $K = 0.824$  and  $K = 0.955$ , which should produce, theoretically, maximum peak gains of 20.31 dB and 32.75 dB, respectively. Moreover, a simple first order LPF of the form  $1/(\tau s + 1)$  has been included where the time constant has been fixed to  $\tau = R_5 C_2 = 31 \mu\text{s}$ . The transfer function of the LPF and  $K$  in terms of the circuit elements is given by

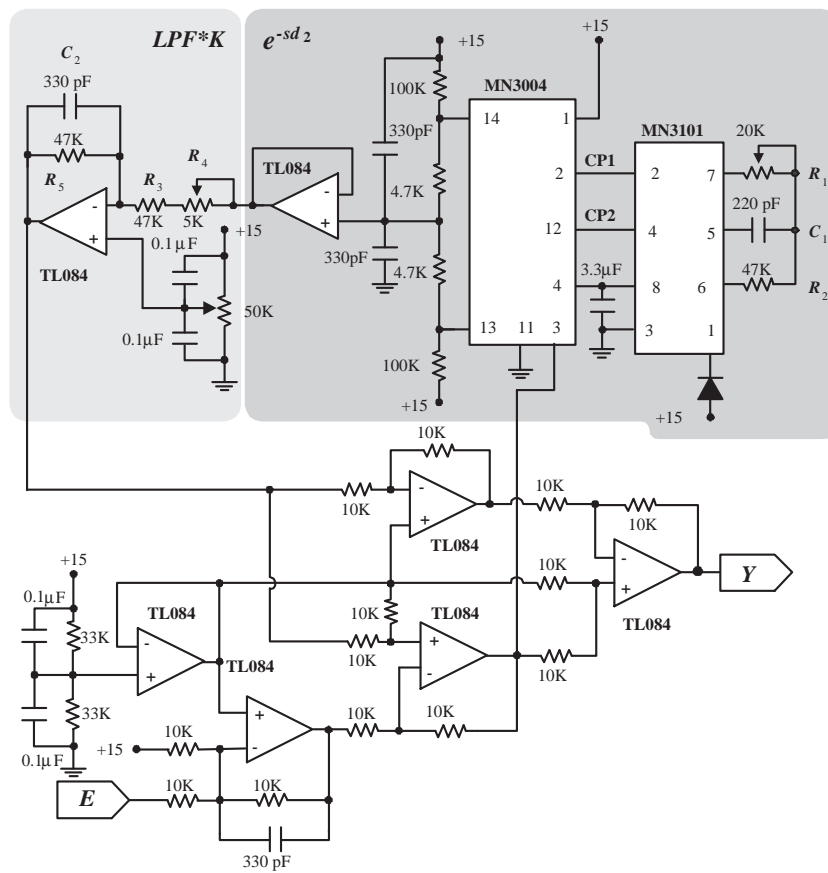


Figure 2.9: Implemented negative feedback feedforward (odd harmonics) compensator.

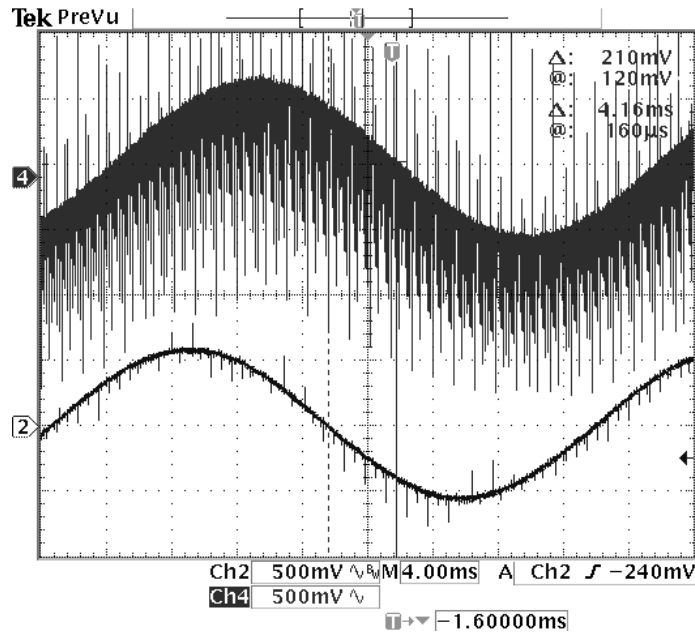


Figure 2.10: Time responses of **(Top)** output signal and **(Bottom)** input signal of the MN3004 circuit.

$$K \frac{1}{\tau s + 1} = \frac{R_5}{R_3 + R_4} \frac{1}{R_5 C_2 s + 1}$$

The experimental frequency responses of the output  $y(t)$ , for the positive and negative feedback compensators with feedforward, are shown in Figs. 2.11 and 2.12, respectively. To obtain these responses, a sinusoidal signal is obtained from a signal generator where the frequency is swept between 1 Hz to 1200 Hz during one second, and the output signal is captured in an oscilloscope operated in FFT mode. The plots show that the circuit contains peaks centered at the expected values, i.e., all harmonics of 120 Hz for the positive feedback, and odd harmonics of 120 Hz for the negative feedback.

The time responses of the controller to sinusoidal inputs are presented for the negative scheme only. Figures 2.13 and 2.15 show the responses of the negative feedback compensator circuit with and without feedforward to a pure sinusoidal signal input. Every figure shows (from top to bottom) the responses of the output  $y(t)$  with feedforward, the output  $y(t)$  without feedforward, and the input signal  $e(t)$ .

Figure 2.13 shows the responses to a sinusoidal signal input with amplitude 50 mV of peak amplitude and frequency 120 Hz, that is at the fundamental frequency. It is observed that the output  $y(t)$  with feedforward compensation reaches a peak amplitude of 2 V, which corresponds to 32 dB, bigger than the 26 dB obtained without feedforward compensation where the output reaches only 1 V of amplitude. Notice that these values are very close to those obtained theoretically.



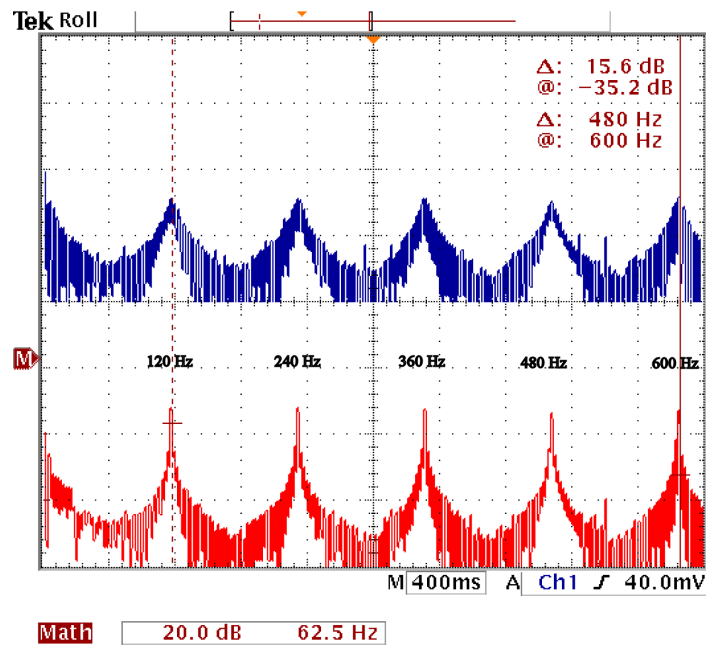


Figure 2.11: Experimental frequency response for the positive feedback compensator with feedforward (x-axis 125 Hz/div and y-axis 10 dB/div): **(top)**  $K = 0.824$ , and **(bottom)**  $K = 0.955$ .

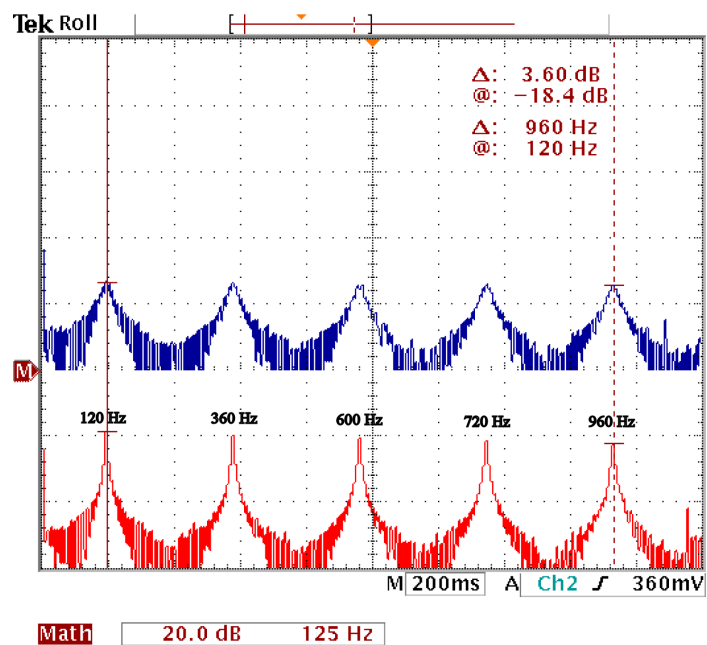


Figure 2.12: Experimental frequency response for the negative feedback compensator with feedforward (x-axis 62.5 Hz/div and y-axis 10 dB/div): **(top)**  $K = 0.824$ , and **(bottom)**  $K = 0.955$ .

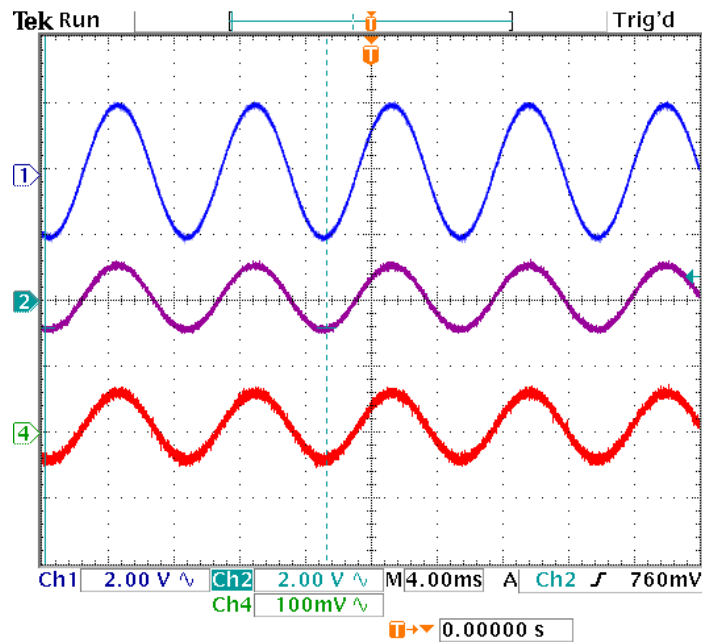


Figure 2.13: Experimental time response for the negative feedback compensator with  $K = 0.955$  to a sinusoidal signal of frequency 120 Hz and amplitude 50 mV (x-axis 4 ms/div). **(from top to bottom)**: output  $y(t)$  with feedforward (y-axis 2 V/div), output  $y(t)$  without feedforward (y-axis 2 V/div), and input  $e(t)$  (y-axis 100 mV/div).

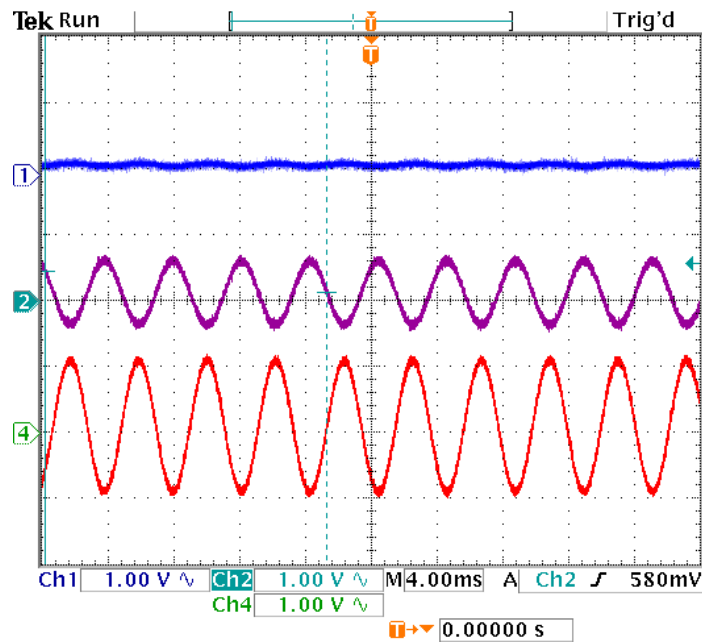


Figure 2.14: Experimental time response for the negative feedback compensator with  $K = 0.955$  to a sinusoidal signal of frequency 240 Hz and amplitude 1 V (x-axis 4 ms/div), (y-axis 1 V/div). **(from top to bottom)**: output  $y(t)$  with feedforward, output  $y(t)$  without feedforward, and input  $e(t)$ .  $K = 0.955$ .

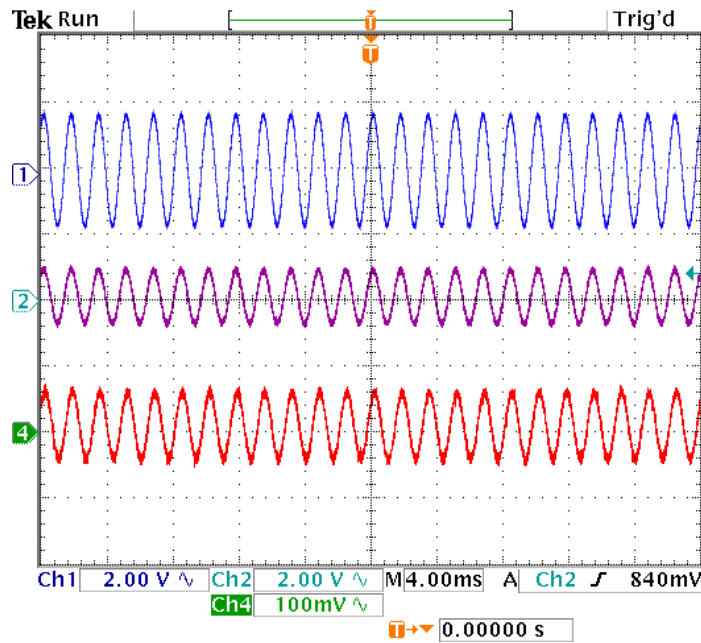


Figure 2.15: Experimental time response for the negative feedback compensator with  $K = 0.955$  to a sinusoidal signal of frequency 600 Hz and amplitude 50 mV (x-axis 4 ms/div). **(from top to bottom)**: output  $y(t)$  with feedforward (y-axis 2 V/div), output  $y(t)$  without feedforward (y-axis 2 V/div), and input  $e(t)$  (y-axis 100 mV/div).

In contrast, Fig. 2.14 shows the responses to a sinusoidal input signal with amplitude 1 V and frequency 240 Hz, that is, coinciding with the frequency of the notch located between peaks of 120 Hz and 300 Hz. As expected, the gain obtained with feedforward compensation reaches -30.45 dB approximately, the output scarcely reaches 0.03 V of amplitude. This gain is clearly much smaller compared to the -6.2 dB obtained without feedforward compensation, where the output reaches 0.5 V of amplitude. For the sake of comparison, the same vertical and horizontal scales have been preserved in this figure.

Finally, Fig. 2.15 shows the time response to a sinusoidal input signal of 50 mV and frequency 600 Hz, i.e., the 5th harmonic of 120 Hz. In this figure similar conclusions as in Fig. 2.13 can be stated, except that, as predicted by the theory, the gain suffers a slight decrease mainly due to the effect of the LPF.

## 2.5 Stability analysis of the closed-loop system

In this section sufficient conditions for BIBO stability are given in terms of *the small gain theorem* [44] for the negative and positive repetitive schemes. For this purpose, consider that either of the repetitive schemes can be connected to a closed loop system as shown in Fig. 2.16, where  $G(s)$

is a proper and, denotes the plant transfer function and  $C(s)$  an appropriate proper stable rational function representing an stabilizing compensator. That is, the studied repetitive schemes can be seen as plug in controllers used as refinement terms dedicated in particular to fulfill the harmonic compensation issue. The overall controller is thus conformed by the parallel connection of the repetitive scheme and the compensator  $C(s)$ .

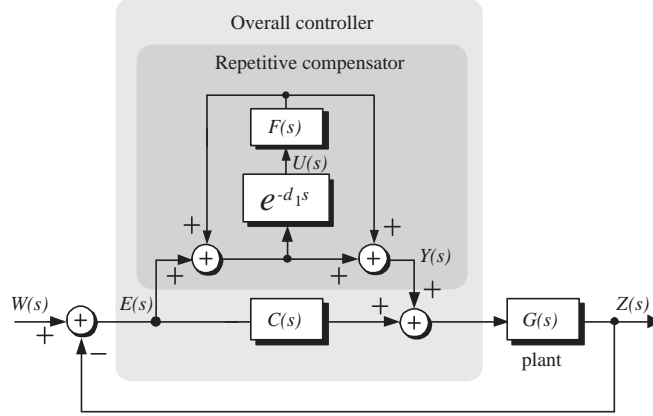


Figure 2.16: General control system with a positive feedback plus feedforward repetitive compensator.

According to Fig. 2.16 the overall repetitive controller is given by  $C(s) + (1 + F(s)e^{-sd_1}) / (1 - F(s)e^{-sd_1})$  for the compensation of all harmonics, and  $C(s) + (1 - F(s)e^{-sd_2}) / (1 + F(s)e^{-sd_2})$  for odd harmonics. The function  $F(s)$  represents the LPF affected by the proportional term  $K$  previously mentioned, i.e.,  $F(s) = K / (\tau s + 1)$  with  $0 < K < 1$ , and thus,  $\|F(s)\|_\infty < 1$ . Signals  $Z(s)$ ,  $W(s)$  and  $E(s)$  correspond to the Laplace transforms of the output  $z(t)$ , the reference  $w(t)$  and the error  $e(t)$  of the system, respectively. Recall that,  $d_1$  denote the delay time for the positive feedback compensator, and  $d_2$  denotes the delay time for the negative feedback compensator. The stability study follows a procedure similar to [21] and considers the BIBO stability for the system shown in Fig.2.16 that is, it considers only the SISO case. In what follows only the positive feedback case is treated in detail, since the negative case is treated in a very similar way. For this latter only the final results are given.

**Proposition 2.3** *The closed loop system formed by an LTI system and a repetitive-base controller shown in Fig. 2.16, is BIBO stable if the following conditions are fulfilled:*

- (i)  $F(s)$  is stable
- (ii)  $(1 + (C(s) + 1)G(s))^{-1}(C(s) + 1)G(s)$  is stable
- (iii)  $\|F(s) (1 + (C(s) + 1)G(s))^{-1} (1 + (C(s) - 1)G(s))\|_\infty < 1$

the error system  $e(t) = \mathcal{L}^{-1}[E(s)]$  is bounded and continuous for all  $w(t)$  bonded.

□

**Proof.**

For the closed-loop system shown in Fig. 2.16, that is, considering the positive feedback plus feedforward case, the following relationships are obtained

$$E(s) = W(s) - Z(s) \quad (2.7)$$

$$Z(s) = G(s)(C(s)E(s) + Y(s)) + \bar{Z}(s) \quad (2.8)$$

$$Y(s) = E(s) + 2F(s)U(s) \quad (2.9)$$

$$U(s) = e^{-sd_1}(E(s) + F(s)U(s)) + \bar{U}(s) \quad (2.10)$$

where terms  $\bar{U}(s)$  and  $\bar{Z}(s)$  correspond to the Laplace transforms of the responses to initial conditions of  $e^{-sd_1}$  and  $G(s)$ , respectively.

The idea behind the stability study followed in [21] is to transform the system to an equivalent one that isolates the delay line from the rest of the system. This remaining part of the system is then grouped as a single block, i.e., a single transfer function, which according to the *small gain theorem* [44] should have a gain less than one. However, as a delay system is involved, special attention should be given to the initial conditions.

to perform this transformation it is necessary to substitute  $Z(s)$  of (2.8) in (2.7) which yields the expression

$$(1 + C(s)G(s))E(s) = -G(s)Y(s) + (W(s) - \bar{U}(s)) \quad (2.11)$$

From (2.9) it is possible to obtain

$$U(s) = \frac{1}{2F(s)}(Y(s) - E(s)) \quad (2.12)$$

Direct substitution of (2.12) in (2.10) yields the following expression

$$Y = (1 - F(s)e^{-sd_1})^{-1}(1 + F(s)e^{-sd_1})E + 2(1 - F(s)e^{-sd_1})^{-1}F(s)\bar{U}(s) \quad (2.13)$$

From (2.11) the following expression can be obtained  $G(s)Y(s) = -(1 + C(s)G(s))E(s) + (W(s) - \bar{U}(s))$  which substituted in (2.13) yields

$$(1 + (C(s) + 1)G)E = e^{-ds}F(s)(1 + (C(s) - 1)G)E(s) + D_e(s) \quad (2.14)$$

After simple manipulations the last expression can be rewritten as

$$E(s) = e^{-sd_1} F(s) 1 + (C(s) + 1)G(s))^{-1} (1 + (C(s) - 1)G(s))E(s) + (I_n + (C(s) + 1)G(s))^{-1} D_e(s) \quad (2.15)$$

where

$$D_e(s) = (1 - F(s)e(-sd_1))(W(s) - \bar{Z}(s)) - 2F(s)G(s)\bar{U}(s) \quad (2.16)$$

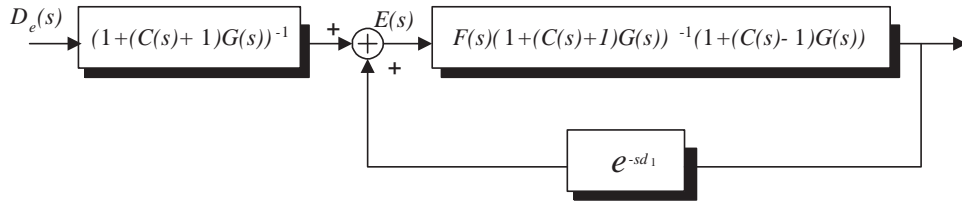


Figure 2.17: An equivalent system for the overall closed-loop system.

A block diagram of this new representation is shown in Fig. 2.17, where the delay line has been isolated.

Suppose that all elements of  $w(t)$  are bounded and continuous periodic signals of period  $d_1$ . Denote this by  $w(t) \in P(d_1)$ . This assumption yields that  $w_0(t)$  is a bounded function, where

$$w_0(t) \triangleq \mathcal{L}^{-1}[(1 - F(s)e^{-d_1s})W(s)]$$

Because  $|e^{-d_1s}| = 1$  and  $F(s)$  is a design parameter and it is chosen stable. This fact, together with (2.15) and (2.16), implies that the equivalent exogenous input  $\mathcal{L}^{-1}[(1 + (C(s) + 1)G(s))^{-1}D_e]$  is a bounded function under the assumption of the asymptotic stability of  $(1 + (C(s) + 1)G(s))^{-1}G(s)$  (condition (ii)).

BIBO stability of the overall system in Fig. 2.17 depends, on the BIBO stability of the input transfer functions, plus the BIBO stability of the close loop system shown in the Fig. 2.17. Notice that the input transfer function can be expressed as:

$$\begin{aligned} \frac{1}{1 + (C(s) + 1)G(s)} &= 1 - \frac{(C(s) + 1)G(s)}{1 + (C(s) + 1)G(s)} \\ &= 1 - \frac{C(s)G(s)}{1 + (C(s) + 1)G(s)} - \frac{G(s)}{1 + (C(s) + 1)G(s)} \end{aligned}$$

since  $(1 + (C(s) + 1)G(s))^{-1}G(s)$  is stable and  $C(s)$  is a stable controller, the input transfer function is stable. The BIBO stability of the stability closed-loop transfer function can be ensured

follow condition (iii)

$$\left\| F(s) \frac{1 + (C(s) - 1)G(s)}{1 + (C(s) + 1)G(s)} \right\|_{\infty} \leq \|F(s)\|_{\infty} \left\| \frac{1 + (C(s) - 1)G(s)}{1 + (C(s) + 1)G(s)} \right\|_{\infty} \leq 1$$

where,  $|e^{-j\omega d_1}| = 1$  and  $\|F(s)\|_{\infty} < 1$  for all  $\omega_0$ , the result follows from *the small gain theorem* [44].

▽▽▽

**Remark 2.4** In the negative feedback case, the following similar representation can be obtained following the same procedure as in the positive feedback case.

$$\begin{aligned} E(s) = & -e^{-d_2s} F(s)(1 + (C(s) + 1)G(s))^{-1}(1 + (C(s) - 1)G(s))E(s) \\ & -(1 + (C(s) + 1)G(s))^{-1}D_e(s) \end{aligned} \quad (2.17)$$

where

$$D_e(s) = -[(1 + F(s)e^{-d_2s}(W(s) - \bar{Z}(s)) + 2F(s)G(s)\bar{U}(s))] \quad (2.18)$$

which has a similar block diagram description as in Fig. 2.17, where the only difference are the signs of the feedback and the input function. Proposition 2.3, with the appropriate changes on the signs, also applies for the negative feedback case.  $\square$





## Chapter 3

# Harmonic compensation in a DC-DC boost converter

---

### *Summary*

This chapter presents the application of the positive feedback plus feedforward repetitive scheme for the control of a DC-DC Pulse Width Modulated (PWM) boost converter. The introduction of the repetitive scheme is aimed to compensate the output voltage ripple due to the harmonic distortion present in the input voltage. The structure of the proposed controller is preserved as close as possible to the conventional one, which includes outer and inner control loops. Thus, in the proposed controller, the repetitive strategy appears as a refinement term added to the inner control loop. An analog implementation of the repetitive based controller is proposed, which represents a cost effective solution in this case, and simplifies enormously the implementation. The repetitive strategy is able to cancel almost every remaining harmonic distortion component while maintaining an acceptable dynamical performance. Experimental results on a boost converter board, using a poorly regulated voltage source, are presented to assess the performance of our approach.

---

### 3.1 Introduction

The interest of the present chapter is the compensation of the output voltage ripple of a DC-DC converter, caused by periodic disturbances present in the input line voltage at frequencies in the audible range (less than 20 kHz). This issue arises in applications where the input voltage may vary on a wide range, such as in power factor correctors (PFC), where the input voltage is mainly polluted by a  $2^{nd}$  harmonic component of the line voltage (due to the rectification process in PFC stage) which is propagated in the form of ripple in the output voltage. This is an issue of vital importance when a high quality DC voltage is demanded, and in addition, it opens the possibility of reducing

the output capacitor, as pointed out in [45] and [46]. In [47], [48] and [49], the authors show that, by simply feedforwarding the input voltage signal, the harmonic distortion appearing in the output voltage may be reduced. Active ripple filtering presented in [45] and [46] is another technique addressing the problem of reducing the output voltage ripple due to switching. In [50], the authors present an extensive and very illustrative analysis of an integral-lead controller for a boost converter. It is shown that this voltage-mode controller significantly improves the audio-susceptibility curve.

As mentioned in previous chapters, repetitive control arises as a practical solution to the tracking or rejection of periodic signals, and it is based in the well-known internal model principle. This fact is the basis of the controller proposed here as explained next. The internal model principle states that the controlled output can track a class of reference commands without a steady error if the generator (or the model) of the reference is included in the stable closed-loop system. It is well known that the generator of a sinusoidal signal, i.e., containing only one harmonic component, is a harmonic oscillator, in other words, a resonant filter. Therefore, following this idea, if a periodic signal has an infinite Fourier series (of harmonic components), then an infinite number of harmonic oscillators are required to track or reject such a periodic signal. Fortunately, the repetitive control approach can be used to fulfill this issue.

This chapter proposes an alternative implementation of the controller presented in [38] and [51]. That controller was very close to the conventional one, i.e., it was composed by an inner and an outer loop, and included a bank of resonant filters aimed to reduce the output voltage ripple. That controller was obtained following adaptive techniques which gave, in principle, a nonlinear controller, however, the authors showed that after some transformations, basically rotations, the adaptive part of the controller became a bank of resonant filters tuned at the frequencies of the harmonics to be compensated, i.e., at the higher harmonics of 120 Hz which is the fundamental frequency of the disturbance to reject. It is shown here that the proposed repetitive scheme, i.e., a positive feedback plus a feedforward path using a delay line, offers a very close behavior to that bank of resonant filters; therefore, they can be replaced by the simpler proposed repetitive controller. The idea behind the controller proposed here is thus, to substitute such a bank of resonant filters in [38] by a repetitive scheme. In particular the positive feedback plus feedforward repetitive scheme has been selected for the compensation of every single harmonic of 120 Hz. The overall repetitive-based controller has been implemented using analog devices which offers a cost effective and rapid solution. The boost converter is fed by a poorly regulated voltage source polluted by harmonics of 120 Hz, i.e., 120 Hz, 240 Hz, 360 Hz, and so on. Finally, some experimental results are shown to assess the performance of the proposed controller.

## 3.2 Problem formulation

A circuit of the boost converter is shown in Fig. 3.1. In this circuit, the equivalent series resistances (ESR) of inductor, capacitor and Mosfet, as well as the voltage drop in the diode have been neglected

without loss of generality.

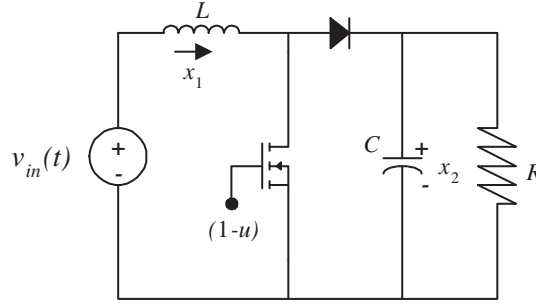


Figure 3.1: Boost converter circuit.

The system dynamics of the boost converter shown in Fig. 3.1 are described by the following expressions

$$L\dot{x}_1 = -ux_2 + v_{in} \quad (3.1)$$

$$C\dot{x}_2 = ux_1 - \frac{x_2}{R} \quad (3.2)$$

where  $x_1$  is the inductor current,  $x_2$  is the capacitor voltage,  $v_{in}$  represents the voltage source (this signal is addressed indistinctly as input voltage or voltage source along the chapter),  $L$  is the inductance,  $C$  is the capacitance and  $R$  is the load resistance. We assume that parameters  $L$ ,  $C$  and  $R$  are unknown positive constants. In the switching model, i.e.,  $u \in \{0, 1\}$ , the value  $u = 0$  corresponds to the situation where the power semiconductor is conducting, while  $u = 1$  corresponds to the case where the power semiconductor is disconnected, and thus the diode is conducting. In the average model [52], it is assumed a sufficiently large switching frequency, hence,  $u$  represents the slew rate of a PWM signal feeding the gate of the boost converter, i.e.,  $u = (1 - D)$  where  $D$  is the duty ratio.

It is assumed that the input voltage  $v_{in}$ , polluted by higher order harmonics of the fundamental frequency  $\omega_0$ , can be represented as:

$$v_{in}(t) = E + \sum_{m \in M} \boldsymbol{\rho}_m^T \mathbf{V}_{s,m} \quad (3.3)$$

$$\boldsymbol{\rho}_m = \begin{bmatrix} \cos(m\omega_0 t) \\ \sin(m\omega_0 t) \end{bmatrix}, \quad \mathbf{V}_{s,m} = \begin{bmatrix} V_{s,m}^r \\ V_{s,m}^i \end{bmatrix}$$

where  $\boldsymbol{\rho}_m$  represents a unitary vector rotating at a frequency  $m\omega_0$  in counterclockwise direction,  $V_{s,m}^r$  and  $V_{s,m}^i$  are the real and imaginary parts of the phasor  $\mathbf{V}_{s,m}$ , and,  $m$  is the set of indices of the harmonic components contained in  $v_{in}$ .

The *control objective* consists in the regulation of the output capacitor voltage  $x_2$  towards a constant reference  $V_d$  despite of the harmonic distortion in the input voltage, that is, the proposed controller should be able to reject harmonic voltage disturbances existent in the source voltage. It is well known that, due to the nonminimum phase nature of this converter, it is preferable to indirectly control the capacitor voltage by first regulating the inductor current towards a constant reference  $I_d$  (this scheme is referred in literature as current or indirect control [53]). This imperfection makes more challenging finding the solution to the harmonic rejection issue. A solution to this problem is obtained by forcing the inductor current to track a harmonic distorted reference instead of the usual constant signal. The idea behind this approach is that, by distorting the inductor current reference, an extra control input is incorporated which allows compensation of harmonics in the capacitor voltage side.

In [38], two stable and robust controllers were proposed for the solution of the problem stated above, a first one that required the measurement of  $v_{in}$  (usually referred as the feedforward term) and a second solution that did not require this signal. In this chapter only the latter is considered, which is specially useful in case that the sensed input voltage signal is lost due to a failure, or simply to eliminate the voltage sensor. In any case, the controller guaranteed a continuous and correct functioning. The idea behind that controller is that the harmonic distortion in the capacitor voltage can be compensated by introducing a certain harmonic distortion in the inductor reference current, that is, by appropriately distorting the inductor reference current. This distortion represents in fact, an extra input which is inserted to allow compensation of harmonics in the capacitor voltage side. As usual in control design for DC-DC converters, the decoupling assumption was appealed, and hence, the final expression of the controller included inner and outer loops. These two loops of the controller proposed in [38] are described next for completeness.

The *inner control loop* was composed by a proportional plus integral term operating on the inductor current error, and the bank of resonant filters operating on the voltage error. The resonant filters appeared as a refinement term, they introduced notches in the audio-susceptibility curve, which were tuned at the harmonics under compensation. Therefore, the bank of resonant filters was able to cancel only a selected set of harmonics while preserving output voltage regulation. The resulting control signal is given by

$$u = \left( k_{p2} + \frac{k_{i2}}{s} \right) \tilde{x}_1 + \sum_{k \in \mathcal{H}} \frac{\gamma_k s}{s^2 + k^2 \omega_0^2} \tilde{x}_2 \quad (3.4)$$

where  $\tilde{x}_1 \triangleq (x_1 - I_d)$ ,  $\tilde{x}_2 \triangleq (x_2 - V_d)$ ,  $k_{p2}$  and  $k_{i2}$  are positive design parameters, the proportional and integral gains, respectively;  $\gamma_k$  is the  $k^{th}$  gain of the resonant filter, with  $k \in \mathcal{H}$  and  $\mathcal{H}$  the selected set of harmonics to compensate, that is, a certain number of odd and even multiples of the fundamental frequency.  $I_d$  is a scalar computed in the outer loop, which corresponds to the usual reference current in the current loop of the conventional controller, and should be driven as close as possible to a constant.

The *outer voltage loop* was formed by a proportional term of limited bandwidth plus an integral

term, both operating on the capacitor voltage error. In this controller, the usual proportional term has been affected by a LPF to prevent the reinjection of further harmonics into the control loop due to the remanent harmonic content in the capacitor voltage.

$$I_d = -\frac{k_p}{\tau s + 1} \tilde{x}_2 - \frac{k_i}{s} \tilde{x}_2 \quad (3.5)$$

where  $k_p$  and  $k_i$  are positive design parameters, the proportional and integral gains, respectively, and  $\tau$  is the time constant of the LPF. A block diagram of controller (3.4)-(3.5) is shown in Fig. 3.2.

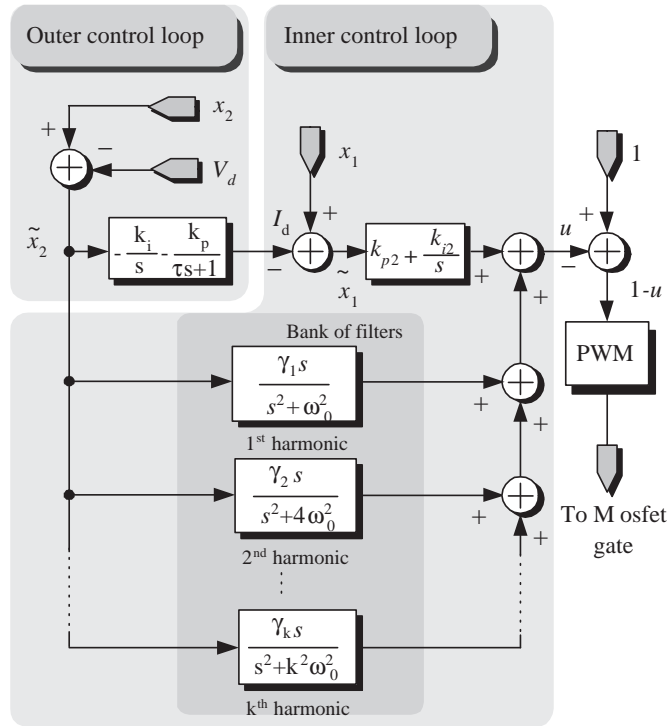


Figure 3.2: Block diagram of the adaptive controller using a bank of resonant filters for the compensation of the output voltage harmonic distortion.

### 3.3 Repetitive-based controller

As even and odd harmonics of the fundamental frequency are considered for compensation, then it is proposed to use the positive feedback plus feedforward repetitive scheme as is shown in Fig. 2.1 (a). In what follows, it is shown that the proposed repetitive scheme, under certain modifications, approaches very close the behavior of the bank of resonant filters previously mentioned. This repetitive scheme, analyzed in Chapter 2, Section 2.2, introduces an infinite number of poles in every single multiple of the fundamental frequency, and thus it is able to compensate for all harmonics. As also explained before, the feedforward path for this scheme improves the selective nature of the controller as it creates an infinite number of zeros located between two consecutive poles. The

transfer function for this scheme is given by

$$R_{pf}(s; d_1) = \frac{1 + e^{-sd_1}}{1 - e^{-sd_1}}$$

As explained in Chapter 2 the transfer function  $R_{pf}(s; d_1)$  has an equivalent expression in terms of an infinite sum of resonant filters tuned at every single harmonic of the fundamental frequency  $\omega_0$ , as expressed in (2.5):

$$R_{pf}(s; d_1) = \frac{2}{s} + \frac{\omega_0}{\pi} \sum_{\ell=1}^{\infty} \frac{4s}{s^2 + (\ell\omega_0)^2}.$$

That is, the repetitive scheme is equivalent to an infinite bank of resonant filters, all connected in parallel, and tuned at every single harmonic of the fundamental.

Clearly some differences arise with respect to the original bank of resonant filters in (3.4) out of which are enumerate next:

- i) Existence of an “extra” integrator.
- ii) The gains are now fixed to  $4/d_1$  for all filters, instead of the independent  $\gamma_k$  for every  $k^{th}$  filter.
- (iii) All harmonics are considered for compensation, that is, there is no more the possibility to compensate for a selected group of them.

It is then clear that, to make the repetitive scheme (2.5) more suitable in the present application it is necessary to make some modifications, as is described next.

In Chapter 2, Section 2.3 some practical modifications are recommended to make this repetitive scheme usable. They consist in the introduction of a gain  $K$  and a LPF with the aim of restricting the gain of the resonant peaks and notches, as well as to limit the bandwidth of the repetitive scheme. Moreover, it was shown that they improve the robustness with respect to frequency variations. In this work a first order LPF of the form  $1/(\tau_1 s + 1)$  is used, where  $1/\tau_1$  is a positive design parameter representing the cut off frequency.

As previously mentioned, the positive feedback compensator contains a pole in the origin (see Fig. 2.1 or eq. (2.1)), i.e., an integrator, which is in most cases undesirable because it may lead to saturation problems and instabilities. To reduce its effect, it is common practice to include at the input of the repetitive scheme a derivative term of limited bandwidth of the form  $H(s) = \tau_2 s / (\tau_2 s + 1)$ , referred here as High Pass Filter (HPF), where  $1/\tau_2$  is a positive design parameter representing the cut off frequency. However, for practical reasons it was more convenient to insert this derivative term inside the loop as shown in Fig. 3.4. This simple modification avoids possible

saturations inside the loop due to the unavoidable offsets in the analog circuitry, besides cancelling the integral effect.

As a consequence of all these modifications, two side effects appear: first, the peaks of resonance and notches are slightly shifted with respect to the corresponding harmonic frequencies, and second, an almost imperceptible phase shift appears at the tuned harmonic frequencies. As is observed in Fig 3.3 the resonant gain at 0 dB can be minimized but a phase shift can be appeared at the first resonant peak.

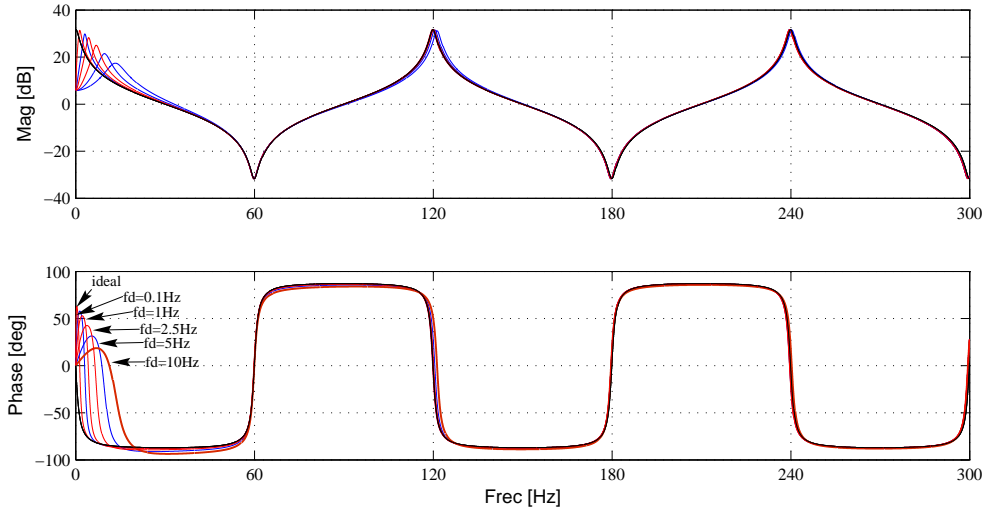


Figure 3.3: Frequency response of the positive feedback feedforward repetitive scheme, with low pass filter with cutoff frequency  $f = 12$  kHz and, different values of cutoff frequency of derivative term of limited bandwidth

The block diagram of the proposed repetitive-based controller is shown in Fig. 3.4. Notice that, the bank of resonant filters has been replaced by the proposed repetitive scheme. Moreover, a gain  $k_r$  has been included to adjust the gain produced in the peaks. Gains  $K$  and  $k_r$  should be combined to obtain the appropriate frequency response.

The investigation of the stability of the proposed scheme appeals to the decoupling assumption, out of which the inductor current dynamics and the capacitor voltage dynamics can be treated separately. Moreover, as the repetitive scheme is intended to deal with the harmonic distortion of the capacitor voltage, then the error dynamics of the harmonic part of the capacitor voltage is considered for this analysis only. The latter is given, according to [38], as

$$C\dot{x}_{2h} = \phi_{\omega_0}(t) - \sum_k \psi_{1,k} - \frac{x_{2h}}{R} \quad (3.6)$$

$$\dot{\psi}_{1,k} = \gamma_k x_{2h} - k\omega_0 \psi_{2,k} \quad \forall k \in \mathcal{H} \quad (3.7)$$

$$\dot{\psi}_{2,k} = k\omega_0 \psi_{1,k} \quad (3.8)$$

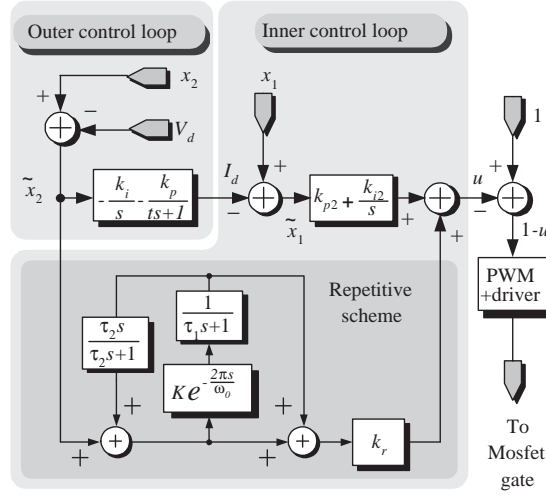


Figure 3.4: Block diagram of the proposed repetitive-based controller.

where  $x_{2h}$  represents the harmonic part of the capacitor voltage;  $\psi_{1,k}$ ,  $\psi_{2,k}$  are the states of a harmonic oscillator;  $\phi_{\omega_0}(t)$  represents the ripple, that is, a periodic disturbance with period  $2\pi/\omega_0$ , and  $\gamma_k$  ( $\forall k \in \mathcal{H}$ ) are positive design constants. Notice that, (3.7)-(3.8) form a bank of harmonic oscillators, that is, a bank resonant filters each tuned at the  $k^{th}$  harmonic component.

It is shown next that the stability property holds after replacing the bank of resonant filters by the repetitive scheme, as shown in the block diagram of Fig. 3.5. The same procedure as in Chapter 2, Section 2.5, is followed to find stability conditions of the closed loop system by appealing the *small gain theorem*. Towards this end, the delay block  $e^{-d_1s}$  is isolated and the remaining part of the system dynamics is concentrated in a single transfer function as described next.

### 3.3.1 Stability analysis

This subsection develops sufficient conditions for the BIBO stability of loop-closed repetitive-base control system described previously for the DC-DC boost converter.

**Proposition 3.1** *The output  $x_{2h}(t)$  of system in Fig. 3.4 is bounded for a bounded input  $\phi(\omega_0)(t)$ , if the following conditions are fulfilled:*

- (i)  $F(s)$  and  $H(s)$  are stable
- (ii)  $(1 + k_r G(s))^{-1} G(s)$  are stable
- (iii)  $\|F(s)(1 + k_r G(s))^{-1}(H(s) - k_r G(s))\|_{\infty} < 1$

□



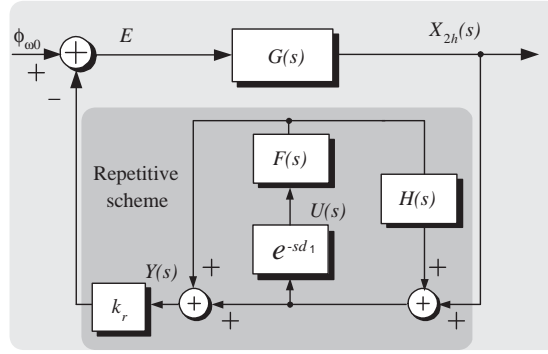


Figure 3.5: Block diagram of the output voltage error dynamics in closed loop with the repetitive scheme.

**Proof.** From the block diagram in Fig. 3.5 the following expressions are derived

$$X_{2h}(s) = G(s)E(s) + \bar{X}_{2h}(s) \quad (3.9)$$

$$E(s) = \phi_{\omega_0}(s) - k_r Y(s) \quad (3.10)$$

$$Y(s) = X_{2h}(s) + F(s)U(s) + F(s)H(s)U(s) \quad (3.11)$$

$$U(s) = e^{-sd_1}(X_{2h}(s) + H(s)F(s)U(s)) + \bar{U}(s) \quad (3.12)$$

where terms  $\bar{U}(s)$  and  $\bar{X}_{2h}(s)$  correspond to the Laplace transforms of the responses for initial conditions of  $e^{-sd_1}$  and  $G(s)$ , respectively. Notice that, the plant is given by  $G(s) = R/(RCs + 1)$  and the filter is defined as  $F(s) = K/(\tau_1 s + 1)$ , where the constant  $K$  is included to add damping to all the poles/zeros by slightly shifting them to the left of the imaginary axis, as described in Chapter 2 and 3 the HPF is of the form  $H(s) = \tau_2 s/(\tau_2 s + 1)$ .

Simple manipulations of (3.9)-(3.12) yield the following expression

$$(1 + k_r G(s))X_{2h}(s) = e^{-d_1 s} F(s)(H(s) - k_r G(s))X_{2h}(s) + D_e(s) \quad (3.13)$$

Out of which

$$X_{2h}(s) = e^{-d_1 s} F(s)(1 + k_r G(s))^{-1}(H(s) - k_r G(s))X_{2h}(s) + (1 + k_r G(s))^{-1} D_e(s) \quad (3.14)$$

where it has been defined

$$D_e(s) = (1 - H(s)F(s)e^{-sd_1})(G(s)\phi_{\omega_0}(s) + \bar{X}_{2h}) - k_r F(s)H(s)G(s)\bar{U}(s) \quad (3.15)$$

A block diagram of this new representation is shown in Fig. 3.6. Notice that, this block diagram has the same structure as the one shown in Fig.2.17.

First it is necessary to state that the input (3.15) of the equivalent system is bounded. This based on the fact that all elements of  $\phi_{\omega_0}(t)$  are bounded and periodic signals. this assumption implies that  $\phi_{0\omega_0}(t)$  the first part of (3.15) is a bounded function, where

$$\phi_{0\omega_0}(t) \triangleq \mathcal{L}^{-1}[(1 - H(s)F(s)e^{-sd_1})G(s)\phi_{\omega_0}(s)]$$

because  $|e^{-j\omega_0 d_1}| = 1$  for all  $\omega_0$  and  $F(s) = K/(\tau_1 s + 1)$ ,  $H(s) = \tau_2 s/(\tau_2 s + 1)$  are a design parameters and they are chosen stables. Notice that the exogenous input is affected by a block transfer function  $(1 + k_r G(s))^{-1}$ , then, under the assumption of the amitotic stability of  $(1 + k_r G(s))^{-1}G(s)$  (condition (ii)), the exogenous input  $\mathcal{L}^{-1}[(1 + k_r G(s))^{-1}D_e(s)]$  is bounded, then the input  $D_e(t)$  is bounded.

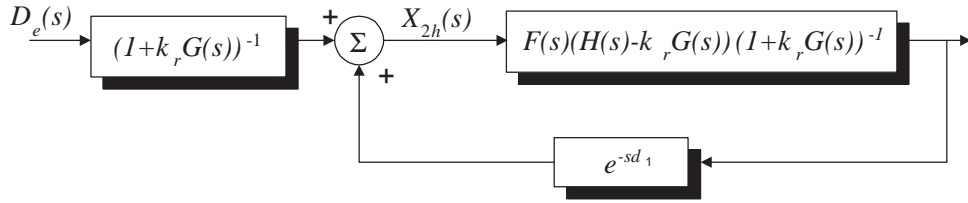


Figure 3.6: Block diagram of the proposed repetitive-based controller.

Moreover, if the exogenous input is  $D_e$  bounded, BIBO stability of the overall system depends on the BIBO stability of the input transfer function and the BIBO stability of the close loop system shown in Fig 3.6. Since,  $(1 + k_r G(s))^{-1} = 1 - (1 + k_r G(s))^{-1}G(s)$ , by condition (ii) the input transfer function is stable. To prove the bounded stability of the close loop system of the Fig. 3.6 formed by  $F(s)(1 + k_r G(s))^{-1}(H(s) - k_r G(s))$  and  $e^{sd_1}$ , it is only necessary to fulfill the condition (iii), since  $|e^{sd_1}| = 1$ , the result follows from *the small gain theorem* [44]. Consider that the norm of  $F(s)$  is bounded by  $\|F(s)\|_\infty < 1$ , where  $F(s) = K * \tilde{F}(s)$  and  $\tilde{F}(s) = 1/\tau_1 s + 1$ . Therefore, condition (iii) can be reduced to

$$\left\| \frac{H(s) - k_r G(s)}{(1 + k_r G(s))} \right\|_\infty \leq 1 \quad (3.16)$$

which holds based on the fact that

$$K \left\| \frac{1}{\tau_1 s + 1} \frac{H(s) - k_r G(s)}{(1 + k_r G(s))} \right\|_\infty < K \left\| \frac{1}{\tau_1 s + 1} \right\|_\infty \left\| \frac{H(s) - k_r G(s)}{(1 + k_r G(s))} \right\|_\infty < 1$$

and considered that  $K$  can take values between  $0 < K < 1$ .

▽▽▽

Moreover, to show that the BIBO stability condition (3.16) is fulfilled for the experimental values used in CD-CD boost converter, the following Bode plot are shown.

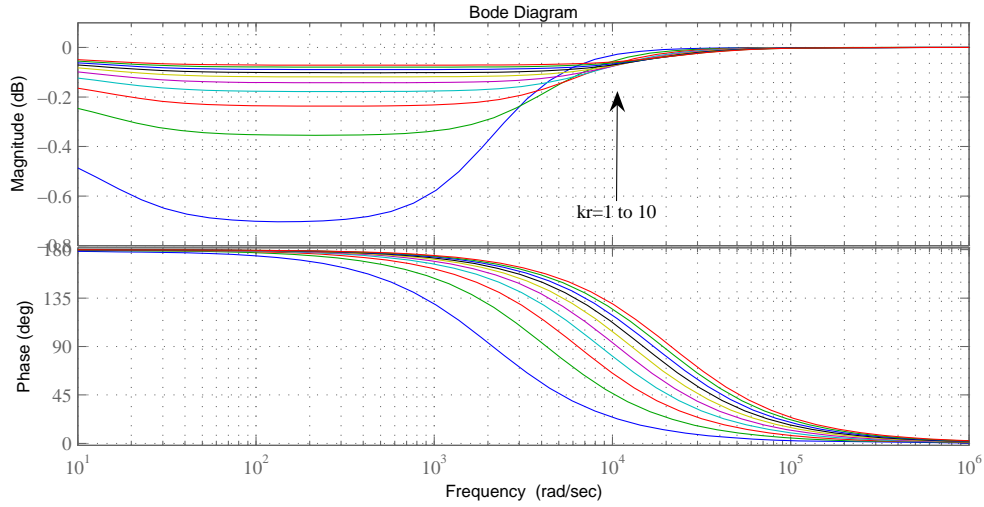


Figure 3.7: Bode plot of the BIBO Stability condition (3.16) for repetitive controller for a DC-DC converter

### 3.4 Experimental results

The proposed controller shown in Fig. 3.4 has been tested in an experimental board of a boost converter with parameters given in Table 3.1. In this experimental board a conventional non regulated power supply using a full bridge diode rectifier with a  $4700\mu\text{F}$  capacitor filter is used as a voltage source. The voltage provided by this source is polluted mainly by harmonic components of 120 Hz (the 2<sup>nd</sup> harmonic of 60 Hz). This harmonic distortion, as expected, increases for a higher current demand. Moreover, the inductor current is sensed via a precision resistor of  $0.05\Omega$  connected in series with the inductor, and a typical circuit SG3524 is used to generate the PWM signal.

Diode	MBR1045
Power Mosfet	IRF540
Inductor	$200\ \mu\text{H}$
Capacitor	$100\ \mu\text{F}$
Load resistor	$12.5$ or $25\ \Omega$
$V_{in}$	$17.6\ \text{v}$
$V_D$	$24\ \text{v}$

Table 3.1: Parameters of the boost converter.

The repetitive part of the compensator (contained in the inner loop) is implemented using analog circuitry. For this purpose, the circuit presented in Fig.2.8 has been used, where the input variable  $u_{in}$  corresponds, in this application, to the capacitor voltage error  $\tilde{x}_2$ , and the output  $y_{out}$  is sent to the gain block  $k_r$ , as shown in Fig. 3.4. The delay time has been fixed to  $d_1 = 8.33\ \text{ms}$  for

compensation of harmonics of  $f_0 = 120$  Hz. The main elements used for the implementation of the delay line are given in Table 3.2. The value of  $K$  is fixed by  $R_3$ ,  $R_4$  and  $R_5$ . A simple first order LPF of the form  $1/(R_5C_2s + 1)$  has been used, where the time constant has been set to  $R_5C_2 = 15.5\mu$  s, and the time constant of the HPF is fixed to  $\tau_2 = 70.5$  ms which is selected as big as possible to minimize the integral effect and without affecting the rest of the frequency response.

The tests performed include:

1. Enabling and disabling the harmonic compensation, that is, connecting and disconnecting the repetitive controller contribution, respectively, while keeping a constant load resistance  $R = 12.5 \Omega$ .
2. Step changes in load resistance between  $12.5 \Omega$  and  $25 \Omega$  to show the robustness of the proposed controller against load variations.

IC 512 stage BBD	MN3004
IC clock	MN3101
potentiometer $R_1$	20 K $\Omega$
resistor $R_2$	47 K $\Omega$
capacitor $C_1$	20 pF

Table 3.2: Elements used to implement the delay line.

Fig. 3.8 shows (from top to bottom) the responses of capacitor voltage  $x_2$ , inductor current  $x_1$  and the DC component of the inductor reference current  $I_d$ . In this figure the harmonic compensation is enabled after a given period of time. Notice that, the distortion in the output voltage capacitor is considerably reduced. Fig. 3.9 shows the same responses in the case that the compensation is disabled after a certain period of time.

Figure 3.10 shows (from top to bottom) the frequency spectrum of  $x_2$  without and during compensation. Notice that, the harmonic component at 120 Hz and 240 Hz decreases about 20 dB while the harmonic at 360 Hz decreases almost 10 dB, and the higher harmonics simply disappear. Moreover, it has been observed that the compensation of harmonic distortion is even more evident for bigger load resistors. Fig. 3.11 the same frequency response but considering a load resistance of  $R = 25 \Omega$ .

Figure 3.12 shows (from top to bottom) the frequency spectrum of the inductor current  $x_1$  disabling and enabling the compensation. As predicted by theory, the harmonic content of the inductor current increases as a consequence of the application of the compensation, roughly speaking, it is necessary to distort the inductor current in such a way to allow compensation in the capacitor voltage  $x_2$ .

Once the system is operating under harmonic compensation, i.e., with the proposed repetitive scheme connected, the load is changed from  $25 \Omega$  to  $12.5 \Omega$ . Figure 3.13 shows (from top to bottom) the transient response of voltage  $x_2$  and inductor current  $x_1$ . Notice that, after a small transient the voltage recuperates, in average, its desired value 24 V. In Fig. 3.14 the inverse process is performed, that is, the load resistance is changed from  $12.5 \Omega$  to  $25 \Omega$ .

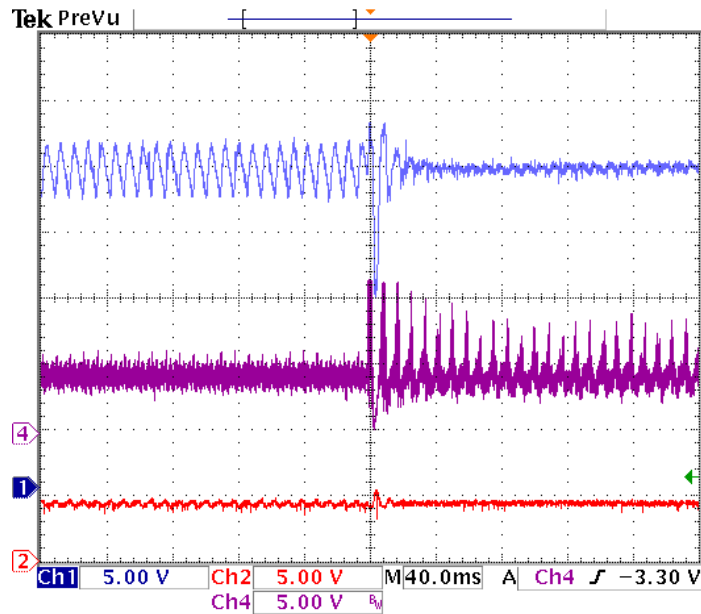


Figure 3.8: Transient responses after enabling the harmonic compensation, with  $R = 12.5\Omega$ . (From top to bottom) Capacitor voltage  $x_2$ , inductor current  $x_1$  and the inductor reference current  $I_d$ .

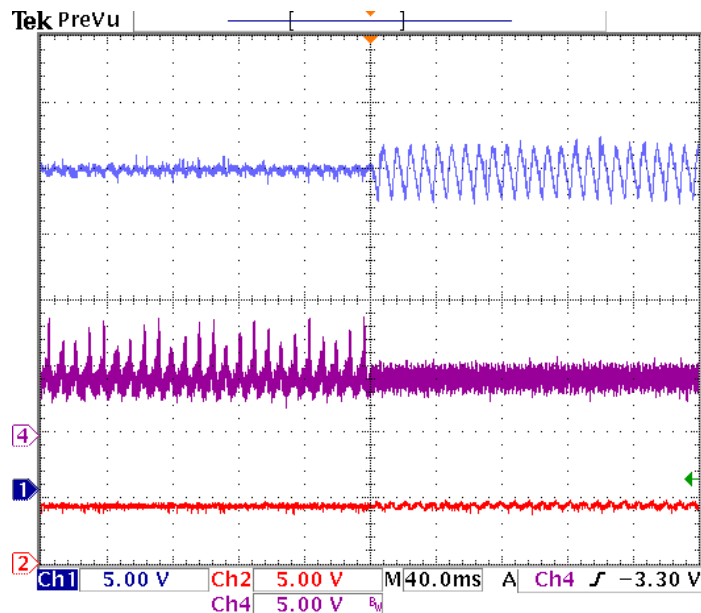


Figure 3.9: Transient responses after disabling the harmonic compensation, with  $R = 25\Omega$ . (from top to bottom) Capacitor voltage  $x_2$ , inductor current  $x_1$  and the inductor reference current  $I_d$ .

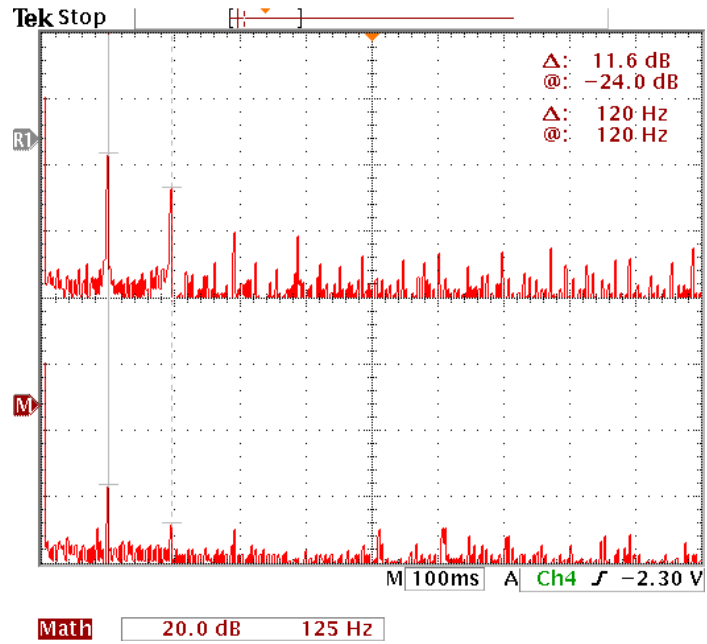


Figure 3.10: Frequency spectrum of capacitor voltage  $x_2$ , with  $R = 12.5\Omega$ . **(top)** Without harmonic compensation, and **(bottom)** under harmonic compensation.

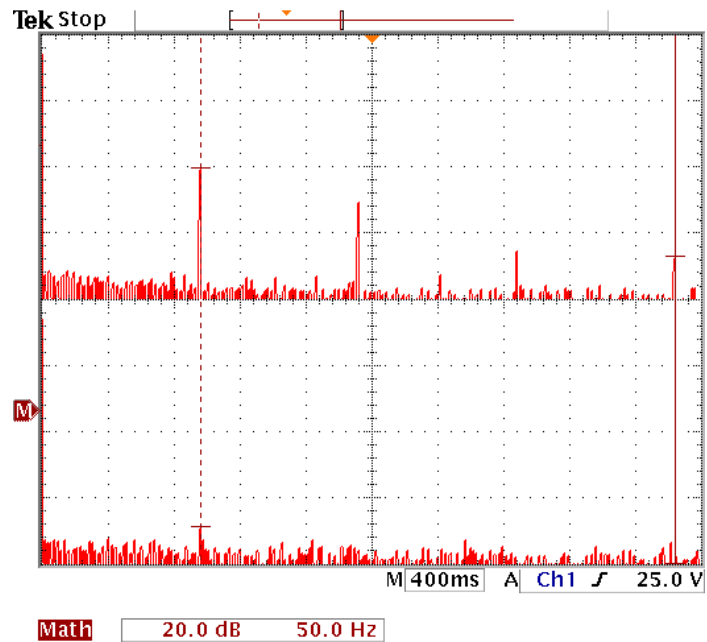


Figure 3.11: Frequency spectrum of capacitor voltage  $x_2$ , with  $R = 25\Omega$ . **(top)** Without harmonic compensation, and **(bottom)** under harmonic compensation.

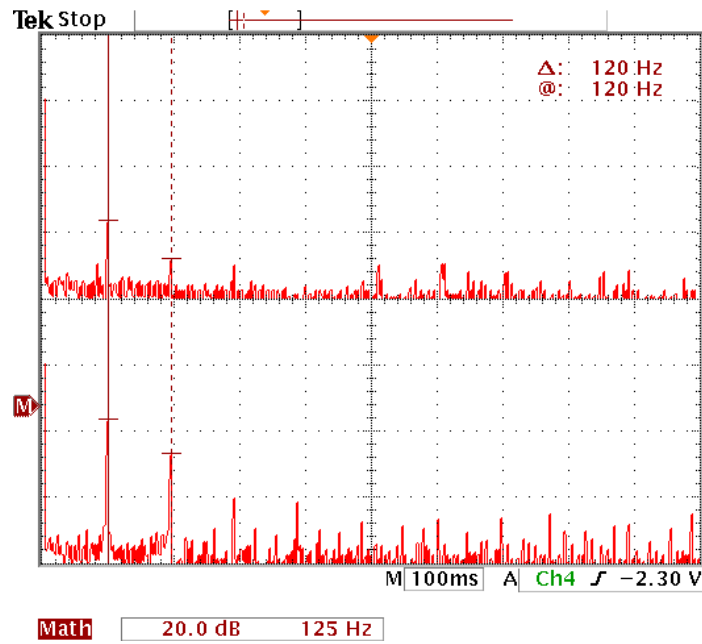


Figure 3.12: Frequency spectrum of inductor current  $x_1$ , with  $R = 12.5\Omega$ . (**top**) Without harmonic compensation, and **bottom** under harmonic compensation.

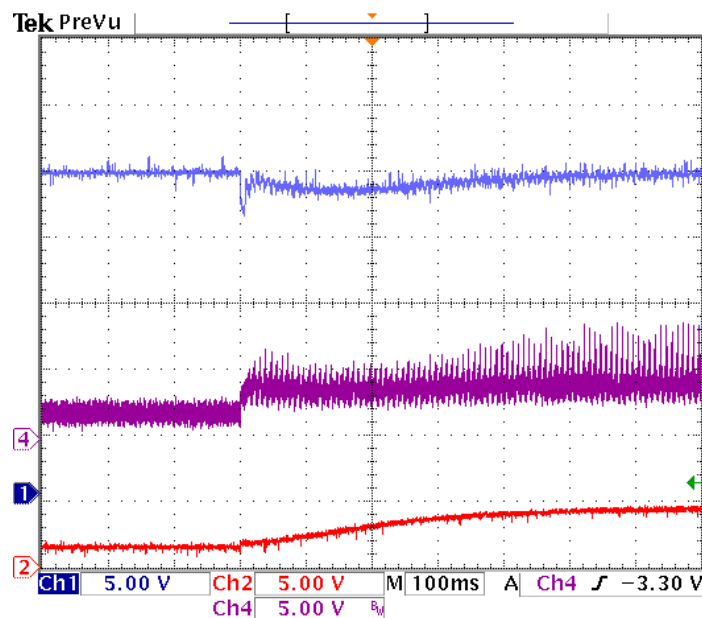


Figure 3.13: Transient response for a load step change from  $R = 25\Omega$  to  $R = 12.5\Omega$ . (**from top to bottom**) Capacitor voltage  $x_2$ , inductor current  $x_1$  and DC component of the inductor reference current  $I_d$ .

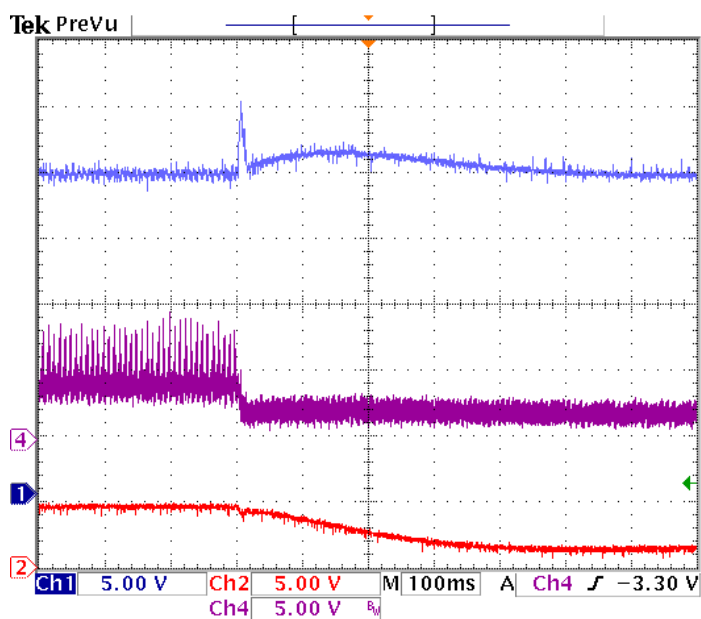


Figure 3.14: Transient response for a load step change from  $R = 12.5\Omega$  to  $R = 25\Omega$ . (from top to bottom) capacitor voltage  $x_2$ , inductor current  $x_1$  and DC component of the inductor reference current  $I_d$ .



## Chapter 4

# Boost-based PFC with harmonic compensation

---

### Summary

This chapter studies a repetitive-based controller for a power factor precompensator. The controller guarantees voltage regulation with a power factor close to unity, despite of the presence of harmonic distortion in the source voltage and uncertainties in the system parameters. A key point in the proposed solution is the expression of the model in terms of the input current instead of the inductor current as usually done. The resulting controller is preserved as close as possible to the conventional one, which is composed by the cascade interconnection of two controllers namely: inner and outer control loops. It is shown that while the latter turns out to be a simple low pass filter plus an integration term, the former is composed by a proportional gain plus a repetitive strategy actuating as a refinement term. It is shown that, the repetitive scheme considered here is, in fact, equivalent to a bank of resonant filters, which has shown to be a useful technique in harmonic compensation. The closed loop BIBO stability analysis of such an infinite dimensional system is performed. Experimental results in a 400 W boost-based PFC, with a fixed point DSP-based implementation of the proposed controller, are provided to assess the performance of the controlled system.

---

## 4.1 Introduction

In the past few years, there has been a growing research on the design and control of power factor compensators (PFC). This is due to the fact that power converters are, generally speaking, an ubiquitous power source whose applicability ranges from electrical appliances and digital computers to industrial electronics and sophisticated communications equipment. This issue has been reflected in several published works [54], [55], [56], [57] and [58] where different new topologies and clever controllers have been proposed. It is clear from all these works that the control design of a PFC faces a twofold problem. First, a controller should be designed to guarantee *output voltage* regulation, and second, a *power factor close to unity* should be guaranteed. In the present work, the boost-based PFC topology shown in Fig. 4.1 is considered, which is perhaps one of the most popular among the different topologies, although it exhibits certain drawbacks, such as a slight deformation in the

input current signal around the zero crossings. This PFC consists of a diode bridge aimed to rectify the voltage coming from an AC power supply, and should deliver a regulated DC voltage using to an associated boost converter.

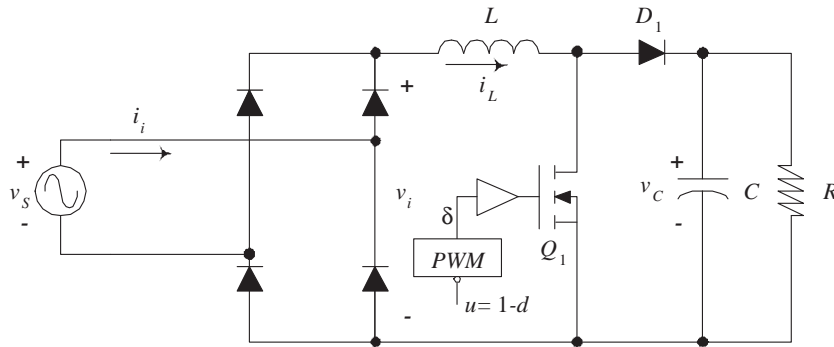


Figure 4.1: Switch-regulated boost-based PFC circuit.

Usually, the control design problem for this PFC topology is split in two loops, namely, the inner and the outer loops. This idea is based on the assumption of decoupling between the inductor current and the capacitor voltage dynamics due to the considerable difference between their time scales, which allows to deal with each dynamics separately. The inner loop, also referred as the current loop, is designed to guarantee the power factor requirement. This part of the controller should guarantee a sort of tracking of the inductor current towards a reference current. Normally, the reference current which is a scaled replica of the rectified source voltage is considered. As a consequence, the controlled system is seen from the power supply as an equivalent resistor, which holds even in the presence of distortion in the voltage source. The outer loop, also referred as voltage loop, indirectly performs the regulation of the output voltage by computing the input current reference amplitude. In the proposed controller, a low pass filter (LPF) has been added to the proportional term to limit the bandwidth of the PI controller to prevent the reinjection of more distortion.

The use of a system representation in terms of the input current, instead of the usual inductor current, is instrumental for our developments. This allows us to treat the problem of harmonic contents in the input voltage in a more natural way, and facilitates considerably the tracking objective. In [4], a controller was obtained following adaptive techniques which gave, in principle, a stable and robust nonlinear controller. Special attention was given to the inner control loop where, the inner loop was composed of a proportional term plus a bank of resonant filters. Those resonant filters acted as a refinement term to guarantee perfect current tracking in steady state. In particular, those resonant filters were tuned at the odd harmonics, which were the main components of the distorted input voltage. However, notice that, there would be as many resonant filters as harmonic components considered for compensation. This may represent a drawback, most of all in the case of highly distorted input voltage signal. To address this issue, it is shown in the present chapter that, the whole bank of resonators can be replaced by a simpler repetitive scheme while preserving a very close performance. In particular, the negative feedback plus feedforward repetitive scheme has been selected for implementation, since the harmonics under consideration are the odd. One of the main contributions of the present chapter is to present a practical application of the repetitive scheme to the boost-based PFC converter, and moreover, to show the connection between these two forms of harmonic compensation. As in [4], the repetitive-based solution considers the main parameters of

the system (the capacitance and the inductance) and the output load resistance as unknowns, and, as already mentioned, it allows for harmonic distortion in the input voltage. Finally in this chapter, an implementation of the controller have been performed for low power applications. The experimental results are presented here to assess the performance of the controlled system.

## 4.2 Switch-regulated boost converter as a PFP

In this section, the control problem of the PFP is formulated. The scheme of the PFC circuit is shown in Fig. 4.1. The differential equations describing the circuit dynamics are:

$$\begin{aligned} L \frac{d}{dt} i_L &= -u v_C + v_i \\ C \frac{d}{dt} \left( \frac{v_C^2}{2} \right) &= u v_C i_L - \frac{v_C^2}{R} \end{aligned} \quad (4.1)$$

where  $i_L$  and  $v_C$  are the inductor current and capacitor voltage variables, respectively; notice that  $i_L = |i_i|$  with  $i_i = \text{sign}(i_i) i_L$  the input current (on the AC power supply side);  $v_i(t) = \text{sign}(i_i) v_S$  is the voltage measured at the diode bridge output;  $R$  represents the load resistance;  $C$  and  $L$  are the capacitance and inductance of the circuit, respectively;  $\delta$ , which takes values in the discrete set  $\{0, 1\}$ , denotes the switch position function and acts as the control input, that is, for  $\delta = 0$  the transistor  $Q_1$  is off, while for  $\delta = 1$  the transistor  $Q_1$  is on. For the controller design purposes the averaged model is considered, i.e., the control input  $u$  is considered as a continuous signal representing the slew rate of a PWM switching sequence of a relative high frequency ( $u = 1 - d$  where  $d$  is the duty ratio of such a PWM switching sequence).

According to [4], to treat the problem of harmonic content in the input voltage  $v_S$  in a more natural way, i.e., to facilitate the current tracking problem, it is very convenient to represent the system model in terms of the input current, instead of the usual inductor current. For this purpose, the following coordinate transformations are used

$$i_i = \text{sign}(i_i) i_L, \quad v_i = \text{sign}(i_i) v_S, \quad e = \text{sign}(i_i) u v_C$$

where  $\text{sign}(x) = 1$  if  $x > 0$ ,  $\text{sign}(x) = -1$  if  $x < 0$  and  $\text{sign}(x) = 0$  if  $x = 0$ .

Thus, in open sets excluding the zero crossing points, i.e.,  $\forall t$  such that  $i_i(t) \neq 0$ , the model can be rewritten as

$$L \frac{d}{dt} i_i = -e + v_S \quad (4.2)$$

$$C \frac{d}{dt} z = e i_i - \frac{2z}{R} \quad (4.3)$$

where  $e$  represents the actual control input and  $z = \frac{v_C^2}{2}$ .

The twofold *control objective* consists in:

- (i) First, to guarantee a power factor near unity, the input current  $i_i$  should follow a signal proportional (same shape and phase) to  $v_S$ , i.e.,

$$i_i \rightarrow i_i^* = g v_S \quad (4.4)$$

where gain  $g$  represents the conductance of the equivalent resistor seen by the power supply for a given load resistance  $R$ , and under a unitary power factor functioning.

It is usual in practice to redefine gain  $g$  by introducing a normalization factor  $1/v_{S,RMS}^2$  as shown below

$$g = \frac{G}{v_{S,RMS}^2} \quad (4.5)$$

where  $G$  is a gain yet to be defined and  $v_{S,RMS}$  is the RMS value of  $v_S$ . This simple transformation is very useful in the implementation process as it prevents numerical errors. However, for the analysis it is more convenient the use of  $g$ .

- (ii) Second, the DC component of output  $v_C$  should be driven to some constant desired value  $V_d > V_i$ , where  $V_i$  is the peak value of the input voltage  $v_i$  (rectified voltage). Here and in what follows the DC component of a signal  $x(t)$  is considered as the average of the signal taken over a period of the fundamental, that is,  $\frac{1}{T} \int_{(t-T)}^t x(\tau) d\tau$ .

It is assumed that the system parameters  $L$ ,  $C$  and the load resistance  $R$  are unknown quantities that may vary slowly or in steps due to changes in the system. Moreover, it is assumed that the source voltage can be described as a Fourier series

$$v_S = \sum_{k \in \mathcal{H}} \rho_k^\top V_{S,k} \quad (4.6)$$

where

$$\rho_k = \begin{bmatrix} \cos(k\omega_0 t) \\ \sin(k\omega_0 t) \end{bmatrix}, \quad V_{S,k} = \begin{bmatrix} V_{S,k}^r \\ V_{S,k}^i \end{bmatrix}$$

Numbers  $V_{S,k}^r, V_{S,k}^i \in \mathbb{R}$  are the  $k^{th}$  harmonic coefficients of the Fourier series description of the source voltage, and  $\omega_0$  represents the fundamental frequency considered as a known constant. The harmonic coefficients are assumed unknown constants (or slowly varying) and  $\mathcal{H} = \{1, 3, 5, 7, \dots\}$  is the set of indexes of the considered harmonic components, in this case the odd harmonics. Supercripts  $(\cdot)^r$  and  $(\cdot)^i$  are used to distinguish the coefficients associated to  $\cos(k\omega_0 t)$  and  $\sin(k\omega_0 t)$ , respectively.

### 4.2.1 Inner control loop

In this subsection, a controller is designed which guarantees tracking of  $i_i$  towards its desired reference  $i_i^*$  computed as in (4.4). It is straightforward to show [58] that the following controller stabilizes subsystem (4.2), and guarantees that  $i_i$  tracks its desired reference  $i_i^*$

$$e = -L \frac{d}{dt} i_i^* + v_S + k_1 \tilde{i}_i \quad (4.7)$$

where  $\tilde{i}_i = i_i - i_i^*$  and  $k_1 > 0$  is a design parameter.

Notice that, both the time derivative of  $i_i^*$  and the parameter  $L$  are required to implement the above controller. In what follows it is shown how this term can be estimated by means of adaptation using the description in Fourier series (in its harmonics components) of the source voltage  $v_S$ .

Using (4.4) and (4.6), the term containing the time derivative can be developed as follows

$$L \frac{d}{dt} i_i^* = L (g \dot{v}_S + \dot{g} v_S) = \sum_{k \in \mathcal{H}} \rho_k^\top L (\dot{g} - k \omega_0 g \mathcal{J}) V_{S,k} \quad (4.8)$$

where it has been used the fact that

$$\dot{v}_S = - \sum_{k \in \mathcal{H}} k \omega \rho_k^\top \mathcal{J} V_{S,k}, \quad \mathcal{J} = -\mathcal{J}^\top = \begin{bmatrix} 0 & -1 \\ 1 & 0 \end{bmatrix}$$

Now, by defining the vector

$$\Phi_k = L (\dot{g} - k \omega_0 g \mathcal{J}) V_{S,k}, \quad k \in \mathcal{H} \quad (4.9)$$

which for each  $k \in \mathcal{H}$  practically converges towards a constant<sup>1</sup>, then (4.8) can be further reduced to

$$L \frac{d}{dt} i_i^* = \sum_{k \in \mathcal{H}} \rho_k^\top \Phi_k$$

where vector  $\Phi_k$  is unknown. Thus, it is proposed to use an estimate  $\hat{\Phi}_k$  in the control expression (4.7) above, this yields the controller

$$e = - \sum_{k \in \mathcal{H}} \rho_k^\top \hat{\Phi}_k + v_S + k_1 \tilde{i}_i \quad (4.10)$$

Subsystem (4.2) in closed loop with controller (4.10) yields the following error dynamics

$$L \frac{d}{dt} \tilde{i}_i = \sum_{k \in \mathcal{H}} \rho_k^\top \tilde{\Phi}_k - k_1 \tilde{i}_i \quad (4.11)$$

where  $\tilde{\Phi}_k \triangleq \hat{\Phi}_k - \Phi_k$ .

The following energy storage function is used to deal with the terms associated with the error signals  $\tilde{\Phi}_k$

$$W = \frac{L}{2} \tilde{i}_i^2 + \sum_{k \in \mathcal{H}} \frac{1}{2\gamma_k} \left[ \left( \tilde{\Phi}_k^r \right)^2 + \left( \tilde{\Phi}_k^i \right)^2 \right]$$

with a time derivative along the trajectories of (4.11) given by

$$\dot{W} = -k_1 \tilde{i}_i^2 + \tilde{i}_i \sum_{k \in \mathcal{H}} \rho_k^\top \tilde{\Phi}_k + \sum_{k \in \mathcal{H}} \frac{\dot{\tilde{\Phi}}_k^\top \tilde{\Phi}_k}{\gamma_k}$$

which is forced to be negative semidefinite if the error on the estimates is constructed according to the following adaptive laws

$$\dot{\tilde{\Phi}}_k^r = -\gamma_k \tilde{i}_i \cos(k \omega_0 t), \quad k \in \mathcal{H} \quad (4.12)$$

$$\dot{\tilde{\Phi}}_k^i = -\gamma_k \tilde{i}_i \sin(k \omega_0 t), \quad k \in \mathcal{H} \quad (4.13)$$

<sup>1</sup>Ideally  $g$  and  $\dot{g}$  should vary slowly and take constant values in the steady state.

or in a more compact form

$$\dot{\hat{\Phi}}_k = -\gamma_k \tilde{i}_i \rho_k, \quad k \in \mathcal{H} \quad (4.14)$$

where  $\gamma_k > 0$ ,  $k \in \mathcal{H}$  are design parameters.

Since  $W$  is radially unbounded, and  $\dot{W}$  is negative semi-definite then  $\tilde{i}_i \in \mathcal{L}_2 \cap \mathcal{L}_\infty$  and  $\tilde{\Phi}_k \in \mathcal{L}_\infty$  for every  $k \in \mathcal{H}$ . From (4.11)  $\dot{\tilde{i}}_i \in \mathcal{L}_\infty$ . Now, since  $\tilde{i}_i \in \mathcal{L}_\infty$  and  $\dot{\tilde{i}}_i \in \mathcal{L}_\infty$ , then  $\tilde{i}_i$  is uniformly continuous, which together with the fact that,  $\tilde{i}_i \in \mathcal{L}_2$  imply that,  $\tilde{i}_i \rightarrow 0$  asymptotically. Out of this  $\tilde{\Phi}_k^p$ ,  $\tilde{\Phi}_k^n$  equal constants  $\forall k \in \mathcal{H}$ , however, for  $\tilde{i}_i = 0$  and from (4.11)  $\sum_{k \in \mathcal{H}} \rho_k^\top \tilde{\Phi}_k = 0$ . Therefore, the only possible solution is  $\tilde{\Phi}_k^p \rightarrow 0$  and  $\tilde{\Phi}_k^n \rightarrow 0$ .

The controller (4.10) with adaptive laws (4.14) can be further simplified using the following transformations

$$\Psi_k^r = -\rho_k^\top \hat{\Phi}_k, \quad k \in \mathcal{H} \quad (4.15)$$

$$\Psi_k^i = -\rho_k^\top \mathcal{J} \hat{\Phi}_k, \quad k \in \mathcal{H} \quad (4.16)$$

The controller (4.10) is reduced to

$$e = \sum_{k \in \mathcal{H}} \Psi_k^r + v_S + k_1 \tilde{i}_i \quad (4.17)$$

and the adaptive laws can be rewritten as

$$\dot{\Psi}_k^r = \gamma_k \tilde{i}_i - k\omega_0 \Psi_k^i, \quad k \in \mathcal{H} \quad (4.18)$$

$$\dot{\Psi}_k^i = k\omega_0 \Psi_k^r, \quad k \in \mathcal{H} \quad (4.19)$$

Expressing the dynamic extension (the adaptations) in the form of transfer functions  $\tilde{i}_i \mapsto \Psi_k^r$  yields

$$\Psi_k^r = \frac{\gamma_k s}{s^2 + k^2 \omega_0^2} \tilde{i}_i, \quad k \in \mathcal{H} \quad (4.20)$$

**Remark 4.1** The previous resulting compensator has a very similar structure as those controllers presented in [59] and [60], which include a bank of resonant filters as the main harmonic compensation element, but they were derived intuitively following the *internal model principle* approach.  $\square$

#### A. Discussion on the repetitive controller

Assuming that an infinite number of odd harmonics is considered for compensation, then a controller comprising the following infinite sum of resonant filters would be required.

$$\sum_{k=1}^{\infty} \frac{\gamma_k s}{s^2 + (2k-1)^2 \omega_0^2} = \frac{2\omega_0}{\pi} \sum_{k=1}^{\infty} \frac{2s}{s^2 + (2k-1)^2 \omega_0^2} \quad (4.21)$$

where  $\gamma_k = 4\omega_0/\pi$ ,  $k \in \{1, \dots, \infty\}$  has been fixed. An interesting observation here is that, out of the selection of that precise  $\gamma_k$ , the expression on the RHS of (4.21) has the following equivalent expression in terms of the hyperbolic tangent [43].

$$\frac{2\omega_0}{\pi} \sum_{k=1}^{\infty} \frac{2s}{s^2 + (2k-1)^2\omega_0^2} = \tanh\left(\frac{s\pi}{2\omega_0}\right)$$

It is described in Chapter 2 that the hyperbolic tangent can be also expressed as

$$\tanh\left(\frac{s\pi}{2\omega_0}\right) = \frac{1 - e^{-\frac{s\pi}{\omega_0}}}{1 + e^{-\frac{s\pi}{\omega_0}}} = \frac{1 - e^{-sd_2}}{1 + e^{-sd_2}} \quad (4.22)$$

where  $d_2 = \pi/\omega_0$  and represent the delay time. The idea is thus, to substitute the infinite bank of resonant filters tuned at odd harmonics by the negative feedback plus feedforward repetitive scheme (4.22), with the appropriate modifications discussed in Chapter 2, Section 2.3, i.e., introduction of a gain  $0 < K < 1$  and a low pass filter  $F(s) = 1/(\tau s + 1)$ . Then the inner loop can thus be rewritten as follows

$$e = k_1 \tilde{i}_i + v_S + \frac{1 - F(s)K e^{-\frac{s\pi}{\omega_0}}}{1 + F(s)K e^{-\frac{s\pi}{\omega_0}}} \quad (4.23)$$

#### 4.2.2 Outer control loop

Direct substitution of controller (4.10) and (4.14) in the second subsystem (4.3), yields the following system (in terms of the reference error)

$$C \dot{\tilde{z}} = -i_i \sum_{k \in \mathcal{H}} \rho_k^\top \hat{\Phi}_k + i_i v_S + i_i k_1 \tilde{i}_i - \frac{2z}{R} \quad (4.24)$$

where  $\tilde{z} = z - \frac{V_d^2}{2}$ .

As pointed out before, it is assumed that the dynamics of subsystem (4.11) are much faster than the dynamics of subsystem (4.24), and moreover, that the control law  $e$  is bounded, which is true if all terms  $\hat{\Phi}_k$  ( $\forall k \in \mathcal{H}$ ) are bounded. Thus, in a relatively short time,  $\tilde{i}_i = 0$  and  $\hat{\Phi} = \Phi$ , and the model reduces to

$$C \dot{\tilde{z}} = -g v_S \sum_{k \in \mathcal{H}} \rho_k^\top \Phi_k + g v_S^2 - P_0 \quad (4.25)$$

where  $P_0$  represents the output power load, it may be a simple constant power source, it may also include the effect of a load resistance<sup>2</sup> or simply a constant current source.

Since the main interest in the outer control loop of a PFC is to regulate in average the output capacitor voltage, then the control objective focus on the dynamics of the DC component of  $\tilde{z}$ . As a consequence the higher order harmonics at the RHS of the above equation (4.25) are neglected. And then a controller is designed with a relatively short bandwidth to attenuate the affects of these neglected higher order harmonics. This limitation directly affects the dynamical response of the system, as the DC voltage responds slowly.

To extract the DC component, a moving average function<sup>3</sup> is applied to the RHS of (4.25), which yields

$$C \dot{\tilde{z}} = -\langle g v_S \sum_{k \in \mathcal{H}} \rho_k^\top \Phi_k \rangle_0 + g \langle v_S^2 \rangle_0 - P_0 \quad (4.26)$$

<sup>2</sup>In most works  $P_0 = \frac{2z}{R}$  is considered.

<sup>3</sup>The moving average function of a signal  $x(t)$  is defined as  $\langle x(t) \rangle_0 = \frac{1}{T} \int_{t-T}^t x(\tau) d\tau$ .

where  $\langle v_S^2 \rangle_0$  is nothing else than the square of the RMS value of  $v_S$ , i.e.,  $v_{S,RMS}^2 = \langle v_S^2 \rangle_0$ .

The first term on the RHS can be rewritten, using (4.6) and (4.9), as

$$\begin{aligned} \langle g v_S \sum_{k \in \mathcal{H}} \rho_k^\top \Phi_k \rangle_0 &= \langle \sum_{k \in \mathcal{H}} g \rho_k^\top V_{S,k} \cdot \sum_{k \in \mathcal{H}} \rho_k^\top L \dot{g} V_{S,k} \rangle_0 \\ &\quad - \langle \sum_{k \in \mathcal{H}} g \rho_k^\top V_{S,k} \cdot \sum_{k \in \mathcal{H}} \rho_k^\top L g k \omega_0 \mathcal{J} V_{S,k} \rangle_0 \end{aligned} \quad (4.27)$$

Notice that, the second term at the right hand side of (4.27) will contain the products of orthogonal rotating vectors at the same angular speed, plus harmonics components of higher order, thus its DC component will be zero. On the other hand, the first term on the RHS contains harmonic components of higher order plus products of parallel rotating vectors which will produce squares of sinusoidal functions (and thus a DC component) plus higher order harmonics. Therefore, (4.27) can be reduced to

$$\langle g v_S \sum_{k \in \mathcal{H}} \rho_k^\top \Phi_k \rangle_0 = L g \dot{g} \sum_{k \in \mathcal{H}} \langle (\rho_k^\top V_{S,k})^2 \rangle_0 = L g \dot{g} v_{S,RMS}^2$$

Finally, the error model can be written as

$$C \dot{\tilde{z}} = -\frac{L G \dot{G}}{v_{S,RMS}^2} + G - P_0 \quad (4.28)$$

where the equivalence (4.5) has been used.

Notice that, the term  $L/v_{S,RMS}^2$  is extremely small, and thus the first term on the RHS of system (4.28) can be neglected as far as  $G$  varies slowly. Following this idea, it is proposed to compute  $G$  as

$$G = -k_i \xi - k_p \zeta \quad (4.29)$$

$$\dot{\xi} = \tilde{z} \quad (4.30)$$

$$\tau \dot{\zeta} = \tilde{z} - \zeta \quad (4.31)$$

where  $k_p$ ,  $k_i$  and  $\tau$  are positive design parameters.

The form of this controller is motivated from the structure of a simple PI, where  $\zeta$  represents the signal  $\tilde{z}$  filtered by means of a first order filter. It has been observed that direct use of  $\tilde{z}$  in the computation of  $G$  (using a normal PI) causes the introduction of more harmonics which will in principle deform the shape of reference  $i_i^*$  causing the degradation of the power factor. The controller (4.29)-(4.31) can be rewritten in the form of a transfer function having as input  $\tilde{z}$  and output  $G$  as follows

$$G = -\frac{k_i}{s} \tilde{z} - \frac{k_p}{\tau s + 1} \tilde{z} \quad (4.32)$$

where  $s$  represents the complex Laplace variable.

Summarizing, in Fig. 4.2 shows the block diagram of the proposed repetitive-based controller, where the original bank of resonant filters has been replaced by the proposed negative feedback repetitive scheme. Hence, similar to the original bank of resonant filters, the repetitive scheme appears as a refinement term to compensate for the harmonic distortion, in this case the odd harmonics. Notice that, a gain  $k_r > 0$  has been also included. The purpose of this gain is to have control over the gain produced by the peaks, and to somehow enlarge their bandwidth, which serves to improve the robustness with respect to frequency variations.



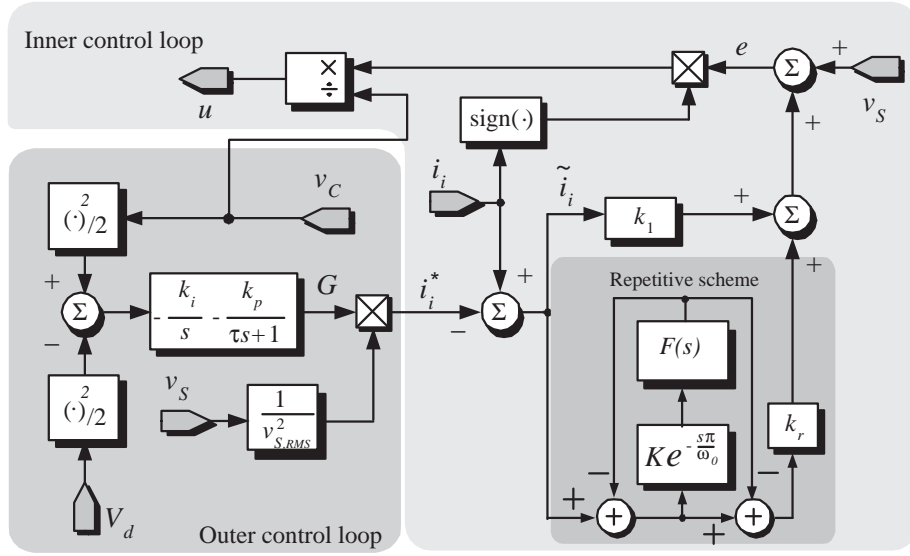


Figure 4.2: Block diagram of the proposed repetitive-based controller for the PFC.

### 4.3 Stability analysis

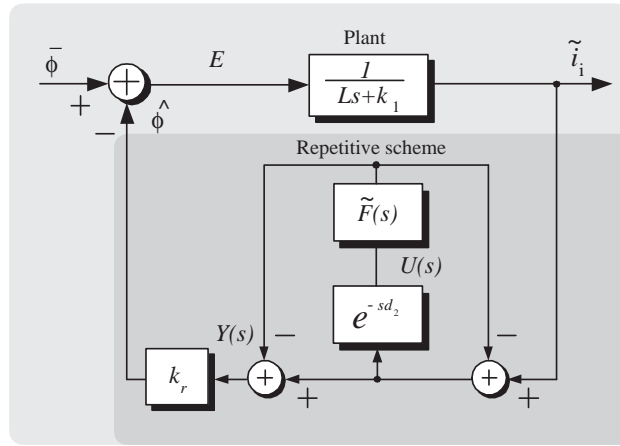


Figure 4.3: Block diagram of the input current error dynamics in closed-loop with the repetitive scheme.

In what follows, a BIBO stability study considering the repetitive scheme is performed based on the well known *small gain theorem*. The study focuses on the input current dynamics  $i_i$  because, these are the dynamics where the harmonic distortion is present, and where the repetitive scheme is applied. Following the decoupling assumption, the current dynamics (4.2) are considered as an independent closed loop system. It is assumed that the damping  $k_1 \dot{i}_i$  and the  $v_s$  cancellation terms in (4.23) have already been applied to the  $i_i$  dynamics (4.2), remaining to consider the harmonics compensation term, i.e., the repetitive scheme. This yields the following input current error dynamics

$$L\dot{\tilde{i}}_i = -\hat{\phi} + \bar{\phi} - k_1 \tilde{i}_i \quad (4.33)$$

where  $\bar{\phi}(t)$  represents a periodical disturbance composed of higher harmonics of the fundamental at  $\omega_0$ , and  $\hat{\phi}(t)$  represents the control signal computed with the proposed repetitive scheme as shown in the block diagram of Fig. 4.3. A first order LPF of the form  $F(s) = 1/(\tau_1 s + 1)$  has been considered, which is necessary to limit the bandwidth of the controller (see Chapter 2, Fig. 2.3). Moreover, both the gain  $K$  and the LPF have been concentrated in a single term, that is,

$$\tilde{F}(s) = \frac{K}{\tau_1 s + 1} \quad (4.34)$$

Let us discuss the error convergence condition or stability condition for the repetitive control system by considering the BIBO stability. The following proposition states the stability result.

**Proposition 4.2** *The system in Fig. 4.4 is BIBO stable from input  $\bar{\phi}$  to output  $\tilde{i}_i$ , if the following conditions are fulfilled.*

- (i)  $F(s)$  is stable
- (ii)  $(1 + k_r G(s))^{-1} k_r G(s)$  is stable
- (iii)  $\left\| (1 + k_r G(s))^{-1} \tilde{F}(s) (k_r G(s) - 1) \right\|_{\infty} < 1$

□

**Proof.** A similar procedure as in Chapter 2 Sec. 2.5 is followed to find an equivalent closed-loop system for the system shown in Fig. 4.3. The equivalent block diagram is shown in the Fig. 4.4, where the following relations are obtained.

$$\tilde{i}_i(s) = -e^{-sd_2} \tilde{G}(s) \tilde{i}_i(s) + D(s) \quad (4.35)$$

where  $\tilde{G}(s)$  is equal to

$$\tilde{G}(s) = (1 + k_r G(s))^{-1} \tilde{F}(s) (k_r G(s) - 1) \quad (4.36)$$

and, the input signal  $D(s)$  is given by

$$D(s) = (1 + \tilde{F}(s)e^{-sd_2})(G(s)\bar{\phi}(s) + \tilde{i}_i(s)) - 2k_r \tilde{F}(s)G(s)\bar{U}(s) \quad (4.37)$$

The plant is defined as  $G(s) = 1/(Ls + k_1)$  which is a stable transfer function, and  $\tilde{i}_i$  and  $\bar{U}$  represent the initial conditions of  $\tilde{i}_i$  and  $e^{sd_2}$ , respectively. Suppose that all elements of  $\bar{\phi}(t)$  are bounded and continuous periodic signals. This assumption yield, that  $\bar{\phi}_0(t)$ , the first part of (4.37), is an bounded function, where

$$\bar{\phi}_0(t) \triangleq \mathcal{L}^{-1}[(1 + \tilde{F}(s)e^{-sd_2})\bar{\phi}(s)]$$

because  $|e^{-sd_2}| = 1$ , and  $\tilde{F}(s) = K/(\tau_1 s + 1)$ , is a design parameter and it is chosen stable. This fact, in addition with the fact that  $G(s)$  is stable for all positive  $L, k_1$  implies that the exogenous input  $\mathcal{L}^{-1}[(1 + k_r G(s))^{-1}]D(s)$  is bounded under the assumption of asymptotic stability of  $(1 - k_r G(s))^{-1}k_r G(s)$ .

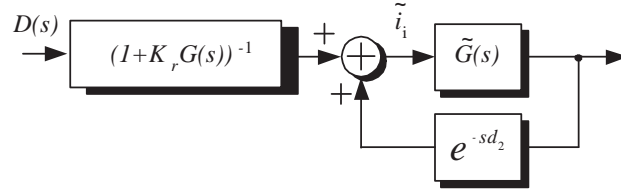


Figure 4.4: Equivalent system of the block diagram shown in Fig. 4.3 for analysis purposes.

Based on condition (ii) it is possible to show that the input transfer function is stable since,  $(1 - k_r G)^{-1} = 1 - (1 + k_r G)^{-1}k_r G$  then  $(1 + k_r G)^{-1}$  is stable. To prove the BIBO stability of the close loop system of the Fig. 4.4 formed by  $e^{-sd_2}$  and  $\tilde{G}(s)$  it is only necessary to fulfill the condition (iii), since  $|e^{sd_2}| = 1$ , the result follows from *the small gain theorem* [44]. Notice that the condition (iii) can be reduces as:

$$K \left\| \frac{1}{\tau_1 s + 1} \frac{s + 1/\tau_a}{s + 1/\tau_b} \right\|_{\infty} < K \left\| \frac{1}{\tau_1 s + 1} \right\|_{\infty} \left\| \frac{s + 1/\tau_a}{s + 1/\tau_b} \right\|_{\infty} < 1 \quad (4.38)$$

where  $1/\tau_a = (k_r - k_1)/L$  and  $1/\tau_b = (k_r + k_1)/L$ . Notice that,  $\|1/(\tau_1 s + 1)\|_{\infty} = 1$  where, the parameter  $\tau_1$  is a design parameter. As stated above,  $k_1$  and  $k_r$  are selected positive, hence,  $|1/\tau_a| < |1/\tau_b|$ , therefore

$$\left\| \frac{s + 1/\tau_a}{s + 1/\tau_b} \right\|_{\infty} \leq 1 \quad (4.39)$$

Condition (iii) is fulfilled if  $0 \leq K < 1$ .

▽▽▽

In other to show that condition (iii) is fulfilled, that is, the infinite norm in 4.39 is less or equal to one, the Bode plot for  $(s + 1/\tau_a)/(s + 1/\tau_b)$  is shown in Figs.4.5 and 4.6. The gains for this simulation have been chosen as:  $k_1 = 8$  and the value of  $k_r$  is varied from 2 to 20, which include the values that are used in the experimental results shown below.

## 4.4 Experimental results

To show the performance of the proposed controller, a boost-based PFC converter has been designed using the parameters shown in Table 4.1. The PFC is feed by a power supply of 120  $V_{RMS}$ , at a fundamental frequency  $\omega_0 = 377$  rad/s ( $f_0 = 60$  Hz). It has been designed to deliver an output voltage of desired average value  $V_d = 375$  Volts, and a power of 400 W. To show the transient response to load variations, the load resistance is commuted between 500  $\Omega$  and 850  $\Omega$ . The switching

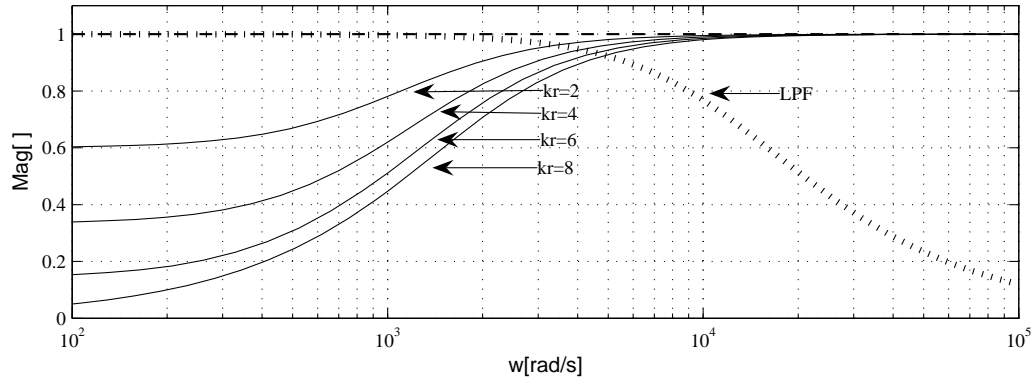


Figure 4.5: Bode plot of  $(s + 1/\tau_a)/(s + 1/\tau_b)$  for different values of  $kr$  to show that their norm is always less than or equal to 1. The Bode plot of  $1/(\tau_1 s + 1)$  is also included where the cutoff frequency of the LPF is fixed to 12 KHz,  $K_1 = 8$  and  $K_r$  is varied from 2 to 8.

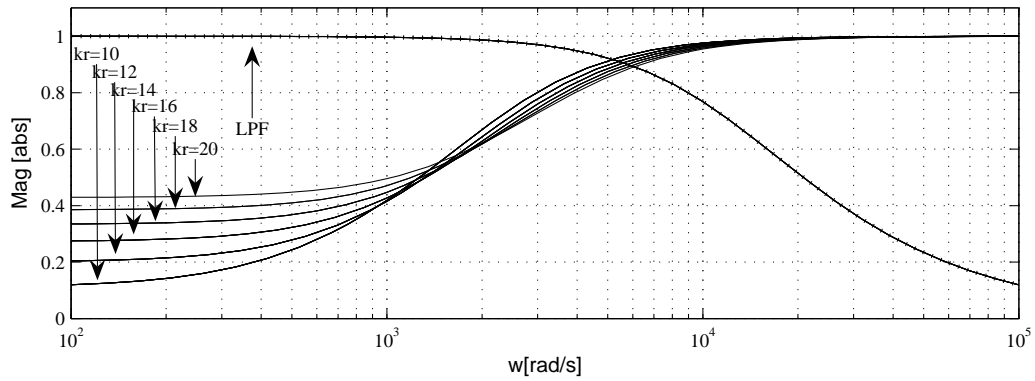


Figure 4.6: Bode plot of  $(s + 1/\tau_a)/(s + 1/\tau_b)$  for different values of  $kr$  to show that their norm is always less than or equal to 1. The Bode plot of  $1/(\tau_1 s + 1)$  is also included where the cutoff frequency of the LPF is fixed to 12 KHz,  $K_1 = 8$  and  $K_r$  is varied from 10 to 20.

frequency of the PWM is fixed to 24 KHz. A fixed point DSP model TMS320LF2407 has been used to implement the controller with a sampling rate fixed to  $f_{DSP} = 24$  kHz. Notice that, the analog implementation of the controller could also be possible.

The time delay has been fixed to  $\pi/\omega_0 = 1/(2f_0) = 1/120 = 8.33$  ms to deal with the odd harmonics of  $f_0 = 60$  Hz. A discrete pure delay of the form  $z^{-d}$  has been used to implement the delay line in the repetitive scheme. Therefore, a  $d = 200$  has been selected to produce the required delay time, i.e.,  $200/24000 = 8.33$  ms for a sampling frequency of 24 kHz. The rest of the control parameters have been fixed to  $k_p = 0.0003$ ,  $k_i = 0.045$ ,  $\tau = 0.001$ ,  $k_1 = 8$ ,  $k_r = 8$ , and  $K = 0.9$ . These parameters have been tuned by trial and error using simulations.

Diode	MUR1560
Power Mosfet	IRFP22N60K
Inductor	8 mH
Capacitor	700 $\mu$ F
Load resistor	500 $\Omega$ , 850 $\Omega$

Table 4.1: Elements used to implement the boost-based PFC converter.

The source voltage  $v_S$  and the magnitude of the magnitude of its FFT are shown in Fig. 4.8. Notice that, this signal is composed of odd harmonics of the fundamental, i.e., 1st, 3rd, 5th, 7th, etc. Hence, the negative feedback repetitive compensator fits perfectly well in this application as it is able to compensate odd harmonics.

The tests performed include steady state responses with and without the harmonic compensation, that is, connecting and disconnecting the repetitive scheme contribution, respectively. The frequency spectrum is included in some cases to exhibit the harmonic content of the signals. Transient responses during step changes in the load resistance between 500  $\Omega$  and 850  $\Omega$ , and back are also included to show the robustness of the proposed controller against load variations.

Figure 4.7 shows the transient response of the output voltage  $v_C$  and the gain  $G$  during a load step change from  $R = 850 \Omega$  to  $R = 500 \Omega$  and back. Notice that, both signals converge towards constants, indeed,  $v_C$  returns to the desired 375 Volts, while  $G$  increases its value for a higher load since it is proportional to the dissipated power.

Figure 4.9 shows that, in the steady state and under the proposed controller, the input current  $i_i$  (middle plot) follows very close the shape of the source voltage  $v_S$  (top plot), and therefore the input current error  $\tilde{i}_i = (i_i - i_i^*)$  (bottom plot) is maintained very close to zero. As a consequence, Fig. 4.10 shows that the input current (bottom plot) has a similar harmonic content as the input voltage  $v_S$  (top plot).

Figure 4.11 compares the input current responses under the harmonic compensation, i.e., with the repetitive scheme connected (top plot), and in the case that only a proportional term is used, i.e., with the repetitive scheme disconnected (bottom plot).

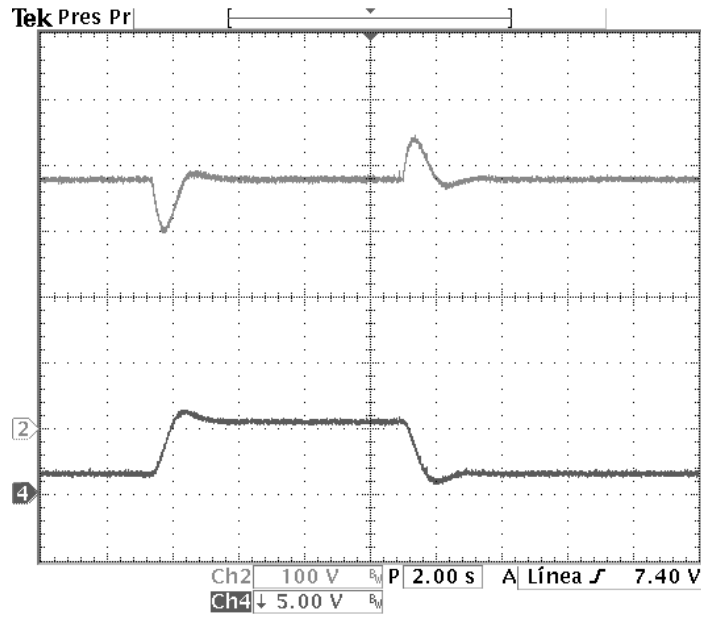


Figure 4.7: Time responses of **(top)** voltage  $v_C$  (y-axis 100 V/div, x-axis 2 s/div), and **(bottom)**  $G$  for a load step change from  $R = 850\Omega$  to  $R = 500\Omega$  and back (y-axis approx. 250 W/div, x-axis 2 s/div).

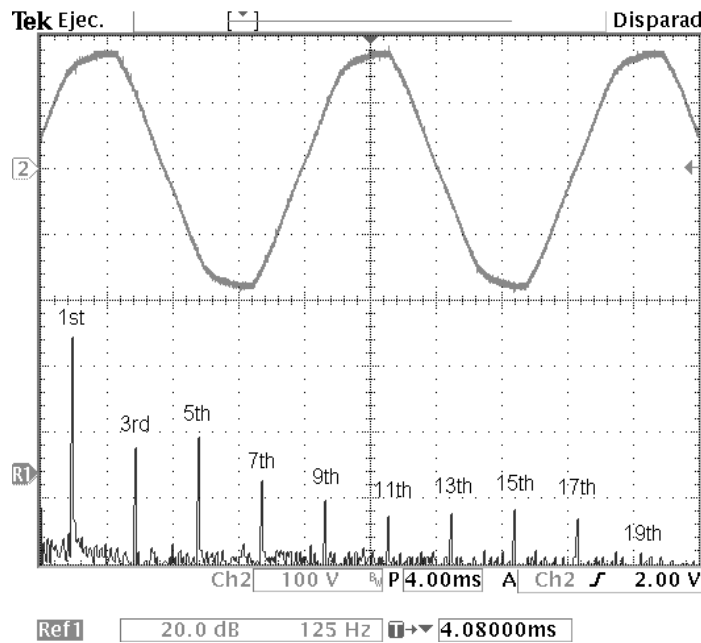


Figure 4.8: **(top)** Source voltage  $v_S$  (y-axis 100 V/div, x-axis 4 ms/div) and **(bottom)** harmonic content of  $v_S$  (y-axis 20 dB/div, x-axis 125 Hz/div).

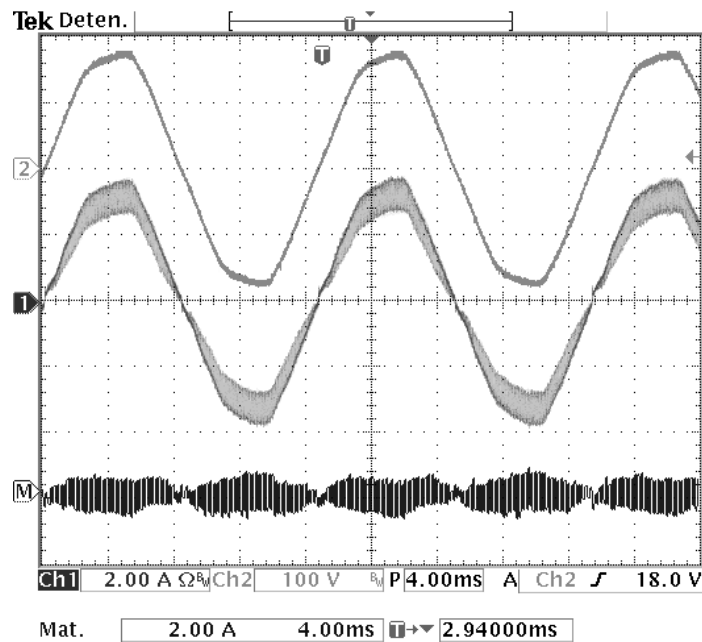


Figure 4.9: (from top to bottom) Source voltage  $v_S(t)$  (y-axis 100 V/div, x-axis 4 ms/div), input current  $i_i(t)$  (y-axis 2 A/div, x-axis 4 ms/div), and input current error  $\tilde{i}_i(t)$  (y-axis 2 A/div, x-axis 4 ms/div), for a load resistance  $R = 500 \Omega$ .

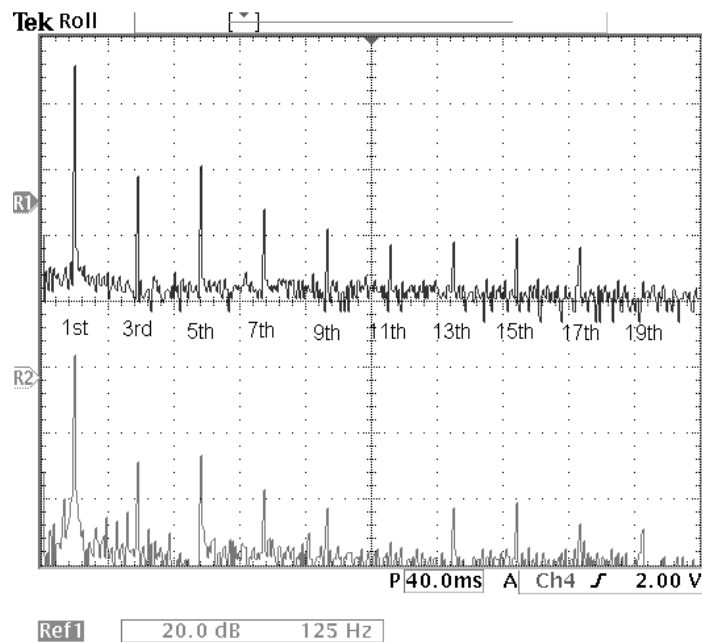


Figure 4.10: Harmonic content of (top) the source voltage  $v_S(t)$  (y-axis 20 dB/div, x-axis 125 Hz/div) and (bottom) the input current  $i_i(t)$  (y-axis 20 dB/div, x-axis 125 Hz/div) under the proposed compensator at a load resistance  $R = 500 \Omega$ .

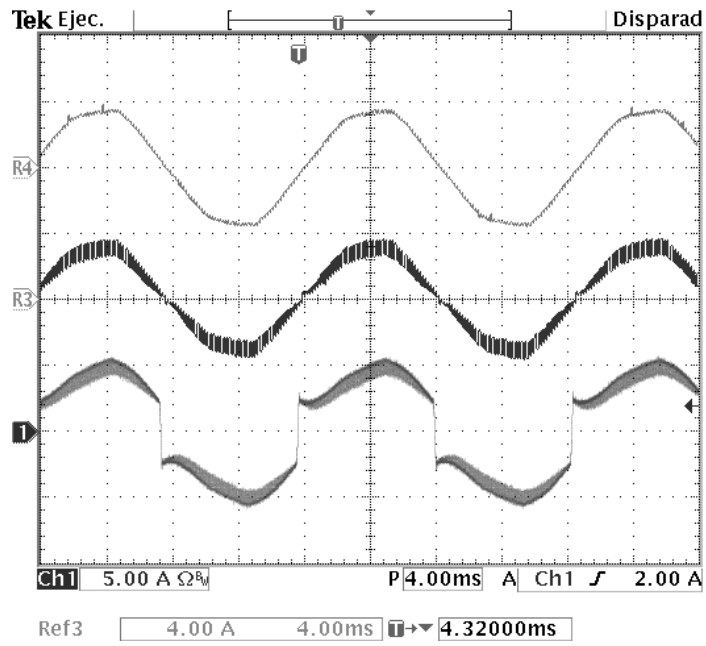


Figure 4.11: Time responses of (from top to bottom) input current reference  $i_i^*(t)$  (y-axis 4 A/div, x-axis 4 ms/div), input current  $i_i(t)$  with harmonic compensation (y-axis 4 A/div, x-axis 4 ms/div), and input current  $i_i(t)$  without harmonic compensation (y-axis 5 A/div, x-axis 4 ms/div), all of them at a load resistance  $R = 500 \Omega$ .



## Chapter 5

# A repetitive controller for a half bridge active filter

---

### *Summary*

This chapter presents a repetitive-based controller for an active filter to compensate reactive power and current harmonic distortion in a single phase system, guaranteeing a power factor close to unity. The half-bridge topology is selected for the active filter consisting of a single branch of two switches plus a branch of two capacitors on the DC side (split DC-capacitor), thus reducing the number of switching devices. The repetitive scheme consists in a negative feedback array plus a feedforward path. In addition, the controller guarantees the regulation and balance of both capacitors voltages. Experimental results are presented to show the performance of the proposed solution.

---

## 5.1 Introduction

The use of electronic equipment drawing highly distorted currents has increased considerably, causing the lowering of the PF. A typical solution for this issue is the use of a power factor correction converter (PFC), which is a system designed to draw sinusoidal current in the source side [4, 56, 57]. This converter substitutes the classical uncontrolled diode-based rectifier commonly found in the power supply of many domestic appliances.

An alternative solution that does not require the redesign of the voltage supply consists in the application of the active filter principle. In this case, an active filter is connected in parallel to the nonlinear load, i.e., the diode-based voltage supply, to inject the distorting harmonic components demanded by the load current. As a result the effect of harmonic distortion due to the nonlinear load can be practically eliminated from the source line. An interesting solution is shown in [61], where a bidirectional DC-DC converter referred as harmonic reducer (HR) is connected in parallel next to the uncontrolled rectifier, i.e. on the DC side. However, a decoupling diode at the load side is also required to guarantee a good performance of the HR. The authors show that, placing such an active filter on the DC side reduces to two the required switches, in contrast to the four switches used in a full-bridge active filter connected on the AC side.

Following with the active filtering idea, the present work shows the use of a single phase shunt active filter connected on the AC side for reactive power and harmonic distortion compensation in the line current. The topology of the active filter used here consists of a half-bridge converter, thus reducing the number of switching devices to two. In return, two capacitors appear on the DC side with their point of common connection grounded, thus maintaining the implementation fairly simple. Moreover, this topology does not require the decoupling diode used in [61], and thus, it is not necessary to make any modification to the power supply.

A controller is proposed for this half-bridge topology to, first, compensate reactive power and current harmonic distortion and, second, to guarantee regulation and balance of both DC-capacitors voltages, simultaneously. It is shown that, the balancing problem can be solved by the introduction of an extra control input that modifies the current reference signal. This extra control input has only effect during the transient, and practically vanishes in the steady state. Moreover, a negative feedback plus feedforward repetitive structure is introduced for the compensation of reactive power and harmonic distortion. This repetitive scheme acts only on the odd harmonics. It is thus expected that, the negative structure based controller will provide better performance and cleaner responses.

The complete controller is composed by the cascade interconnection of a current and a voltage loop. The repetitive scheme appears as a refinement term in the current loop, aimed to compensate the harmonic distortion. In this dissertation, an analog implementation has been selected for the overall controller. Finally, experimental results are provided to assess the performance of the control law.

## 5.2 System Description

In the present chapter the single phase active filter shown in Fig. 5.1 is considered. The model of this system is described by the equations (5.1)-(5.3):

$$L\dot{x}_1 = L\frac{d}{dt}i_0 - (2u - 1)\frac{x_2}{2} - \frac{x_3}{2} + v_S \quad (5.1)$$

$$C\dot{x}_2 = (2u - 1)(x_1 - i_0) - \frac{x_2}{R} \quad (5.2)$$

$$C\dot{x}_3 = (x_1 - i_0) - \frac{x_3}{R} \quad (5.3)$$

$$e = ux_2 + \frac{x_3 - x_2}{2} = u(v_{C1} + v_{C2}) - v_{C2} \quad (5.4)$$

where  $x_1 \triangleq i_S$  is the line current, i.e., the current observed by the source,  $x_2 \triangleq (v_{C1} + v_{C2})$  the sum of the capacitors voltage, and  $x_3 \triangleq (v_{C1} - v_{C2})$  their difference which is a measure of the unbalance;  $i_0(t)$  represents the load current and  $v_S(t)$  the line voltage;  $i(t)$  is the injected current. The parameter  $L$  represents the inductance of the input inductor and  $C$  the capacitance of the DC-side capacitors. It is assumed that both capacitors have the same capacitance. Notice that, both switching devices work in a complementary way. The switch position function  $\delta$  takes values in the set  $\{0, 1\}$ , that is, for  $\delta = 1$  the upper switch is turned on, while for  $\delta = 0$  the lower switch is turned on. For control design purposes, an averaged model is considered instead, therefore the switching position function is replaced by a continuous variable  $u$  which represents the duty

ratio of a PWM (at a relatively high switching frequency) generating the switching sequence  $\delta$ . Variable  $u$  is considered as the control input taking values in the interval  $[0, 1]$ . The injected voltage is represented by  $e$ . Switching and other losses are collected and modelled as unknown constant resistive elements  $R$ .

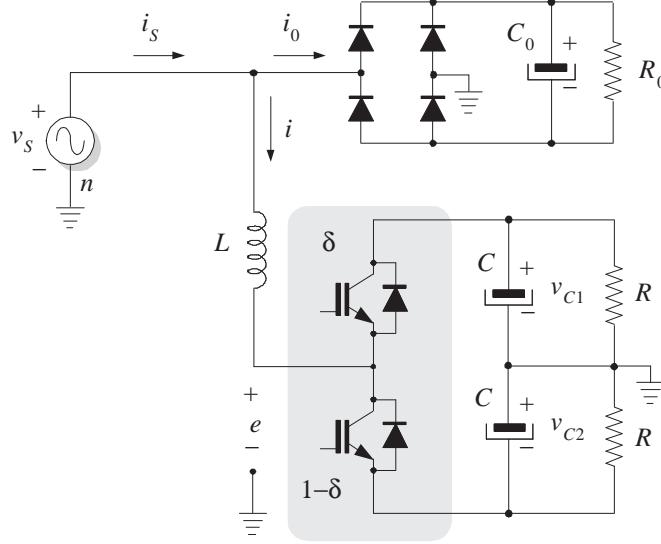


Figure 5.1: Single phase half bridge shunt active filter.

The *control objectives* can be associated to the design of the following three control loops:

(i) A *current tracking control loop* is designed to guarantee the tracking of the line current towards a reference current signal proportional to the line voltage, i.e.,  $x_1 \rightarrow x_1^*$ , in other words, the *same* apparent resistance is observed by the voltage source, which is equivalent to have a power factor close to unity. The current reference is computed as

$$x_1^* = (G/v_{S,RMS}^2)v_S - \zeta \quad (5.5)$$

where the scalar variable  $G/v_{S,RMS}^2$  represents the apparent conductance,  $v_{S,RMS}$  is the RMS value of  $v_S$ , and  $\zeta$  is used as an extra control input aimed to balance the capacitors voltage. Notice that,  $\zeta$  modifies the current reference signal during the transient, however, it vanishes in the steady state as will become clear later. The simple and useful normalization  $G/v_{S,RMS}^2$  prevents  $G$  of taking very small values, which may cause further distortion due to numerical errors.

(ii) A *regulation control loop* drives the sum of the capacitors voltages towards its desired constant reference  $V_d$ , that is,  $x_2 \rightarrow V_d$ . Regulation of these voltages sum is equivalent to guarantee that enough energy has been stored in the capacitors for the correct fulfillment of the previous objective. Out of this control loop, a value for the scalar  $G$  is obtained, which is required to construct the reference  $x_1^*$  as stated above.

(iii) A *balancing control loop* forces the difference of the capacitors voltages to reach zero (at least in average), i.e.,  $x_3 \rightarrow 0$ , in other words, guarantees convergence of both capacitors voltages to the same constant value.

*General assumptions:*

**A1.** [decoupling assumption] It is assumed that, the inductor current dynamics are faster than the capacitor voltage dynamics. Thus based on the time scale separation principle, the control design is split in two parts: a current control loop and a voltage control loop.

**A2.** The load current  $i_0$  and source voltage  $v_S$  are periodic signals that contain higher odd harmonics of the fundamental frequency  $\omega_0 = 2\pi f_0$ , which is considered as a known constant, and have the following Fourier series description.

$$v_S = \sum_{k \in \mathcal{H}} \rho_k^\top V_{S,k}, \quad i_0 = \sum_{k \in \mathcal{H}} \rho_k^\top I_{0,k} \quad (5.6)$$

where

$$\rho_k = \begin{bmatrix} \cos(k\omega_0 t) \\ \sin(k\omega_0 t) \end{bmatrix}, \quad V_{S,k} = \begin{bmatrix} V_{S,k}^r \\ V_{S,k}^i \end{bmatrix}, \quad I_{0,k} = \begin{bmatrix} I_{0,k}^r \\ I_{0,k}^i \end{bmatrix}$$

Numbers  $I_{0,k}^r$ ,  $I_{0,k}^i$ ,  $V_{S,k}^r$  and  $V_{S,k}^i \in \mathbb{R}$  are the  $k^{\text{th}}$  harmonic coefficients of the Fourier series description (also referred as the phasors) of the load current and source voltage, respectively. The harmonic coefficients are assumed to be unknown constants (or slowly varying) and  $\mathcal{H} = \{1, 3, 5, \dots\}$  is the set of indexes of the considered odd harmonic components. Superscripts  $(\cdot)^r$  and  $(\cdot)^i$  are used to distinguish the coefficients associated to  $\cos(k\omega_0 t)$  and  $\sin(k\omega_0 t)$ , respectively.

**A3.** It is assumed that, the system parameters  $L$ ,  $C$  and  $R$  are unknown positive constants. However, a nominal value of this parameters is required for the tuning process of the controller.

## 5.3 Controller design

To facilitate the control design, it is more convenient to rewrite the model (5.1)-(5.3) using the following coordinate transformations  $\varepsilon \triangleq (2u - 1)x_2$ ,  $z_2 \triangleq x_2^2/2$ , which yields

$$L\dot{x}_1 = L \frac{d}{dt} i_0 - \frac{\varepsilon}{2} - \frac{x_3}{2} + v_S \quad (5.7)$$

$$C\dot{z}_2 = (x_1 - i_0)\varepsilon - \frac{2z_2}{R} \quad (5.8)$$

$$C\dot{x}_3 = (x_1 - i_0) - \frac{x_3}{R} \quad (5.9)$$

where  $\varepsilon$  represents the actual control input. The regulation objective becomes now  $z_2 \rightarrow \frac{V_d^2}{2}$ .

### 5.3.1 Inner control loop

The design starts with the inner loop controller. In this case, an adaptive technique is proposed to cancel out a selected group of harmonic components of the disturbance. The idea behind the adaptation is to estimate the frequency domain quantities of the periodic disturbances so they can be cancelled. These adaptations are then reduced, by suitable transformations, to a bank of harmonic oscillators. As already shown in previous chapters, this infinite bank of harmonic oscillators tuned at odd harmonics is equivalent to a negative feedback plus feedforward path repetitive scheme. Therefore, the original bank of harmonic oscillators can be replaced for this fairly simple algorithm.

If the parameters are fully known, case the following controller stabilizes subsystem (5.7) and guarantees that  $x_1$  tracks its desired reference  $x_1^*$ .

$$\varepsilon = 2 \left( -\frac{x_3}{2} + v_S + k_1 \tilde{x}_1 - \phi \right) \quad (5.10)$$

where  $\tilde{x}_1 \triangleq x_1 - x_1^*$ ,  $k_1 > 0$  is a design parameter, and  $\phi \triangleq L \frac{d}{dt}(x_1^* - i_0)$ , which, based on assumption **A1**, can be considered as a harmonic disturbance and thus it can be expressed as

$$\phi = \sum_{k \in \mathcal{H}} \rho_k^\top \Phi_k \quad (5.11)$$

According to assumptions **A2**,  $G$  is considered in the current dynamics as a constant and thus,  $\Phi_k$  ( $k \in \mathcal{H}$ ) can also be considered as an unknown constant. In what follows, it is shown how this term can be estimated by means of adaptation.

Based on the structure of (5.10), the following controller is proposed, where the disturbance has been replaced by its estimate according to (5.11)

$$\varepsilon = 2 \left( -\frac{x_3}{2} + v_S + k_1 \tilde{x}_1 - \sum_{k \in \mathcal{H}} \rho_k^\top \hat{\Phi}_k \right) \quad (5.12)$$

Subsystem (5.7) in closed-loop with controller (5.12) yields the following error dynamics

$$L \dot{\tilde{x}}_1 = -k_1 \tilde{x}_1 + \sum_{k \in \mathcal{H}} \rho_k^\top \tilde{\Phi}_k \quad (5.13)$$

where  $\tilde{\Phi}_k \triangleq \hat{\Phi}_k - \Phi_k$  for every  $k \in \mathcal{H}$ .

The adaptive laws to reconstruct the estimates  $\hat{\Phi}_k$  are obtained by proposing the following energy storage function

$$W = \frac{L}{2} \tilde{x}_1^2 + \sum_{k \in \mathcal{H}} \frac{1}{2\gamma_k} \|\tilde{\Phi}_k\|^2$$

where  $\gamma_k > 0$  is a design parameter. The time derivative of  $W$  along the trajectories of (5.13) is given by

$$\dot{W} = -k_1 \tilde{x}_1^2 + \tilde{x}_1 \sum_{k \in \mathcal{H}} \rho_k^\top \tilde{\Phi}_k + \sum_{k \in \mathcal{H}} \frac{\dot{\tilde{\Phi}}_k^\top \tilde{\Phi}_k}{\gamma_k}$$

which is made negative semidefinite by constructing the estimates according to the following adaptive law

$$\dot{\hat{\Phi}}_k = -\gamma_k \tilde{x}_1 \rho_k, \quad k \in \mathcal{H} \quad (5.14)$$

Given that  $W$  is radially unbounded and  $\dot{W}$  is negative semi-definite, then  $\tilde{x}_1 \in \mathcal{L}_2 \cap \mathcal{L}_\infty$  and  $\tilde{\Phi}_k \in \mathcal{L}_\infty$  for every  $k \in \mathcal{H}$ . From (5.13)  $\dot{\tilde{x}}_1 \in \mathcal{L}_\infty$ . Now, since  $\tilde{x}_1 \in \mathcal{L}_\infty$  and  $\dot{\tilde{x}}_1 \in \mathcal{L}_\infty$ , then  $\tilde{x}_1$  is uniformly continuous, and given that,  $\tilde{x}_1 \in \mathcal{L}_2$  imply that,  $\tilde{x}_1 \rightarrow 0$  asymptotically. Out of this  $\tilde{\Phi}_k^p, \tilde{\Phi}_k^n$  equal constants  $\forall k \in \mathcal{H}$ , however, for  $\tilde{x}_1 = 0$  and from (5.13)  $\sum_{k \in \mathcal{H}} \rho_k^\top \tilde{\Phi}_k = 0$ . Therefore, the only possible solution is  $\tilde{\Phi}_k^p \rightarrow 0$  and  $\tilde{\Phi}_k^n \rightarrow 0$ .

The controller (5.12) with adaptive laws (5.14) can be further simplified using the following transformations

$$\phi_k = \rho_k^\top \hat{\Phi}_k, \quad k \in \mathcal{H} \quad (5.15)$$

$$\psi_k = \rho_k^\top \mathcal{J} \hat{\Phi}_k, \quad k \in \mathcal{H} \quad (5.16)$$

which applying a similar procedure that in Sec. 4.2.1 yields the expression

$$\varepsilon = 2 \left( -\frac{x_3}{2} + v_S + k_1 \tilde{x}_1 + \sum_{k \in \mathcal{H}} \frac{2\gamma_k s}{s^2 + k^2 \omega_0^2} \tilde{x}_1 \right) \quad (5.17)$$

where  $s$  is the complex Laplace variable.

Notice that, harmonic oscillators tuned at odd harmonics have come out, which are aimed to compensate harmonic distortion containing mainly odd components, thus confirming the *internal model principle* [35].

### A. Substitution of the bank of harmonic oscillators by the repetitive scheme

In equation (2.6) of Chapter 2, an equivalence between the previous bank of harmonic oscillators tuned at odd harmonics and the negative feedback plus feedforward path repetitive scheme was established. Therefore, it is proposed to replace the bank of harmonic oscillators by such a repetitive scheme, which will, in principle, reduce considerably the implementation effort. After substitution of the bank of harmonic oscillators by the repetitive scheme, the inner control loop can be rewritten as

$$\varepsilon = 2 \left[ k_1 \tilde{x}_1 + v_S - \frac{x_3}{2} + k_r \left( \frac{1 - K e^{-\frac{s\pi}{\omega_0}}}{1 + K e^{-\frac{s\pi}{\omega_0}}} \right) \tilde{x}_1 \right] \quad (5.18)$$

Notice that, a gain  $k_r$  has been introduced in the repetitive scheme to allow additional control over the gain produced in the resonance peaks. The block diagram of the inner loop (tracking) controller is shown in Fig. 5.2.

Notice that, the BIBO stability analysis of the proposed repetitive-based controller can be study in the same way as in Chapters 3 and 4, where an equivalent representation can be found and the stability proof is developed from Preposition 2.3. For this purpose, only the inner loop is considered, based upon the decoupling assumption **A1**.

## 5.3.2 Voltage control loops

### A. Voltage balance

In what follows, according to the decoupling assumption **A1**, it is assumed that in a relatively short time  $x_1 = x_1^* = (G/v_{S,RMS}^2)v_s - \zeta$ , and  $\hat{\Phi} = \Phi$ . Therefore, subsystem (5.9) can be rewritten as

$$C \dot{x}_3 = (G/v_{S,RMS}^2)v_s - \zeta - i_0 - \frac{x_3}{R}$$

which is a first order linear system perturbed by a harmonic distortion.

As stated above, the objective is to regulate  $x_3$  to zero by means of the extra control input  $\zeta$ . However,  $\zeta$  is a term affecting directly the current reference  $i_S^*$  as shown in (5.5). Therefore, it would be interesting to propose a  $\zeta$  that tends to zero in the steady state. Notice that, introduction of an integral effect is not recommended since it may introduce a DC offset in the current reference, which should be, in principle, a non biased periodical signal in the steady state. In fact, these two requirements cannot be fulfilled completely. In what follows, a controller that keeps the trajectories of both  $x_3$  and  $\zeta$  inside a ball containing the origin is proposed. This controller consists of a simple damping term with limited bandwidth, which improves the low pass filtering capability.

$$\zeta = k_d \eta, \quad \tau_d \dot{\eta} = -\eta + x_3 \quad (5.19)$$

where  $k_d$  is the proportional gain, and  $1/\tau_d$  the cutoff frequency of the LPF. It is clear that, to avoid reinjection of distortion, the real part of the closed loop poles should be kept smaller than the fundamental frequency.

## B. Voltage regulation

As before, according to the decoupling assumption **A1**, subsystem (5.8) can be rewritten as

$$C \dot{z}_2 = 2(x_1^* - i_0) \left( v_S - \frac{x_3}{2} + L \frac{d}{dt} (i_0 - x_1^*) \right) - \frac{2z_2}{R} \quad (5.20)$$

For the sake of simplicity, consider that, a controller is designed in such a way that the dynamics of  $z_2$  are much slower than the the dynamics of  $(x_3, \eta)$ , and thus, it can be assumed that,  $(x_3, \eta)$  reach arbitrarily small values in a relatively short time. Out of this, the system can be further reduced to

$$\frac{C}{2} \dot{z}_2 = \frac{G v_s}{v_{S,RMS}^2} - i_0 v_S - (i_0 - x_1^*) L \frac{d}{dt} (i_0 - x_1^*) - \frac{z_2}{R} \quad (5.21)$$

Notice that, due to the unavoidable harmonic distortion entering in this system, the regulation objective can only be fulfilled in average. Therefore it is proposed to focus in the DC component of (5.21) by applying the moving average function<sup>1</sup> which yields the following system

$$\frac{C}{2} \dot{z}_{20} = G - P_0 - \frac{z_{20}}{R} \quad (5.22)$$

where  $z_{20} = \langle z_2 \rangle_0$  represents the DC part of the state  $\tilde{z}_2$ , and  $P_0 = \langle v_S i_0 \rangle_0$  represents the average output power, which is considered an unknown constant. Moreover, it has been used the fact  $v_{S,RMS}^2 = \langle v_S^2 \rangle_0$ .

**Remark 5.1** As the high harmonic distortion has been neglected, the controller should be proposed with a short bandwidth with the aim of reducing such distortion. This has the disadvantage of making slow the dynamical response of the output capacitor voltage. As the current reference amplitude is modulated by the output voltage loop, then, the current dynamics is affected too.  $\square$

<sup>1</sup>The extraction of the the DC component (or moving average function) of a scalar  $x$  is defined at time  $t$  by the following averaging operation  $\langle x \rangle_0(t) = \frac{1}{T} \int_{t-T}^t x(\tau) d\tau$ .

A controller that guarantees  $z_{20} \rightarrow V_d^2/2$  consists in a proportional plus integral action with limited bandwidth given by

$$G = -k_i \xi - k_p \chi \quad (5.23)$$

$$\dot{\xi} = \left( z_{20} - \frac{V_d^2}{2} \right) \quad (5.24)$$

$$\tau \dot{\chi} = \left( z_{20} - \frac{V_d^2}{2} \right) - \chi \quad (5.25)$$

where  $k_p, k_i$  are the proportional and integral gains of a PI controller, respectively, and  $\tau$  the time constant of a LPF affecting the proportional term.

Relying on the LPF capability of the PI, similar results are obtained if  $z_{20}$  is replaced by  $z_2$ , this yields the following controller which is written in its transfer function form as follows

$$\frac{G(s)}{\tilde{z}_2(s)} = -\frac{k_i}{s} - \frac{k_p}{\tau s + 1} \quad (5.26)$$

where  $\tilde{z}_2 \triangleq (z_2 - \frac{V_d^2}{2})$ .

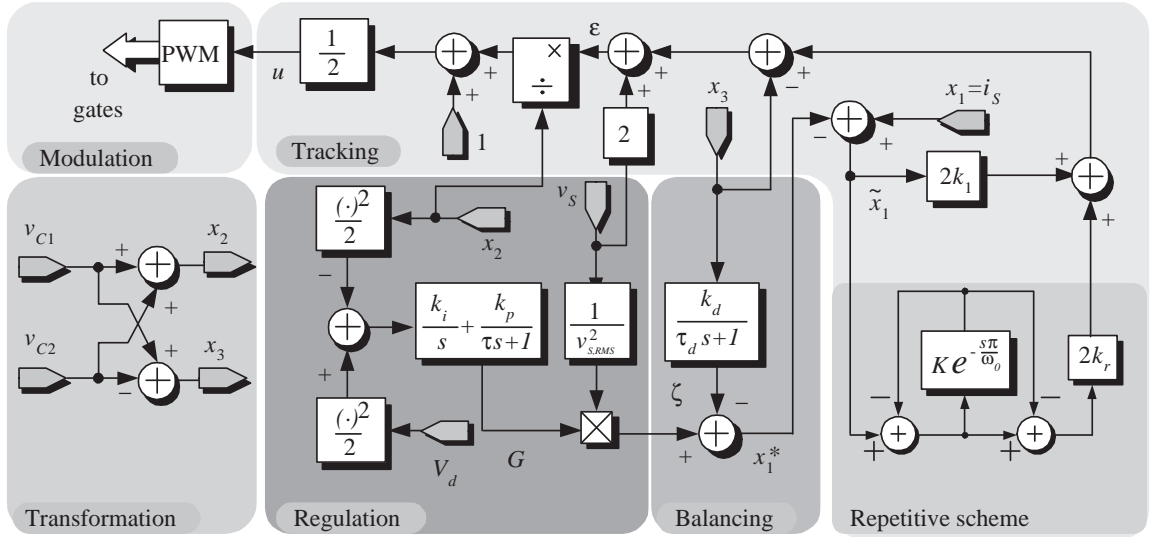


Figure 5.2: Block diagram of the proposed controller.

Summarizing, the expression for the final proposed controller is given by

(i) *Current tracking*

$$u = \frac{1}{2} \left( \frac{\varepsilon}{x_2} + 1 \right) \quad (5.27)$$

$$\varepsilon = 2 \left[ k_1 \tilde{x}_1 + v_S - \frac{x_3}{2} + k_r \left( \frac{1 - K e^{-\frac{s\pi}{\omega_0}}}{1 + K e^{-\frac{s\pi}{\omega_0}}} \right) \tilde{x}_1 \right] \quad (5.28)$$

(ii) *Voltage balance*



$$x_1^* = \frac{Gv_s}{v_{S,RMS}^2} - \frac{k_d x_3}{\tau_d s + 1} \quad (5.29)$$

(iii) Voltage regulation

$$G = - \left( \frac{k_i}{s} + \frac{k_p}{\tau s + 1} \right) \tilde{z}_2 \quad (5.30)$$

where  $\tilde{x}_1 \triangleq (x_1 - x_1^*)$ ,  $\tilde{z}_2 \triangleq (z_2 - \frac{V_d^2}{2})$  and  $z_2 \triangleq \frac{x_2^2}{2}$ .

## 5.4 Experimental results

An academic prototype of low power for the harmonic reducer under study has been implemented to test the performance of the proposed controller. The analog implementation of the proposed controller is shown in Fig. 5.3, and the power stage for the half bridge single phase active filter is shown in Fig. 5.4 . A voltage source of  $12 V_{rms}$  at a frequency of  $f_0 = 60$  Hz ( $\omega_0 = 377$  rad/s) is considered. The load is composed of an uncontrolled diode bridge rectifier feeding a resistive load  $R_0$  which switches between  $25 \Omega$  and  $12.5 \Omega$ , and a capacitor of  $C_0 = 470 \mu F$ . The half bridge topology active filter is constructed with discrete MOSFET transistors, and capacitors of  $C = 4700 \mu F$  each. The active filter is connected to the line by means of an inductor of  $L = 2$  mH. The implementation of the overall controller is performed with analog circuits. The controller parameters have been fixed to  $k_d = 6.7$ ,  $\tau_d = 0.15$ ,  $k_p = 5$ ,  $k_i = 5.5$ ,  $\tau = 0.00125$ ,  $k_1 = 4$ ,  $K = 0.95$  and  $k_r = 1$ . These parameters have been selected by trial and error by means of numerical simulations.

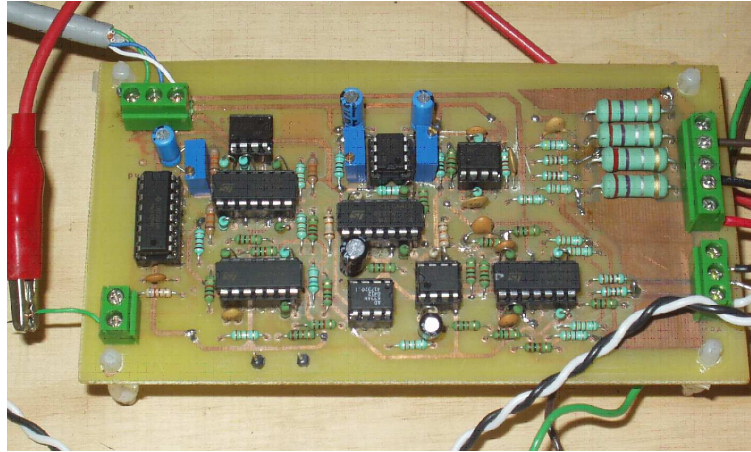


Figure 5.3: The analog implementation of the proposed controller for a half bridge active filter

Figure 5.5 shows that the line current  $i_S$  (middle plot) has a wave form proportional to the voltage source  $v_S$  (top plot). Notice that, the current error (bottom plot) is almost zero in steady state. Notice that, in spite of the slight deformation of the source voltage, the proposed controller accomplishes the tracking objective since the algorithm has been designed to deal with both, the

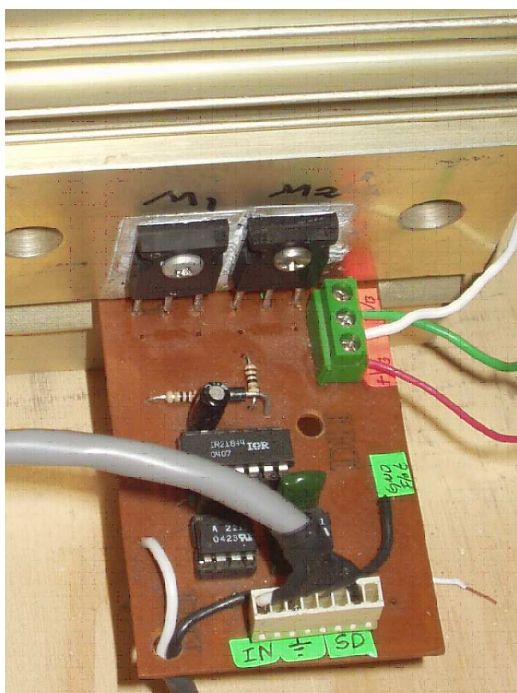


Figure 5.4: Power leg of the half bridge active filter.

deformation in the load current and in the source voltage. As a consequence, the harmonic contents of both,  $v_S$  and  $i_S$  are quite similar, as demonstrated in Fig. 5.6. Notice that, the slight source voltage distortion produces the 3rd, 5th and 7th harmonics.

Figure 5.7 shows the compensated line current  $i_S$  (top plot) as a result of the addition of the injected current  $i$  (generated by the active filter) to the load current  $i_0$  (bottom plot).

Figure 5.8 shows that, both capacitor voltages  $v_{C1}$  and  $v_{C2}$  (top) reach the desired voltage reference set at  $26 V_{DC}$  making a total sum of  $52 V_{DC}$ . The transients are due to changes in the load resistance  $R_0$  going from  $12.5 \Omega$  to  $25 \Omega$  and back. Notice that, the voltages difference  $x_3$  (middle plot) is almost zero with an almost imperceptible transient, therefore, guaranteeing a voltages balance in both capacitors. The bottom plot shows the equivalent conductance  $G/v_{S,RMS}^2$  observed by the source which, as expected, is proportional to the dissipated power in the load. It is important to remark that bigger  $C_0$  would produce a more distorted load current. This highly distorted current might be difficult to compensate because of limitations on the bandwidth of the current controller, as well as physical limitations on the control amplitude. To somehow alleviate this issue it would be necessary to redesign the converter parameters, and perhaps to increase the DC voltage reference.

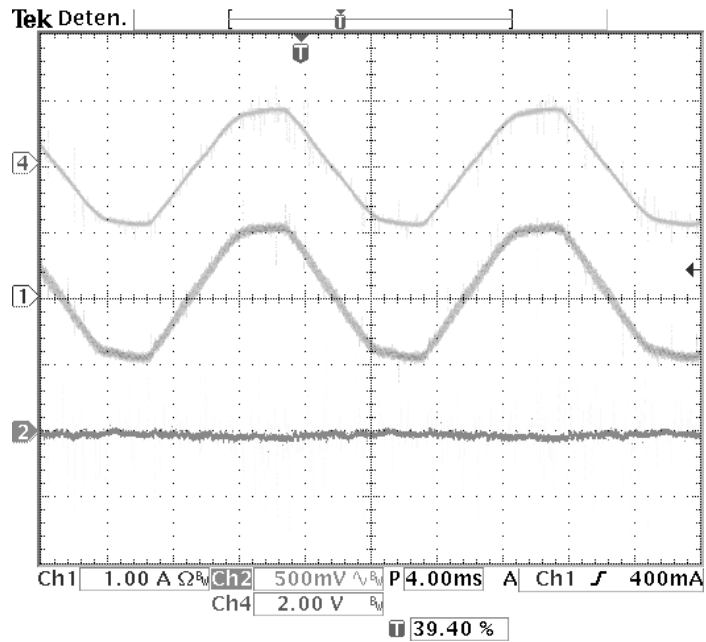


Figure 5.5: Time waveforms of (from top to bottom) line voltage  $v_S$  (real scale 20 V/div), compensated line current  $x_1 = i_S$  (real scale 2.5 A/div), and current error  $\tilde{x}_1$  (real scale 0.5 A/div).

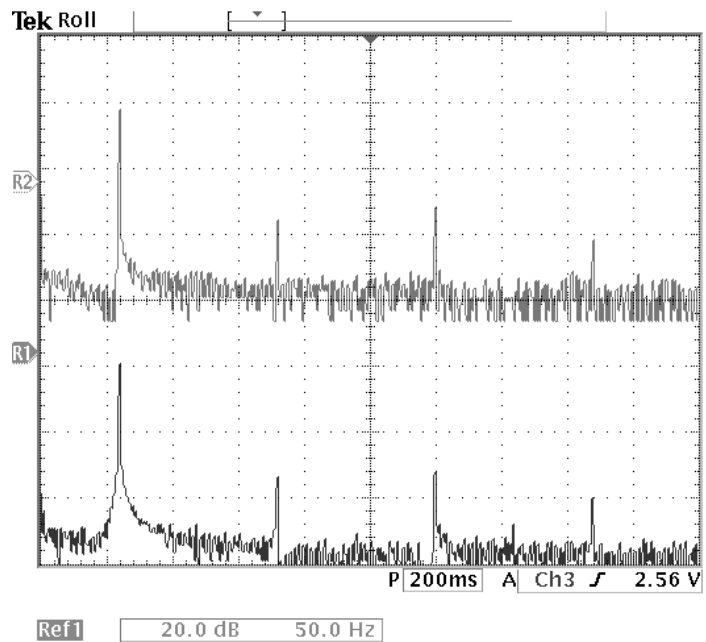


Figure 5.6: (top) Frequency spectrum of  $v_S$  (20 dB/div), and (bottom) frequency spectrum of  $x_1 = i_S$  (20 dB/div).

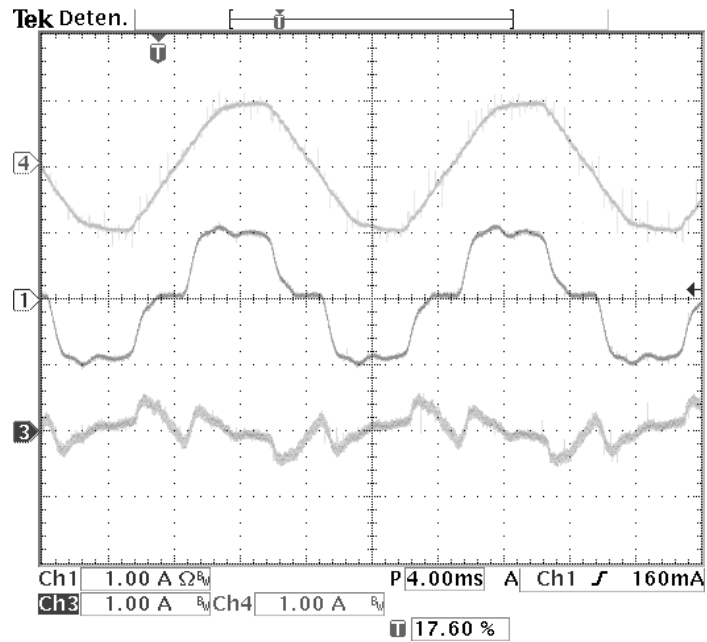


Figure 5.7: Time waveforms of (from top to bottom) compensated line current  $i_S$  (real scale 2.5 A/div), distorted load current  $i_0$  (real scale 2.5 A/div), and injected current  $i$  (real scale 2.5 A/div).

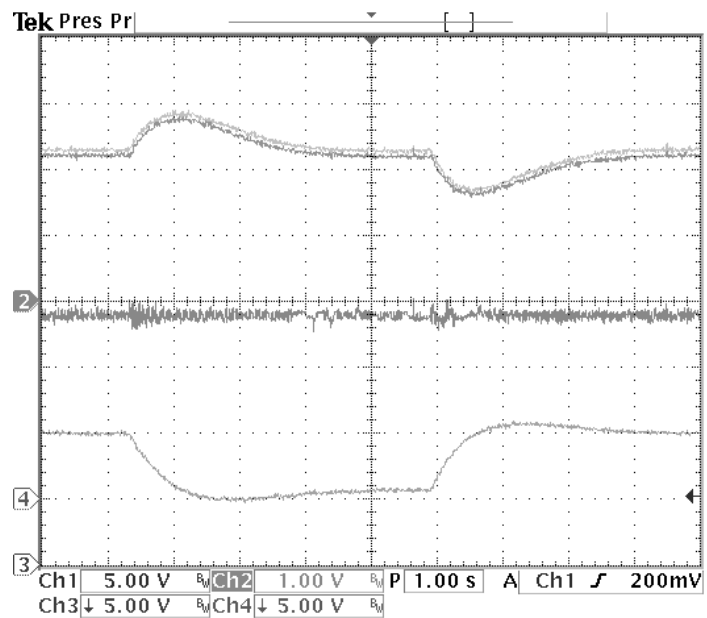


Figure 5.8: Transient responses of (from top to bottom) capacitor voltages  $v_{C1}$  and  $v_{C2}$  (5 V/div), voltages difference  $x_3 = (v_{C1} - v_{C2})$  (1 V/div) and scaled equivalent conductance  $G$  (10 W/div) during load step changes.

## Chapter 6

# A repetitive controller for a single phase active filter

---

### *Summary*

This chapter presents a controller for a single-phase active filter with a repetitive-based control strategy aimed to compensate reactive power and current harmonic distortion. The topology selected for the active filter consists of a single phase full-bridge VSI. Following an adaptive control approach, it is possible to find a control law to compensate the current harmonics. This adaptive control law provides a bank of resonant filters as a refinement term for compensation of selected harmonics, in particular for odd harmonics. The equivalences between a negative scheme of the repetitive compensator, and the bank of resonant filters tuned at odd harmonics found in previous chapters is used here too. The proposed control scheme has been experimentally tested in a 1.5 kVA prototype and the results are presented here.

---

## 6.1 Introduction

Recently, the use of electronic equipment drawing highly distorted current from the AC mains has been increasing considerably, causing low power factor, low efficiency, increasing of EMI, overheat of passive elements, among others. These issues have received special attention in the power electronics and power systems applications, where the disturbances to cancel are composed of specific higher harmonics of the fundamental frequency of the power supply. It is important to remark that the harmonic pollution in the current is basically composed of odd harmonics of the fundamental in single phase AC systems. An interesting solution to alleviate such problems, caused by a distorted load current, is the use of active filters based on VSI. These filters are connected in parallel with the non-linear loads as shown in Fig.6.1. In this type of applications, the active filter is used as a current source which injects the higher harmonic components demanded by the distorted load, thus, eliminating their effect on the source side. In particular, this chapter studies an active filter based on the single phase full bridge topology, which is aimed to compensate for reactive power and current harmonic distortion.

Usually, a decoupled technique is used to design the control of these systems and generally two control loops arise, namely inner and outer loops. Normally, the inner loop controls the current

dynamics while the outer loop guarantees regulation of the voltage level in the capacitors. Thus, the harmonic compensation is performed in the inner loop, where the disturbance rejection problem can be recast as a tracking objective, as will be shown later. It has been reported that conventional techniques [54] and [62], used for active power filters, exhibit a limited achievable performance mainly due to the limited control bandwidth and to the delay caused by the digital implementation. These techniques may even exhibit stability problems due to the high gain techniques used in the inner loop. To overcome such issues, it is proposed here to follow an adaptive approach, just as in the previous chapter, to estimate the unknown system parameters and frequency domain quantities of the periodic disturbance. The adaptive part of this controller is later reduced, by suitable transformations, to a bank of resonant filters. This observation is supported by the well known *internal model principle* [35]. These harmonic oscillators are tuned at selected harmonics, in particular, the odd harmonics, which seem to be the main components of usual single phase nonlinear loads. As it has been shown previously, there is an equivalence between an infinite bank of harmonic oscillators tuned at odd harmonics and a negative feedback plus feedforward repetitive scheme, hence, the bank of oscillators can be replaced by the repetitive scheme. This latter, as discussed previously, represents an interesting and easy to implement solution.

It is important to remark that the proposed control design is based on the measurements of line currents instead of inductance currents as in conventional controllers. This modification is fundamental for the development of the control law, and allows to treat the problem in a more natural way. The resulting controller will have a familiar and simple form which is very similar to the conventional controller, and thus it is suitable for implementation.

## 6.2 Problem formulation

Consider the single-phase active filter shown in Fig. 6.1. The system dynamics are described by (6.1)-(6.2)

$$L \frac{di_S}{dt} = L \frac{d}{dt} i_0 - uv_C + v_S \quad (6.1)$$

$$C \frac{dv_C}{dt} = u(i_S - i_0) - \frac{v_C}{R} \quad (6.2)$$

where parameters  $L$  and  $C$  are the input inductance and DC side capacitance of the active filter, respectively,  $i_S$  is the current in the source,  $v_C$  the capacitor voltage;  $i(t)$  is the injected current;  $i_0(t)$  represents the current load;  $v_S(t)$  the line voltage; and  $u(t)$ , which takes values in the discrete set  $\{-1, 0, 1\}$ , denotes the switch position function and acts as the control input, that is, for  $u = 1$  transistors  $Q_1$  and  $Q_4$  are turned on, while transistors  $Q_2$  and  $Q_3$  are turned off, and the opposite for  $u = -1$ . Moreover, for  $u = 0$ , either,  $Q_1$  and  $Q_2$  are both on, or  $Q_3$  and  $Q_4$  are both on. The term  $R$  is a resistive element modeling the switching and other losses in the system, it is considered an unknown constant.

The *control objectives* for the single phase full bridge active filter are:

(i) *Tracking of the source current* towards a reference current signal proportional to the line voltage, that is,  $i_S \rightarrow i_S^* = \eta v_S$ , where  $i_S^*$  represents the current reference, with  $\eta$  a scalar representing the apparent conductance observed by the source. This is equivalent to seek for a power factor close to unity.

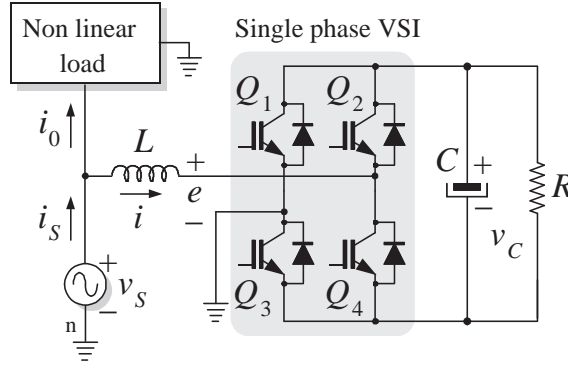


Figure 6.1: Single phase full-bridge shunt active filter.

(ii) *Regulation of the capacitor voltage* towards a desired constant reference  $V_d$ , that is,  $v_C \rightarrow V_d$ . This condition guarantees that enough energy has been stored in the capacitor for the correct fulfillment of the previous objective.

*Main assumptions:*

**A1.** For controller design purposes, the averaged model is considered, i.e., the control input  $u$  is considered as a continuous signal taking values in the range  $[-1, 1]$ .

**A2.** It is assumed that the controller design is performed in such a way that, in the closed loop, the inductor current dynamics are faster than the capacitor voltage dynamics. Therefore, and maintaining the time scales of both dynamics sufficiently separated (at least ten times), it is possible to split the control design in two loops, an inner current loop and an outer voltage loop. This is referred as the decoupling assumption, since both dynamics can be treated separately. Evidently this restriction will impose limitations on the control parameters.

**A3.** The load current  $i_0$  and source voltage  $v_S$  are periodic signals that contain higher odd harmonics of the fundamental frequency  $\omega_0 = 2\pi f_0$ . They can be described by their Fourier series as follows

$$v_S = \sum_{k \in \mathcal{H}} \rho_k^\top V_{S,k}, \quad i_0 = \sum_{k \in \mathcal{H}} \rho_k^\top I_{0,k} \quad (6.3)$$

where

$$\rho_k = \begin{bmatrix} \cos(k\omega_0 t) \\ \sin(k\omega_0 t) \end{bmatrix}, \quad V_{S,k} = \begin{bmatrix} V_{S,k}^r \\ V_{S,k}^i \end{bmatrix}, \quad I_{0,k} = \begin{bmatrix} I_{0,k}^r \\ I_{0,k}^i \end{bmatrix}$$

Notice that, the values  $I_{0,k}^r$ ,  $I_{0,k}^i$ ,  $V_{S,k}^r$  and  $V_{S,k}^i \in \mathbb{R}$  are the  $k^{\text{th}}$  harmonic coefficients of the Fourier series, and  $\omega_0$  represents the fundamental frequency considered as a known constant.

The harmonic coefficients in both series are assumed unknown constants (or sufficiently slow variables). Furthermore,  $\mathcal{H} = \{1, 3, 5, 7, \dots\}$  is the set of indexes of the considered harmonic components present in the load current and source voltage. Superscripts  $(\cdot)^r$  and  $(\cdot)^i$  are used to distinguish the relation of the coefficient with the  $\cos(k\omega_0 t)$  and  $\sin(k\omega_0 t)$ , respectively.

**A4.** It is also assumed that the system parameters  $L$ ,  $C$  and  $R$  are unknown positive constants, although a nominal value for them is required for the tuning process of the control parameters.

### 6.2.1 Inner control loop

In this subsection, a controller which guarantees tracking of  $i_S$  towards its desired reference  $i_S^*$  is designed. For the control design purpose, it is more convenient to rewrite the model (6.1)-(6.2) using the following coordinate transformations

$$x_1 = i_S, \quad x_2 = \frac{v_C^2}{2}, \quad e = uv_C$$

After these transformations, the model can be rewritten as

$$L\dot{x}_1 = L\frac{d}{dt}i_0 - e + v_S \quad (6.4)$$

$$C\dot{x}_2 = e(i_S - i_0) - \frac{2x_2}{R} \quad (6.5)$$

where  $e$ , the injected voltage, represents the actual control input. Notice that, to accomplish the twofold control objective,  $x_1$  should track the reference  $x_1^* = \eta v_S$  while  $x_2$  should be driven towards  $V_d^2/2$ .

It is straightforward to show that the following control law guarantees a stable tracking of subsystem (6.4)

$$e = L\frac{d}{dt}(i_0 - x_1^*) + v_S + k_1\tilde{x}_1 \quad (6.6)$$

where  $\tilde{x}_1 = x_1 - x_1^*$  represents the current error, and  $k_1 > 0$  is a constant design parameter.

It is important to remark that the inductance value  $L$  and the  $\frac{d}{dt}(i_0)$  are required to implement the above control law. However, as  $L$  and the load current time derivative are considered unknown, then it is proposed to estimate the disturbance term  $L\frac{d}{dt}(i_0 - x_1^*)$  by means of adaptation. As shown below, the estimation can be considerably simplified if the disturbances are expressed as Fourier series.

Using (6.3) it is possible to express the disturbances of the system as

$$L\frac{d}{dt}(i_0 - x_1^*) = \sum_{k \in \mathcal{H}} \rho_k^\top \Phi_k \quad (6.7)$$

where it has been defined  $\Phi_k \triangleq L(\dot{g} - k\omega_0 g \mathcal{J})V_{S,k} + Lk\omega_0 \mathcal{J}I_{0,k}$  ( $k \in \mathcal{H}$ ) and the following matrix rotation has been used.

$$\mathcal{J} = -\mathcal{J}^\top = \begin{bmatrix} 0 & -1 \\ 1 & 0 \end{bmatrix} \quad (6.8)$$

The time derivatives of the load current and supply voltage are given by

$$\dot{v}_S = -\sum_{k \in \mathcal{H}} k\omega_0 \rho_k^\top \mathcal{J}V_{S,k}, \quad \frac{di_0}{dt} = -\sum_{k \in \mathcal{H}} k\omega_0 \rho_k^\top \mathcal{J}I_{0,k}$$

According to the decoupling assumption, vector  $\Phi_k$  ( $k \in \mathcal{H}$ ) converges towards a constant<sup>1</sup>. It is then proposed to use an estimate  $\hat{\Phi}_k$  in the control expression (6.6) instead of the term  $\Phi_k$ . This

<sup>1</sup>Ideally  $g$  and  $\dot{g}$  should vary slowly and take constant values in steady state.



yields the controller

$$e = v_S + k_1 \tilde{x}_1 + \sum_{k \in \mathcal{H}} \hat{\Phi}_k \quad (6.9)$$

The error dynamics of subsystem (6.4) in closed loop with controller (6.9) can be expressed as follows

$$L \dot{\tilde{x}}_1 = \sum_{k \in \mathcal{H}} \rho_k^\top \tilde{\Phi}_k - k_1 \tilde{x}_1 \quad (6.10)$$

where  $\tilde{\Phi}_k \triangleq \hat{\Phi}_k - \Phi_k$  for every  $k \in \mathcal{H}$  represent the estimation errors.

Based on the structure of the error function (6.10) (see (4.11) and (5.13)), a similar procedure as in previous chapters can be followed here, that is, an energy storage function  $W$  is proposed as follows

$$W = \frac{L}{2} \tilde{x}_1^2 + \sum_{k \in \mathcal{H}} \frac{1}{2\gamma_k} \left[ \left( \tilde{\Phi}_k^r \right)^2 + \left( \tilde{\Phi}_k^i \right)^2 \right]$$

The time derivative of  $W$  along the trajectories of (6.10) yields

$$\dot{W} = -k_1 \tilde{x}_1^2 + \tilde{x}_1 \sum_{k \in \mathcal{H}} \rho_k^\top \tilde{\Phi}_k + \sum_{k \in \mathcal{H}} \frac{\dot{\tilde{\Phi}}_k^\top \tilde{\Phi}_k}{\gamma_k}$$

which is made negative semidefinite by proposing the following adaptive laws

$$\dot{\tilde{\Phi}}_k = -\gamma_k \tilde{x}_1 \rho_k, \quad k \in \mathcal{H} \quad (6.11)$$

where  $\gamma_k > 0 \forall, k \in \mathcal{H}$  are design parameters.

The proof of convergence and stability is not included here, as it follows a similar procedure as that presented previously for the PFC and half bridge active filter in Chapters 4 and 5, respectively.

The following transformations are used to further simplify the controller (6.9) and adaptations (6.11).

$$\begin{aligned} \Psi_k^r &= -\rho_k^\top \hat{\Phi}_k, \quad k \in \mathcal{H} \\ \Psi_k^i &= -\rho_k^\top \mathcal{J} \hat{\Phi}_k, \quad k \in \mathcal{H} \end{aligned}$$

After these transformations, the controller (6.9) is reduced to

$$e(s) = \sum_{k \in \mathcal{H}} \Psi_k^r + v_S + k_1 \tilde{x}_1 \quad (6.12)$$

where the adaptive laws can be rewritten as

$$\dot{\Psi}_k^r = \gamma_k \tilde{x}_1 - k\omega_0 \Psi_k^i, \quad k \in \mathcal{H} \quad (6.13)$$

$$\dot{\Psi}_k^i = k\omega_0 \Psi_k^r, \quad k \in \mathcal{H} \quad (6.14)$$

Expressing the adaptive laws in the form of transfer functions  $\tilde{x}_1 \mapsto \Psi_k^r$  ( $k \in \mathcal{H}$ ) yields

$$\Psi_k^r(s) = \frac{\gamma_k s}{s^2 + k^2 \omega_0^2} \tilde{x}_1(s), \quad k \in \mathcal{H} \quad (6.15)$$

Summarizing, the expression for the inner current controller is given by

$$e(s) = k_1 \tilde{x}_1 + v_S + \left( \sum_{k \in \mathcal{H}} \frac{2\gamma_k s}{s^2 + k^2 \omega_0^2} \tilde{x}_1 \right) \quad (6.16)$$

Clearly, the interesting part in the inner loop is the bank of resonators tuned at odd frequencies ( $\mathcal{H} = \{1, 3, 5, 7, \dots\}$ ) of the fundamental  $\omega_0$ , each with an associated gain  $\gamma_k$ ,  $k \in \mathcal{H}$ . As it has been done in previous chapters, the bank of resonant filters inside the parenthesis are equivalent to a negative feedback plus feedforward repetitive compensator, and thus, the former can be replaced by the repetitive scheme ensuring a similar performance.

After substitution of the bank of harmonic oscillators by the repetitive scheme, the inner control loop can be rewritten as follows:

$$\varepsilon = k_1 \tilde{x}_1 + v_S + k_r \left( \frac{1 - K e^{-\frac{s\pi}{\omega_0}}}{1 + K e^{-\frac{s\pi}{\omega_0}}} \right) \tilde{x}_1 \quad (6.17)$$

Notice that, the gain  $\gamma_k$  is fixed as  $\gamma_k = 4\omega_0/\pi$ , where, the gain  $k_r$  in the repetitive scheme allows additional control over the gain produced by the resonant peaks.

A block diagram of the inner current control loop is shown in Fig. 6.2(a), where a LPF of the form  $F(s) = K/(\tau s + 1)$  is proposed according to the practical modifications suggested in Chapter 2, in particular in Sections 2.2 and 2.3, respectively. In Fig. 6.2 (b) an equivalent block diagram is shown, where  $\xi = i_0 - i_S^*$  and  $i$  represent the injected output current. Notice that the block diagram of Fig. 6.2b has the same structure of the system in Fig. 2.16 used to study the BIBO stability in Chapter 2. In fact, it is easy to show that this system satisfies all conditions of Proposition 2.3, and thus it is BIBO stable.

## 6.2.2 Outer control loop

As pointed out before, it is considered that the dynamics of subsystem (6.1) are much faster than the dynamics of subsystem (6.2), and moreover, that the controller  $e$  is bounded, which is true if all terms  $\hat{\Phi}_k$  ( $\forall k \in \mathcal{H}$ ) are bounded. Thus, in a relatively short time  $\tilde{x}_1 = 0$  and  $\hat{\Phi}_k = \Phi_k$ ,  $\forall k \in \mathcal{H}$ . Hence, subsystem (6.5) can be written in terms of the reference error for  $x_2$  as

$$\begin{aligned} C\dot{\tilde{x}}_2 &= \left( L \frac{d}{dt} (i_0 - x_1^*) + v_S \right) (x_1^* - i_0) - \frac{2x_2}{R} = \\ &= \eta v_S^2 - v_S i_0 - L \frac{d}{dt} (i_0 - x_1^*) (x_1^* - i_0) - \frac{2x_2}{R} \end{aligned} \quad (6.18)$$

where the quadratic error of the capacitor voltage is represented and defined as  $\tilde{x}_2 \triangleq (x_2 - \frac{V_d^2}{2})$ .

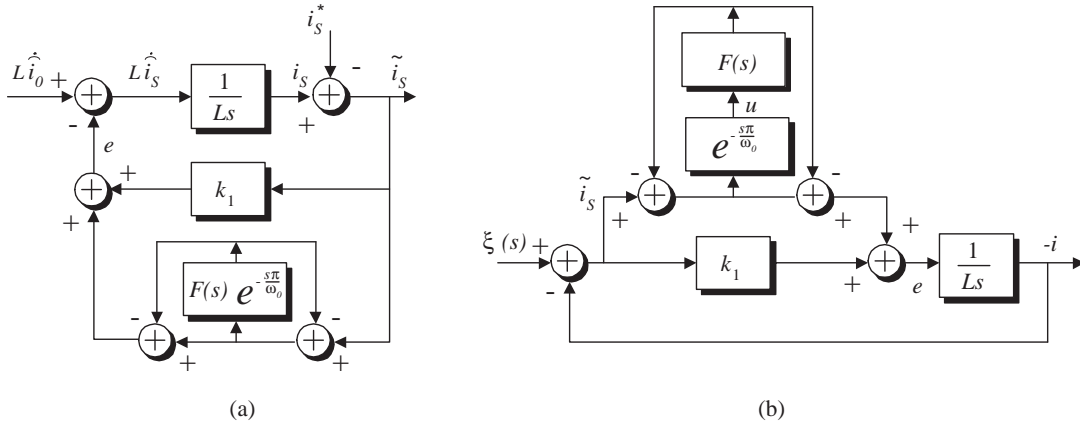


Figure 6.2: Block diagram of the inner control loop.

Moreover, since the main interest is about the behavior of the dynamics of the DC component of  $\tilde{x}_2$ . This component is extracted from (6.18) by applying a moving average function to subsystem (6.18). The so-called DC model of the dynamics of the capacitor voltage is given by

$$C\dot{\tilde{x}}_{20} = \eta v_{S,RMS}^2 - p_0 - \frac{2x_{20}}{R}$$

where  $\tilde{x}_{20}$  represents the DC component of state  $x_2$ ; the extraction of the DC component of a scalar  $x$  is defined at time  $t$  by the following averaging operation  $\langle x \rangle_0(t) = \frac{1}{T} \int_{t-T}^t x(\tau) d\tau$ . Therefore,  $p_0 = \langle v_S i_0 \rangle_0$  represents the average output power, considered as an unknown constant, while  $v_{S,RMS}^2 = \langle v_S^2 \rangle_0$  is the square of the RMS value of  $v_S$  which is also a constant.

Similar to the PFC in Chapter 2, it is proposed to compute the current reference  $x_1^*$  as follows

$$x_1^* = \delta \left( \frac{v_S}{v_{S,RMS}^2} \right) \quad (6.19)$$

which is equivalent to make the following transformation in our developments

$$\delta = \eta v_{S,RMS}^2$$

It has been observed that this simple transformation keeps the values of most variables on the same order, and thus reduces the risk of numerical errors since the value of  $\eta$  is usually very small.

The error model can be rewritten as

$$C\dot{\tilde{x}}_{20} = \delta - p_0 - \frac{2x_{20}}{R} \quad (6.20)$$

A controller that guarantees  $\tilde{x}_{20} \rightarrow 0$  is

$$\dot{\delta} = -k_i \xi - k_p \zeta \quad (6.21)$$

$$\dot{\xi} = \tilde{x}_{20} \quad (6.22)$$

$$\tau \dot{\zeta} = \tilde{x}_{20} - \zeta \quad (6.23)$$

where  $k_p$ ,  $k_i$  are the proportional and integral gains of a PI controller, and  $\tau$  the time constant of a LPF.

Relying in the filtering capability of such a PI controller, it is proposed to use  $x_2$  instead of  $x_{20}$  for the control implementation. The controller (6.21)-(6.23) can thus be rewritten in the form of a transfer function as follows

$$\frac{\delta(s)}{\tilde{x}_2(s)} = -\frac{k_i}{s} - \frac{k_p}{\tau s + 1} \quad (6.24)$$

Summarizing, the overall proposed controller is given by

$$e = k_1 \tilde{x}_1 + v_S + k_r \left( \frac{1 - K e^{-\frac{s\pi}{\omega_0}}}{1 + K e^{-\frac{s\pi}{\omega_0}}} \right) \tilde{x}_1 \quad (6.25)$$

$$\delta = -\left( \frac{K_i}{s} + \frac{K_p}{\tau s + 1} \right) \tilde{x}_2 \quad (6.26)$$

$$x_1^* = \delta \frac{v_S}{v_{S,RMS}^2} \quad (6.27)$$

where a gain  $k_r$  has been included to have control over the gain produced in the resonant peaks. The block diagram of the overall proposed repetitive-based controller is shown in Fig. 6.3. Notice that, the bank of resonant filters has been replaced by the proposed repetitive scheme.

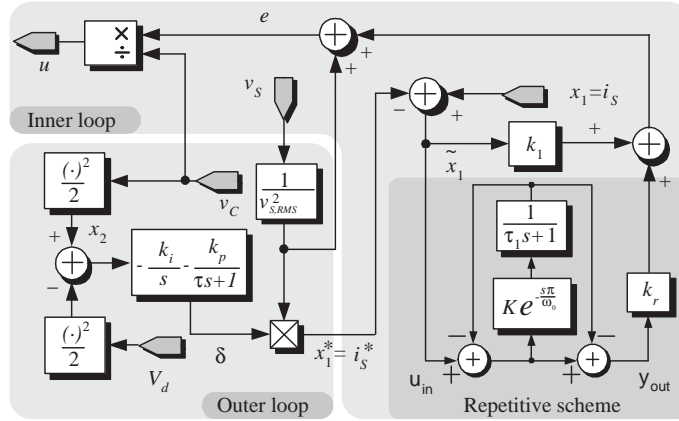


Figure 6.3: Block diagram of the proposed repetitive-based controller.

### 6.3 Experimental results

To test the proposed controller, a prototype of 1.5 KVA of a single phase shunt active filter was designed. The complete prototype is shown in Fig.6.4. The prototype is connected to a voltage source of 127 V<sub>RMS</sub>,  $f_0=60$  Hz ( $\omega_0=377$  rad/s) with a THD of 4.8%. The nonlinear load is composed of a diode bridge based rectifier connected in parallel with a resistor load of 100  $\Omega$ . The latter is included to increase the amplitude of the load current without increasing the distortion, as the resistor adds only a sinusoidal component. The diode bridge based rectifier contains a DC capacitor of 330  $\mu$ F feeding a resistor of either, 40  $\Omega$  or 80  $\Omega$ . The nonlinear load produces a distorted current containing all odd harmonics of the fundamental frequency (60Hz). The active filter has been designed

with the following parameter values:  $L = 4$  mH,  $C = 6800$   $\mu$ F,  $R = 22$  k $\Omega$ . This  $R$  is used to safely discharge the capacitor. A fixed point digital signal processor TMS320LF2407A from Texas Instruments has been used to implement the controller. Sampling and switching frequencies are fixed to 24 kHz. A discrete pure delay of the form  $z^{-d}$  has been used to implement the delay line in the repetitive scheme. Therefore, a  $d = 200$  produces the required delay time (to compensate the odd harmonics of 60 Hz), i.e.,  $200/24000 = 8.33$  ms for a sampling frequency of 24 kHz. That is, a stack of 200 memory locations has been reserved to generate a required delay. The other control parameters are fixed to  $k_p = 0.018$ ,  $k_i = 0.01$ ,  $k_1 = 10$ ,  $K = 0.944$  and  $k_r = 0.75$ . All these control parameters have been obtained by trial and error using a numerical simulation.



Figure 6.4: Prototype of single Phase active filter

Figure 6.5 shows (from top to bottom) the steady state responses of the source voltage, compensated line current, load current and injected current. This figure shows that the compensated line current  $i_S(t)$  presents a proportional wave form to the voltage supply  $v_S(t)$ , despite of the highly distorted load current  $i_0(t)$  (47% of THD). Notice that, even though the voltage source has a slight deformation corresponding to the 4.8% of THD, as mentioned above, the proposed algorithm has been designed to deal with the deformation in both, the load current and the voltage source .

Figure 6.6 shows (from top to bottom) the source voltage  $v_S$ , the line current  $i_S$  with harmonic compensation (including the repetitive scheme), and the line current  $i_S$  without harmonic compensation. Notice that, there is a considerable improvement in the current wave form when the repetitive scheme is introduced.

Figure 6.7 shows the transient responses of the capacitor voltage  $v_C$  and scaled apparent conductance  $\delta = v_{S,RMS}^2 \eta(t)$  when the load in the diode bridge rectifier is changed from  $80\Omega$  to  $40\Omega$  and back to  $80\Omega$ . It is shown that after a relatively small transient, the capacitor voltage  $v_C(t)$  converges towards its reference  $250 V_{DC}$ , while the scaled apparent conductance  $\delta(t)$  reaches (in average) a constant value which depends on the load characteristics.

Figure 6.8 shows the spectrum of the compensated current  $i_S$  in comparison with the spectrum of the line voltage  $v_S$ . It is shown that, as expected,  $i_S$  has a similar harmonic content as  $v_S$ , which is mainly composed by a fundamental harmonic. The compensated current reaches a THD of 6%, compared to the 4.8% of THD in the line voltage and the 47% of THD in the load current.

**Remark 6.1** As established in the control objective, the line current is forced to track a waveform proportional to the supply voltage, therefore, the compensated current should be as distorted as the source voltage. Clearly, the harmonics of the compensated current are similar to the harmonic content of the supply voltage. Therefore, with the fulfillment of the control objective, current harmonics are reinjected into the grid. This is preferred here to exhibit the ability of the proposed controller to deal with distortion in the supply voltage. An alternative objective to avoid the reinjection of current harmonics consists in simply taking the fundamental component of the supply voltage to build the current reference.  $\square$

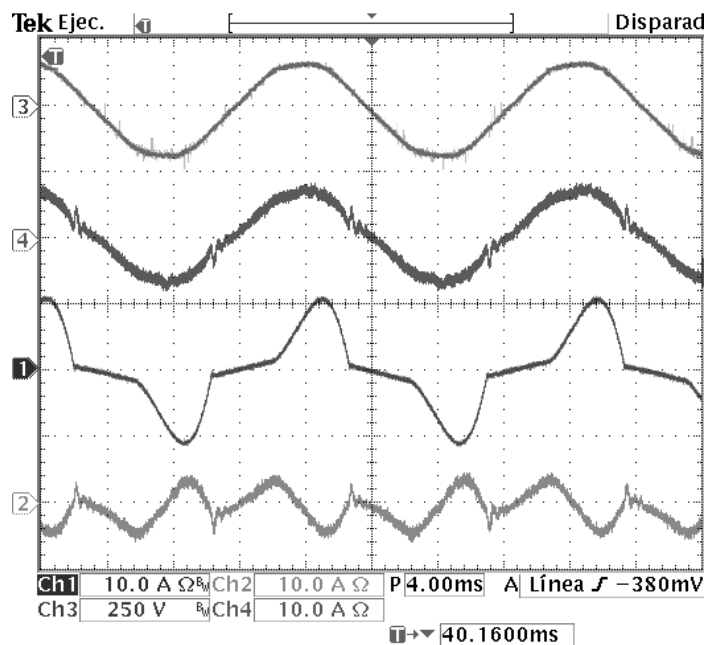


Figure 6.5: Time responses with the proposed controller of: (from top to bottom) line voltage  $v_S(t)$  (250 V/div), compensated current  $i_S(t)$  (10 A/div), current load  $i_0(t)$  (10 A/div), and injected current  $i(t)$  (10 A/div).

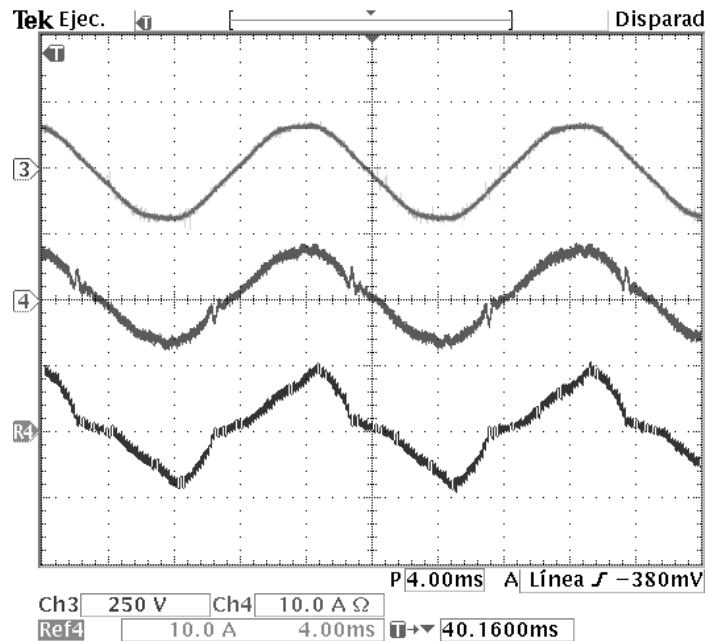


Figure 6.6: (from top to bottom) Source voltage  $v_S(t)$  (250 V/div), source current  $i_S(t)$  with harmonic compensation (10 A/div), and source current  $i_S(t)$  without harmonic compensation (10 A/div).

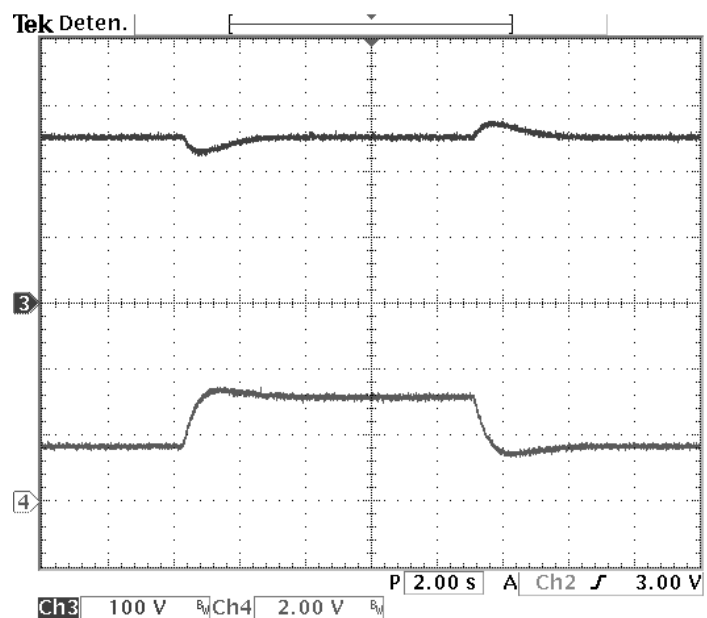


Figure 6.7: Transient responses during a load step change of (top) capacitor voltage  $v_C(t)$  (100 V/div), and (bottom) scaled apparent conductance  $\delta(t) = v_{S,RMS}^2 \eta(t)$  observed by the source (500 W/div).

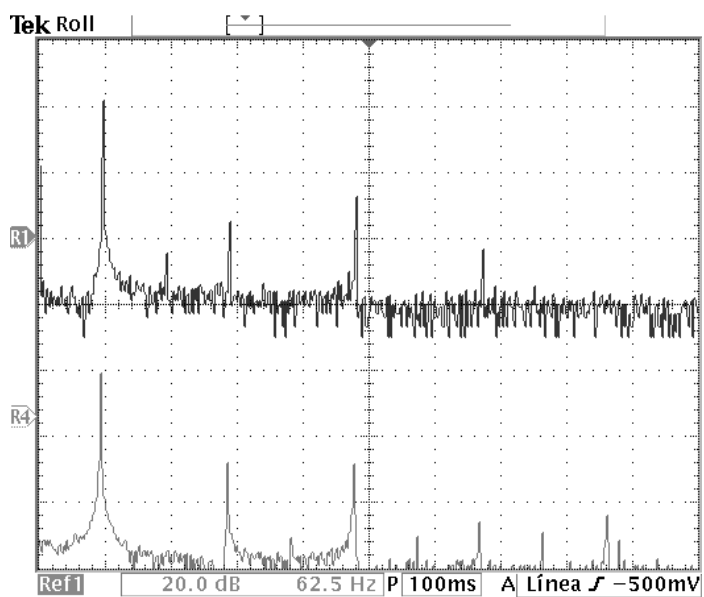


Figure 6.8: Spectra of **(top)** the line voltage  $v_S$  (20 dB/div), and **(bottom)** the compensated current  $i_S$  (20 dB/div).



## Chapter 7

# Concluding remarks and future work

### 7.1 Concluding remarks

The present dissertation work was interested in the solution of the harmonic compensation issue in different power electronics systems. For this purpose, the problem of harmonic compensation was recast as a tracking problem, where the disturbance signal was assumed as a periodical signal. To facilitate the study, the disturbance was expressed as a Fourier series composed by an infinite number of terms, referred as harmonic components. The methodology for the solution of this problem was based originally on adaptive techniques. Several remarks of interest are highlighted next:

- ▷ The adaptations proposed to compensate the periodic disturbances could be transformed, by suitable rotations, into a bank of resonant filters, which was in agreement with the *internal model principle*.
- ▷ An infinite bank of resonant filters tuned at odd harmonics was equivalent to a hyperbolic tangent function, which is equivalent to the proposed negative feedback repetitive scheme .
- ▷ An infinite bank of resonant filters tuned at every single multiple of the fundamental frequency, including the dc component, was equivalent to a hyperbolic cotangent function, which is equivalent to the proposed positive feedback repetitive scheme.
- ▷ Implementation of these control schemes were based on a feedback array of a simple transport delay. In contrast to conventional schemes, the two proposed schemes include a feedforward path.
- ▷ These schemes could be implemented digitally or using analog components. In this work, simple analog circuits to implement both positive and negative feedback schemes were described also. The proposed circuits used a BBD circuit thoroughly used in the music industry to generate reverberant and echo effects. The tuning for these circuits was performed by two trimming resistors, one devoted to set the correct time delay and therefore fix the resonant frequencies, and one more to fix the gain and bandwidth of the peaks at the resonant frequencies. These circuits turned out to be well suited for applications of harmonic compensation in low power electronics systems.

- ▷ It has been shown that the negative feedback scheme produces poles located at odd harmonics, while the positive feedback scheme produces poles at every single multiple of the fundamental frequency. Moreover, due to the feedforward path, zeros are included in between every two consecutive poles. It is thus clear that, the implementation of these schemes generate an infinite set of peaks centered at higher order harmonic frequencies, and due to the feedforward term, notches were inserted in between two consecutive peaks. The latter allows peaks of higher gain and enhanced selectivity, therefore improving considerably the performance.
- ▷ Some modifications for the proposed schemes were given to make them suitable for real applications, as the introduction of a LPF and a limiting gain  $K$ .
- ▷ A BIBO stability proof was developed for both schemes when they were used in a quite general closed loop control system.

Therefore, the bank of resonant filters, a scheme thoroughly used in controllers for harmonic compensation in different power electronic systems, could be replaced by these simpler repetitive schemes. This facilitated the controller implementation enormously. Originally, a resonant filter was required for each harmonic to compensate, which tuned out to be more involved as more harmonics were considered resulting in an unpractical solution. Thus, the two repetitive schemes, above described, represented an interesting approach particularly useful in control systems with periodic reference signals or disturbances.

This work presents also a collection of applications of repetitive based schemes to several representative systems in the power electronics field which are described next:

- ▷ A repetitive-based controller has been applied to the dc-dc boost converter whose control structure was very close to a conventional one. The main difference consisted in the introduction of a repetitive strategy aimed to compensate for harmonic distortion contained in the output capacitor voltage. This type of disturbance was mainly due to a voltage source polluted by harmonics in the audible range. This controller took the same structure as the one presented in [38] and [51], where the repetitive scheme replaced the bank of resonant filters. The idea behind these controllers was to distort the inductor reference current to incorporate an extra control input to allow harmonic compensation on the capacitor voltage side. A series of tests were carried out in an experimental prototype to assess the performance of the proposed controller. The experimental results compared the responses obtained with and without the harmonic compensation term. Transient responses to step changes in the load were also presented to exhibit the robustness of the proposed controller against load variations.
- ▷ A repetitive-based controller for a boost-based PFC was presented. This controller guaranteed voltage regulation with a power factor close to unity. The proposed controller was composed of the cascade interconnection of inner and outer loops, just as in the conventional controller. The outer loop consisted of a low pass filter plus an integral term, while the inner loop was composed by a negative feedback repetitive scheme plus the usual proportional term. In this case, the repetitive scheme could replace the bank of resonant filters tuned at odd harmonics, which represented a considerable reduction on the computational load. Experimental results in a 400 W boost-based PFC were obtained to show the effectiveness of the proposed control law.
- ▷ A repetitive based controller was presented for a half-bridge active filter working as a harmonic reducer. This system was connected in parallel with the supply voltage of a non

controlled full bridge rectifier to correct the power factor. The controller also guaranteed regulation and balance of both capacitors voltages present in the half-bridge topology. The controller was composed of three control loops, namely, tracking (inner), regulation and balance control loops. A first contribution was that, to allow the voltage balance, an extra control input was included in the line current reference whose effect practically vanished in steady state. A second contribution of this work was the use of a negative feedback repetitive scheme in the tracking (inner) control loop to guarantee current tracking and disturbance rejection. Finally, experimental results were obtained with a low power laboratory prototype to show the effectiveness of the proposed controller.

- ▷ A repetitive based controller for a full bridge shunt active filter was presented. This controller was integrated by the cascade interconnection of inner and outer loops. The latter was designed as a low pass filter plus an integral term, while the former was composed of a negative feedback repetitive scheme plus the usual proportional term. The idea behind the repetitive scheme was to compensate for odd harmonic components of a highly distorted load current. Finally, experimental results in a 1.5 KVA prototype were obtained to show the effectiveness of the proposed control law.

## 7.2 Future Work

The following issues are still under study and the results will appear in future works:

- ▷ Performance analysis of the controllers presented in this work.
- ▷ The study of singular perturbation techniques to relax the decoupling assumption in the control of power electronics systems.
- ▷ The study of the passivity proprieties of the proposed repetitive base controllers.
- ▷ A formal study of the parameters tuning process in the proposed controllers
- ▷ The use of direct power control to propose control laws for power electronics systems.
- ▷ The study of practical modifications in repetitive scheme to improve the phase distortion caused by practical modifications in feedback feedforward repetitive structures.
- ▷ The study of hybrid solutions, i.e. combination of active and passive filters for the harmonic compensation issue in a single phase systems.
- ▷ The study of sensorless techniques for power electronics system.



# Bibliography

- [1] Muhammad H. Rashid. *Power Electronics Handbook*. Academic Press, 1st edition, 2001. ISBN0-12-581650-2.
- [2] J. Schlabbach, D. Blume and T. Stephanblome. *Voltage Quality In electrical Power System*. The Institution of Electrical Engineers, 1st edition, 2001. ISBN0-85296-975-9.
- [3] G. Escobar, P.R. Martínez and J. Leyva-Ramos. Analog circuits to implement repetitive controllers with feedforward for harmonic compensation. *IEEE Trans. on Ind. Electr.*, 53(6):1–7, 2006.
- [4] G. Escobar, A.M. Stanković. and D. Perrault. Regulation and compensation of source harmonics for the boost-converter based power factor precompensator. *Proc. 32th IEEE Power Electr. Spec. Conf. PESC*, 1:1–6, 2001.
- [5] C. D. Schauder and S. A. Moran. Multiple reference frame controller for active filters and power line conditioners. *US Patent*, No. 5309353 (USA):1, 1994.
- [6] P. Mattavelli. Synchronous-frame harmonic control for high-performance ac power supplies. *IEEE Trans. on Ind. App.*, 37(3):864–872, 2001.
- [7] T. W. Rowan and R. J. Kerkman. A new synchronous current regulator and an analysis of current-regulated pwm inverters. *IEEE Trans. on Ind. App.*, IA(22):678–690, 1986.
- [8] C. D. Schauder and R. Caddy. Current control of voltage source inverters for fast four quadrant drive performance. *IEEE Trans. on Ind. App.*, IA(18):163–171, 1982.
- [9] M. Bojrup, P. Karlsson, M. Alakula and L. Gertmar. A multiple rotating integrator controller for active filters. 1:1–9, 1999.
- [10] I. Etxeberria-Otadui, A. Lopez-de-Heredia, H. Gaztañaga S. Bacha and R. Reyer. A single synchronous frame hybrid (ssf) multifrequency controller for power active filters. *IEEE Trans. on Ind. Electr.*, 53(5):1640–1648, 2006.
- [11] G. Escobar, A. Stankovic and P. Mattavelli. An adaptive controller in stationary reference frame for d-statcom in unbalanced operation. *IEEE Trans. on Ind. Electr.*, 51(2):401–409, 2004.
- [12] G. Escobar, A. M. Stankovic and P. Mattavelli. Adaptive controller for d-statcom in the stationary reference frame to compensate for reactive and harmonic distortion under unbalanced conditions. *US Patent*, No. 6862199 B2:1, 2005.
- [13] D. N. Zmood, D. G. Holmes and G. Bode. Frequency domain analysis of three phase linear current regulators. *Conf. Rec. IEEE-IAS Annual Meeting*, 1:818–825, 1999.

- [14] C. B. Jacobina, R.O. de Carvalho Jr., M. B. R. Correa, A. M. N. Lima and E. R. C da Silva. Digital current controller of unbalanced three-phase power electronic systems,. *Proc. IEEE Pow. Elec. Spec. Conf. (PESC)*, 2:767–772, 1999.
- [15] S. Fukuda and T. Yoda. Investigation of current controller for single phase pwm converters based on the internal model principle. 1:1–6, 1999.
- [16] S. Fukuda and T. Yoda. A novel current tracking method for active filters based on a sinusoidal internal model. 1:1–6, 2000.
- [17] X. Yuan, W. Merk, H. Stemmler and J. Allmeling. Stationary-frame generalized integrators for current control of active power filters with zero steady-state error for current harmonics of concern under unbalanced and distorted operating onditions. *IEEE Trans. on Ind. App.*, 38(2):523–532, 2002.
- [18] S. Hara, T. Omata and M. Nakano. Synthesis of repetitive control of a proton synchrotron magnet power supply. *Proc. 8th. IFAC World Congress*, 2:216–221, 1981.
- [19] S. Hara, T. Omata and M. Nakano. Synthesis of repetitive control of systems and its applications. *Proc. 24th. IEEE Conf. Decision Contr.*, 3:1387–1392, 1981.
- [20] T. Omata, S. Hara and M. Nakano. Repetitive control for linear periodics systems. *Elect. Eng. Jpn.*, 105:131–138, 1985.
- [21] S. Hara, Y. Yamamoto, T. Omata and M. Nakano. Repetitive control systems: A new type servo systems for periodic exogenous signals. *IEEE Trans. on Automat. Contr.*, 33-7:659–668, 1988.
- [22] Y. Yamamoto and S. Hara. Relationships between internal and external stability for infinite-dimencional systems whit applications to a servo problem. *IEEE Trans. on Automat. Contr.*, 33-11:1044–1053, 1988.
- [23] Brad Paden Ghosh and Jayati. Nolinear repetitive control. *IEEE Trans. on Automat. Contr.*, 45-5:949–954, 1988.
- [24] Steinbuch Maarten. Repetitive control for systems whit uncertain period-time. *Automatica*, 38:2103–2109, 2002.
- [25] M. Tomizuca, T. Tsao and K. chew. Discrete-time domain analisys and synthesis of repetitive controller. *Proc. American Control Conference*, 1:860–866, 1988.
- [26] M. Tsai, G. Anwar and M. Tomizuca. Discrete time repetitive controllers for robots manipulators. *Proc. IEEE Conf. Robotics Automat.*, 3:1341–1346, 1988.
- [27] H. L. Broberg and R. G. Molyet. Reduction of repetitive errors in tracking of periodical signals: theory and application of repetitive control. *Proc. IEEE Conf. Robotics Automat.*, 3:1341–1346, 1988.
- [28] P. Mattavelli and F. P. Marafao. Selective active filters using repetitive control techniques. *IEEE Transactions On Industrial Electronics*, 51-5:1018–1024, 2004.
- [29] Shunxiao Xu and Fuwen Yang. A novel three-phase ac/dc converter without front-end filter based on repetitive control technique. *Proc. 3rd International Power Electronics and Motion Control Conference: PIEMC'00*, 3:1111–1115, 2000.

- [30] Ying-Yu Tzou, Shih-Liang Jung and Hsin-Chung Yeh. Adaptive repetitive control of pwm inverters for very low thd ac-voltage regulation with unknown loads. *IEEE Trans. on Pow. Electronics*, 14-5:973–981, 1999.
- [31] Kai Zhang, Jian Xiong, Yong Kang and Jian Chen. Direct repetitive control of spwm inverter for ups purpose. *IEEE Trans. on Pow. Electronics*, 18-3:784–792, 2003.
- [32] R. Costa-Castelló and R. Griñó. A repetitive controller for discrete-time passive systems. *Automatica*, 42:1605–1610, 2006.
- [33] G. Escobar, P. R. Martínez, J. Leyva-Ramos and P. Mattavelli. A negative feedback repetitive control scheme for harmonic compensation. *IEEE Trans. on Ind. Electr.*, 53(4):1383–1386, 2006.
- [34] J. Leyva-Ramos, G. Escobar, P. R. Martínez and P. Mattavelli. Analog circuits to implement repetitive controllers for tracking and disturbance rejection of periodic signals. *Transactions On Circuits and SystemsII: Express Briefs*, 52(8):466–470, 2005.
- [35] B. Francis and W. Wonham. The internal model principle for linear multivariable regulators. *Applied Mathematics and Optimization*, 2:170–194, 1975.
- [36] J. Leyva-Ramos, G. Escobar, P. R. Martínez and P. Mattavelli. Analog circuits to implement a repetitive controller for harmonic compensation. *Proc. IEEE International Congress of Power Electronics 2004*, 1:1–6, 2004.
- [37] G. Escobar, J. Leyva-Ramos, P. R. Martínez and A. A. Valdez. A repetitive-based controller for the boost converter to compensate the harmonic distortion of the output voltage. *Trans. on Control Systems Technology*, 13(3):500–508, 2005.
- [38] G. Escobar, A. Valdez, J. Leyva-Ramos and P.R. Martínez. A controller for a boost converter with harmonic reduction. *Proc. 29th Int. Conf. Ind. Elec., Contr., and Instr.: IECON '03*, 1:1–6, 2003.
- [39] G. Escobar, P. R. Martínez, J. Leyva-Ramos, A. A. Valdez and M. Hernandez-Gomez. A repetitive-based controller for a power factor precompensator with harmonic compensation. *Proc. 36th IEEE Power Electr. Spec. Conf. PESC*, 1:2363–2369, 2005.
- [40] P. R. Martínez, G. Escobar, Hernandez-Gomez and R. E. Torres-Olguín. Power factor correction with an active filter using a repetitive controller. *Proc. IEEE International Symposium on Industrial Electronics IEEE ISIE*, 1:1395–1399, 2006.
- [41] G. Escobar, P. R. Martínez, M. Hernandez-Gomez and S. C. Ynez-Campos. A repetitive-based controller for a single-phase shunt active filter. *Proc. IEEE International Congress of Power Electronics 2006*, 1:1, 2006.
- [42] R. Griñó and R. Costa-Castelló. Digital repetitive plug-in controller for odd-harmonic periodic references and disturbances. *Automatica*, 41:153–157, 2005.
- [43] I. S. Gradshteyn and I.M. Ryzhik. *Table of integrals, series, and products*. Academic Press, 6th edition, 2000. ISBN0-12373-637-4.
- [44] Jhon C. Doyle Kemin Zhou. *Essentials of Robust control*. Prentice Hall, 2nd edition, 1996. ISBN0-13-525833-2.

- [45] A. C. Chow and D. Perreault. Design and evaluation of a hybrid passive/active ripple filter with voltage injection. *IEEE Trans. on Aerospace and Electronic Systems*, 39-2:471–480, 2003.
- [46] S. Y. M. Feng, W. A. Sander III and T. G. Wilson. Small-capacitance nondissipative ripple filters for dc supplies. *IEEE Trans. on Magnetics*, MAG-6:137–142, 1970.
- [47] M. K. Kazimierczuk and L. A. Starman. Dynamic performance of pwm dc-dc boost converter with input voltage feedforward control. *Transactions On Circuits and SystemsI: Fundamental Theory And Applications*, 46-12:137–142, 1999.
- [48] M. K. Kazimierczuk and A. Massarini. Feedforward control of dc-dc pwm boost converter. *Transactions On Circuits and SystemsI: Fundamental Theory And Applications*, 44:143–148, 1997.
- [49] B. Arbetter and D. Maksimović. Feedforward control of dc-dc pwm boost converter. *IEEE Trans. Power Electronics*, 42:361–368, 1997.
- [50] M. K. Kazimierczuk and R. Cravens II. Closed-loop characteristics of voltage-mode controlled pwm boost converter with an integral-lead controller. *Journal of Circuits, Systems and Computers*, 4-2:429–458, 1994.
- [51] G. Escobar, A. A. Valdez, J. Leyva-Ramos and P. R. Martínez. A controller for a boost converter with harmonic reduction. *Trans. on Control Systems Technology*, 12(5):717–726, 2004.
- [52] J. G. Kassakian, M. Schlecht and G. C. Verghese. *Principles of Power Electronics*. Addison–Wesley, 1st edition, 1991. ISBN0-201-09689-7.
- [53] P. T. Krein. *Elements of Power Electronics*. Oxford University Press, New York, 0 edition, 1998. ISBN0-19-511701-8.
- [54] F. Pottker and I. Barbi. Power factor correction of non-linear loads employing a single phase active power filter: control strategy, design methodology and experimentation. *Proc. 28th IEEE Power Electr. Spec. Conf. PESC*, 1:412–417, 1997.
- [55] F. Pottker and I. Barbi. Analysis and performance limits of continuous-mode boost converters for power-factor-correction applications. *Proc. IEEE International Symposium on Circuits and Systems ISCAS*, 1:877–880, 1997.
- [56] O. García, J.A. Cobos, R. Prieto, P. Alou and J. Uceda. Single phase power factor correction: A survey. *IEEE Trans. Power Electronics*, 18(3):749–755, 2003.
- [57] G. Escobar and H. Sira-Ramirez. A passivity-based sliding mode control approach for the regulation of power factor precompensators. *Proc. IFAC NOLCOS*, 1:1–6, 1998.
- [58] R. Ortega, P. J. Nicklasson, A. Loria and H. Sira-Ramirez. *Passivity-based control of Euler-Lagrange systems*. Springer-Verlag, 1st edition, 1998. ISBN1-85233-016-3.
- [59] D. G. Holmes. D. N. Zmood. Stationary frame current regulation of pwm inverters with zero steady-state error. *IEEE Trans. Power Electronics*, 18(3):814–822, 2003.
- [60] S. Fukuda and R. Imamura. Application of a sinusoidal internal model to current control of three phase utility-interface-converters. *IEEE Trans. on Ind. Electr.*, 52(2):420–426, 2005.
- [61] O. García, María Dolores Martínez-Avial, J. A. Cobos, J. Uceda, J. González and J. A. Navas. Harmonic reducer converter. *IEEE Trans. on Ind. Electr.*, 50(2):322–327, 2003.



- [62] H. Akagi and A. Nabae. Control strategy of active power filters using multiple voltage source pwm converters. *IEEE Trans. on Ind. App.*, IA-22(3):460–465, 1986.